Aus dem Institut für Immunologie im Biomedizinischen Centrum

Institut der Ludwig-Maximilians-Universität München

Vorstand: Prof. Dr. rer. nat. Thomas Brocker

Analysis of phosphatidylserine-positive $CD8^+$ T cells during viral infections

Dissertation

zum Erwerb des Doktorgrades der Naturwissenschaften

an der Medizinischen Fakultät der

Ludwig-Maximilians-Universität München

vorgelegt von

Lisa Rausch

aus Ludwigsburg

2021

Mit Genehmigung der Medizinischen Fakultät

der Universität München

Betreuer:	Prof. Dr. Thomas Brocker
Zweitgutachterin:	Prof. Dr. Carolin Daniel
Dekan:	Prof. Dr. med. Thomas Gudermann
Tag der mündlichen Prüfung:	20. Juni 2022

Eidesstattliche Versicherung

Lisa Rausch

Name, Vorname

Ich erkläre hiermit an Eides statt, dass ich die vorliegende Dissertation mit dem Titel:

Analysis of phosphatidylserine-positive $CD8^+$ T cells during viral infections

selbständig verfasst, mich außer der angegebenen keiner weiteren Hilfsmittel bedient und alle Erkenntnisse, die aus dem Schrifttum ganz oder annähernd übernommen sind, als solche kenntlich gemacht und nach ihrer Herkunft unter Bezeichnung der Fundstelle einzeln nachgewiesen habe.

Ich erkläre des Weiteren, dass die hier vorgelegte Dissertation nicht in gleicher oder in ähnlicher Form bei einer anderen Stelle zur Erlangung eines akademischen Grades eingereicht wurde.

Melbourne, 20.6.22 — Lisa Rausch

Ort, Datum — Unterschrift Doktorandin

This work contains work presented in the following publication:

Kranich, J., N.-K. Chlis, L. Rausch, A. Latha, M. Schifferer, T. Kurz, A. Foltyn-Arfa Kia, M. Simons, F.J. Theis, and T. Brocker, *In vivo identification of apoptotic and extracellular vesicle-bound live cells using image-based deep learning.* Journal of Extracellular Vesicles, 2020. **9**(1): p. 1792683-1792683.

Table of Contents

List of figures

Abbreviations

Ab	antibody
AF	autofluorescence
Ag	antigen
APC	antigen-presenting cell
BCL-2	B cell lymphoma 2
BDS score	Bright Detail Similarity Score
BF	bright field
BSA	bovine serum albumin
CAE-RF	convolutional autoencoder followed by a random forest classifier
CD	cluster of differentiation
CTL	cytotoxic T lymphocyte
DCs	dendritic cells
Eomes	eomesodermin
ESCRT	endosomal sorting complexes required for transport
EVs	extracellular vesicles
FCS	fetal calf serum
FDC	follicular dendritic cell
GC	germinal centre
GSK3	glycogen synthase kinase 3
i.v.	intravenously
IFC	Imaging flow cytometry
IFN-γ	interferon-γ
KLRG1	killer cell lectin-like receptor subfamily G member1
LCMV	lymphocytic choreomeningitis Virus
LFA-1	lymphocyte function-associated antigen-1
MFG-E8	milk fat globule-EGF factor 8
MFI	median fluorescence intensity
MFI	mean fluorescence intensity
MPEC	memory precursor effector cell
MS	mass spectrometry
MVE	multivesicular endosome
MVs	microvesicle
NFAT	nuclear factor of T cell activation
NK cells	natural killer cells
p.i.	post-infection
pMHC	peptide-loaded major histocompatibility complex
PS	phosphatidylserine
SLEC	short-lived effector cell
SS	Similarity Score
TCR	T cell receptor
TEM	transmission electron microscopy

1 Abstract

Apoptosis, the programmed cell death, is a central part of every immune response. Apoptotic host cell death occurs in response to pathogen infection, during lymphocyte-mediated cytolysis or T cell contraction following pathogen clearance. The presence of phosphatidylserine (PS) on the outer leaflet of the plasma membrane is a classic feature of apoptosis. In addition, extracellular vesicles (EVs) exhibit PS on their surface. EVs are a heterogeneous population of lipid bilayer-enclosed particles secreted into the extracellular space and are considered to modulate immune and T cell responses during infection and cancer.

However, the *in situ* detection of apoptotic and EV-bound cells, the properties of naturally produced EVs and their contribution to the regulation of T cell immunity *in vivo* is unknown. Here, upon intravenous injection of the PS-binding reporter molecule Milk fat globule-EGF factor 8 (MFG-E8)-eGFP followed by deep learning-based image analysis, we could reliably visualise and quantify apoptotic and EV-decorated cells *in vivo* during acute LCMV infection. Unexpectedly, we detected only low frequencies of apoptotic $CD8^+$ T cells but a significant fraction, preferentially effector $CD8^+$ T cells, associated with free PS^+ EVs in LCMV-infected mice and human vaccinees. $CD8^+$ T cell-associated EVs are of antigen-presenting cell (APC) origin. They carry MHC-II and costimulatory molecules, and their binding to T cells correlated with increased T cell receptor signalling and an activated phenotype. At later time points of infection, particularly cells displaying characteristics of memory precursor cells were EV^+.

Our results propose that APC-derived EVs signal an ongoing infection. Therefore, EVs may represent a mechanism to continuously stimulate primed $CD8^+$ T cells and keep them in an activated state to support virus elimination. Furthermore, EVs potentially influence the effector $CD8^+$ T cell fate during the contraction phase. Hence, we suggest that free APC-derived EVs contribute to the regulation of antiviral T cell responses *in vivo*.

This study contributes to a better understanding of naturally occurring EVs, their characteristics and complex roles during acute infections. The *in vivo* analysis of EV-T cell interactions may support the development of EV-based therapies for infectious diseases and cancer and may provide new insights into the potential use of EVs as biomarkers.

2 Zusammenfassung

Der programmierte Zelltod, auch Apoptose genannt, ist ein zentraler Bestandteil von Immunantworten. Apoptose von Zellen tritt während der Pathogeninfektion, der Lymphozyten-vermittelten Zytolyse oder während der Kontraktion der T Zellen am Ende einer Immunantwort auf. Die Exposition von Phosphatidylserin (PS) auf der Zelloberfläche ist ein charakteristisches Merkmal der Apoptose, allerdings weisen auch extrazelluläre Vesikel (EVs) PS auf ihrer Oberfläche auf. EVs sind eine heterogene von einer Lipid-Doppelschicht umgebene Strukturen, welche in den extrazellulären Raum sezerniert werden und möglicherweise die T-Zell Immunantworten während Infektionen und Krebs regulieren. Allerdings wurde die *in situ* Detektion von apoptotischen und EV-gebunden Zellen, die Eigenschaften von natürlich produzierten EVs und ihr Beitrag zu der Regulierung der Immunität *in vivo* noch nicht beschrieben. Durch die intravenöse Injektion des PS-bindenden Reportermoleküls *milk fat globule-EGF factor 8*(MFG-E8)-eGFP und einer auf *deep learning* basierenden Bildanalyse, konnten wir apoptotische und EV-gebundene Zellen zuverlässig *in vivo* während akuter Infektionen visualisieren und quantifizieren. Unerwarteter Weise entdeckten wir nur einen geringen Prozentsatz an apoptotischen $CD8^+$ T Zellen aber ein großer Teil der Zellen, präferenziell Effektor $CD8^+$ T Zellen, waren mit freien PS^+ EVs in LCMV-infizierten Mäusen und Gelbfieber-Virus-Vakzine geimpften Probanden assoziiert. Diese EVs stammen von Antigen-präsentieren Zellen (APCs) ab, tragen MHC-II und kostimulatorische Moleküle und ihre Bindung an $CD8^+$ T Zellen korrelierte mit einer erhöhten T Zellrezeptor-vermittelten Signaltransduktion und einem aktivierten Phänotyp. Zu späteren Zeitpunkten der Infektion sind vor allem Zellen, welche Charakteristika von Vorläufern von Gedächtniszellen aufweisen mit EVs dekoriert. Unsere Ergebnisse zeigen, dass EVs eine aktuelle Infektion indizieren und einen von APCs verwendeten Mechanismus darstellen könnten, um bereits aktivierte $CD8^+$ T Zellen kontinuierlich zu stimulieren und diese dadurch bis zum Ende der Immunantwort in einem aktivierten Zustand zu halten. Zusätzlich könnten EVs das Schicksal von Effektor $CD8^+$ T Zellen während der Kontraktionsphase beeinflussen und daher zur Regulierung von anti-viralen T Zellantworten *in vivo* beitragen.

Diese Arbeit trägt zu einem besseren Verständnis der Eigenschaften und der möglichen Rolle von natürlichen EVs während akuten Infektionen bei. Die *in vivo* Analyse von EV-T Zell Interaktionen könnte die Entwicklung von auf EV-basierenden Therapien gegen Infektionskrankheiten und Krebs unterstützen und neue Erkenntnisse über den potentiellen Einsatz von EVs als Biomarker liefern.

3 Introduction

3.1 The immune system

Our body encounters millions of potential pathogens, which rarely cause disease. The ability to avoid infections relies on our immune system, which evolved a variety of defence mechanisms to eliminate invading pathogens.

The vertebrate immune system comprises two arms, the innate and the adaptive immune system. Pathogens that succeed to cross the physical barriers of the innate immune system, such as epithelia and mucus, are immediately attacked by antimicrobial peptides and proteins of the complement system as a first defence mechanism. Additionally, innate immune cells, including phagocytic macrophages, dendritic cells (DCs) and natural killer (NK) cells, are activated that directly kill and engulf pathogens. These cells recognise molecular structures present on microbes by a limited number of germ-line encoded receptors, enabling the discrimination of self from non-self. However, when the innate immune response fails to eliminate invading pathogens, the adaptive immune system is required. Its activation crucially depends on professional antigen-presenting cells (APCs), such as DCs [1, 2].

The adaptive immune system is composed of two types of highly specialised lymphocytes, the B and T cells. B cells originate from the bone marrow and differentiate into antibody-producing plasma cells upon activation. T cells, after their development in the thymus, either express the co-receptor CD4 or CD8 and differentiate into cells that regulate lymphocyte activation ($CD4^+$ helper T cells) or kill infected and transformed cells, respectively ($CD8^+$ cytotoxic T lymphocytes (CTLs)). Unlike receptors of the innate immune system, the antigen-receptor of B (BCR) and T cells (TCR) are generated through the rearrangement of genomic DNA segments, and each B and T cell clone possesses a unique antigen specificity. The BCR and TCR are highly specific for and bind with high affinity to a particular antigen, enabling a more efficient clearance of the ongoing infection. Furthermore, in contrast to the innate immune system, lymphocytes can generate long-lasting immunological memory characterised by an immediate and enhanced response to repeated encounters with the same pathogen [3].

3.2 Activation of CD8$^+$ T cell by APCs

CD8$^+$ T cells play a crucial role in the protection against intracellular pathogens and transformed cells. T cell responses are initiated when a naïve T cell encounters its cognate antigen (Ag) in peripheral lymphoid organs [reviewed in 4, 5].

For its activation, a mature APC must provide at least two signals to naïve T cells. Signal 1 is Ag-dependent and achieved by the binding of the TCR and the CD4/CD8 co-receptor to its specific Ag in the form of a peptide fragment loaded on a major histocompatibility complex (pMHC) on the surface of APCs. CD8$^+$ T cells recognise pathogen-derived peptides presented by MHC class I molecules, while CD4$^+$ T cells bind to pMHC class II. Signal 2 is provided by co-stimulatory receptors including CD80/CD86 and intracellular adhesion molecule 1 (ICAM-1) on APCs that interact with CD28 and lymphocyte function-associated antigen-1 (LFA-1) on T cells, respectively [reviewed in 6]. Co-stimulatory signals amplify signal 1, promoting T cell proliferation and survival [reviewed in 6, 7]. However, the absence of co-stimulatory signalling or the interaction with inhibitory receptors (including cytotoxic T-lymphocyte antigen-4 (CTLA-4)) leads to T cell anergy and the termination of immune responses by restricting T cell activation, proliferation, and effector differentiation [reviewed in 8, 9].

Besides TCR and co-stimulatory signals, cytokines such as Interleukin-12 (IL-12) or Type I interferons (IFNs) drive proliferation, effector functions and survival of CD8$^+$ T cells, representing signal 3 of the T cell activation program [10-12].

Once all three signals are delivered, APC-T cell interactions continue for around a day, during which naïve CD8$^+$ T cells undergo clonal expansion and differentiate into potent killer cells of identical antigen specificity [13, 14].

The transition from naïve to effector CD8$^+$ T cells is associated with drastic changes in the overall gene expression profile and crucially depends on transcription factors that regulate the expression of effector functions [reviewed in 15, 16]. TCR and IL-12 receptor signalling induce an early expression of the T-box transcription factor T-bet that, together with eomesodermin (Eomes), is essential to produce antiviral IFN-γ and cytotoxic molecules, such as granzyme B and perforin [17, 18]. Furthermore, during effector differentiation, T cells lose the expression of the lymphoid homing molecules CD62L and C-C chemokine receptor type 7 (CCR7) [19, 20]. However, effector CD8$^+$ T cells display increased levels of the adhesion molecules CD44 and activated LFA-1, enabling their migration into infected or transformed tissues, where they kill pMHC-bearing target cells by cytolysis [19-22].

3.3 Ca^{2+}-Calcineurin-NFAT signalling in $CD8^+$ T cells

Another essential transcription factor activated within 3 min after TCR, and co-stimulatory signalling is the nuclear factor of T cell activation (NFAT) [23]. The NFAT family comprises five members: NFATc1 (NFAT2), NFATc2 (NFAT1), NFATc3 (NFAT4), NFATc4 (NFAT3) and NFAT5 [reviewed in 24]. All NFAT proteins have highly conserved DNA-binding domains, while only four of them translocate to the nucleus upon Ca^{2+}-induced dephosphorylation [25-27]. NFATc1-3 and NFAT5 are expressed in T cells, where they play essential roles in regulating T cell development, activation and effector functions [reviewed in 27]. Notably, NFATc1 has recently been demonstrated to be crucial for the cytotoxicity of $CD8^+$ T cells against tumour cells and during infection [28].

NFAT proteins are activated by signalling pathways triggered following TCR engagement [reviewed in 29, 30]. Briefly, TCR stimulation results in the activation of receptor-associated tyrosine-kinases that, in turn, phosphorylate and activate phospholipase C-γ (PLC-γ) (Fig. 1). Activated PLC-γ cleaves the membrane protein phosphatidylinositol-4,5-bisphosphate to generate the second messengers, inositol-1,4,5-triphosphate ($InsP_3$) and diacylglycerol (DAG). The binding of $InsP_3$ to its receptor in the endoplasmatic reticulum (ER) causes the release of Ca^{2+} into the cytosol. Decreased Ca^{2+} concentrations in the ER induce the opening of Ca^{2+}-release-activated Ca^{2+} (CRAC) channels in the plasma membrane, resulting in Ca^{2+}-influx, further elevating intracellular Ca^{2+} levels. Cytoplasmic Ca^{2+} then forms a complex with calmodulin, which binds to and activates the calmodulin-dependent phosphatase calcineurin. Calcineurin dephosphorylates NFAT, unmasking its nuclear-localisation signal (NLS) and inducing nuclear translocation. Nuclear NFAT interacts with various transcription factors, including activator protein 1 (AP1), activated upon TCR and co-stimulatory receptor ligation, to regulate gene expression [reviewed in 27, 29]. Nuclear NFAT proteins control cell-cycle progression and induce the expression of cytokines and effector molecules, including granzyme B, T-bet, IFN-γ, tumor necrosis factor (TNF) [28, 31-33].

When TCR signalling is terminated, and calcineurin activity decreases, NFAT-mediated transcription is rapidly inhibited by kinases such as glycogen-synthase kinase 3 (GSK3) [23, 34, 35]. Activated GSK3 rephosphorylates nuclear NFAT, thereby promoting its export back to the cytosol [34, 35]. However, the transcriptional activity can also be extended, e.g. by co-stimulatory signals [reviewed in 27, 36]. CD28 signalling activates Akt, which negatively regulates GSK3, preventing dephosphorylation and the export of nuclear NFAT [36, 37].

Together, NFAT proteins integrate multiple signalling pathways that tightly regulate their activity, thereby controlling T cell function [reviewed in 27].

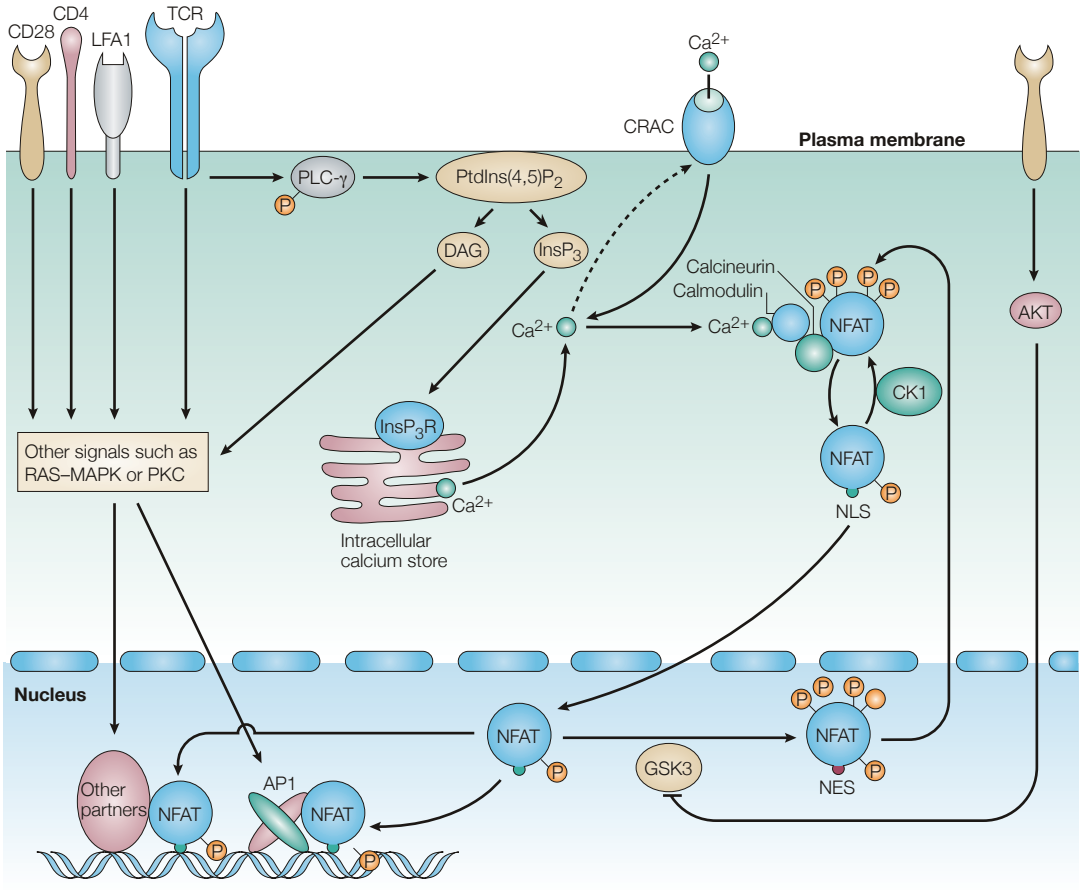

Figure 1: The regulation of NFAT activity.
TCR signalling induces the activation and phosphorylation of PLC-γ, which generates $InsP_3$ and DAG. $InsP_3$ triggers the release of Ca^{2+} from the ER to the cytosol. Increased Ca^{2+} levels, in turn, result in the opening of CRAC channels in the plasma membrane, maintaining high intracellular Ca^{2+} concentrations. Cytoplasmic Ca^{2+} binds to calmodulin which activates calcineurin. Activated calcineurin dephosphorylates NFAT resulting in the exposure of the NLS and its translocation to the nucleus. In the nucleus, NFAT associates with several transcription factors, for example, AP1, to induce the expression of effector genes. These transcription factors are activated upon TCR and co-stimulatory receptor signalling, including the RAS-mitogen-activated protein kinase (MAPK) pathway or protein kinase C pathway. NFAT activity is negatively regulated by kinases such as GSK3, which rephosphorylates nuclear NFAT, causing its return to the cytosol. The kinase Akt, which is activated upon CD28 ligation, inhibits the GSK3 activity. The figure is modified from [27].

3.4 $CD8^+$ T-cell memory differentiation during acute infection

The $CD8^+$ T-cell immune response has at least two important outcomes. The first outcome is the generation of a large number of cytotoxic T cells that eliminate invading pathogens. The second is the generation of long-lived memory cells that protect against repetitive encounters with the same pathogen. A typical T cell response to an acute infection encompasses three

different phases [reviewed in 38]. Upon infection, naïve Ag-specific $CD8^+$ T cells are activated and massively expand to give rise to CTLs that kill infected cells during the effector phase [reviewed in 7, 39]. After pathogen clearance, a contraction phase occurs, during which most Ag-specific effector $CD8^+$ T cells die via apoptosis. A small fraction (usually 5-10 %) survives and develops into protective, long-lasting memory $CD8^+$ T cells [reviewed in 15]. In the memory phase, surviving cells progressively acquire several memory characteristics, such as accelerated, more robust immune responses to secondary exposure with the same pathogen. Furthermore, in addition to lymphoid organs, memory cells reside in non-lymphoid and mucosal tissues, where they are maintained in an Ag-independent, cytokine-dependent manner by homeostatic proliferation [reviewed in 15, 40].

Kaech and Cui proposed that the differentiation of $CD8^+$ T cells into either short-lived effector cells (SLECs) that display decreased proliferative capability and longevity or into surviving memory precursor cells (MPECs) that develop into cells of the memory pool is not arbitrary [reviewed in 15]. By receiving specific signals, some cells might be more suitable to form memory T cells than others [reviwed in 15]. Several studies demonstrated that a high expression of the IL-7 receptor subunit-α (CD127) and anti-apoptotic B cell lymphoma 2 (Bcl-2) and a low expression of killer cell lectin-like receptor G1 (KLRG1) on effector $CD8^+$ T cells is associated with their selective survival and a preferential differentiation into memory cells [15, 41-44]. In contrast, SLECs, prone to die, display a low expression of CD127 and a higher expression of KLRG1 [41-43].

However, the molecular mechanisms that control the SLEC or MPEC potential of effector $CD8^+$ T cells are still incompletely understood. In a proposed “gradient model”, the transcriptional programs that determine the fate of effector $CD8^+$ T cells are regulated by a graded expression and activity of several antagonistic pairs of transcription factors [reviewed in 15]. In turn, these transcriptional regulators are controlled by multiple signals such as TCR strength and duration, type of co-stimulation, inflammatory cytokines and mTOR signalling [reviewed in 15, 40]. T-bet expression correlates with TCR signal strength during acute infections and is amplified by IL-12 signalling, while Eomes is induced by weak TCR signals and repressed by IL-12 [17, 42, 45]. Accordingly, a gradient of T-bet expression levels is established, which, by exceeding a certain molecular threshold, induces the differentiation into $KLRG1^{hi}CD127^{lo}$ terminally differentiated $CD8^+$ T cells [15, 42, 46]. In contrast, low T-bet expression and increased expression of Eomes prevent SLEC differentiation and promote cells to become part of the $CD8^+$ T cell memory pool [17, 42, 45]. Together, the long-term fate of effector $CD8^+$ T cells during acute infections is

coordinated by the expression levels of opposing sets of transcription factors that integrate multiple signals [reviewed in 15].

3.5 The LCMV infection model

LCMV is one of the best-characterised model systems of viral infection. Several fundamental concepts of $CD8^+$ T cell biology have been discovered by using LCMV as a model pathogen. The best example is the "MHC restriction", for which Peter Doherty and Rolf Zinkernagel were awarded the Nobel Prize in 1996 [47, 48]. Further fundamental discoveries include the basic principles of immunological memory [41, 49, 50], immunopathology in disease [51-53] and T cell exhaustion [54-57].

LCMV is an RNA virus belonging to the family of *Arenaviridae* and was isolated by Charles Armstrong from a monkey with acute lymphocytic choriomeningitis ($LCMV_{Arm}$) in 1933 [58, 59]. In its natural host, the mouse, $LCMV_{Arm}$ induces an acute infection triggering a vigorous CTL response, which is critical for viral elimination around day 8 post-infection (p.i.) [60-62]. LCMV is a spherical enveloped virus between 60-300 nm in diameter. The genome of LCMV consists of two negative single-stranded segments [63]. The large segment (L) encodes an RNA-dependent RNA polymerase and a small RING (really interesting new gene) finger motif protein [64]. The short (S) fragment encodes the structural proteins of the virus: the nucleoprotein (NP) and a precursor polypeptide, GP-C [65]. In infected cells, GP-C is post-translationally cleaved into the peripheral glycoprotein GP1 and the transmembrane glycoprotein GP2 [66].

LCMV replicates in several tissues, including the spleen, liver, lung, lymph nodes and brain [67]. The main cellular receptor of LCMV is α-dystroglycan (α-DG), a widely expressed cell surface receptor, which is mainly found on $CD11c^+$ and $DEC\text{-}205^+$ DCs and macrophages [68-70]. The GP1 protein of LCMV mediates receptor binding, and only in the absence of CTLs, LCMV-neutralising antibodies (nAb) are generated against GP1 one month after infection [71, 72]. However, CTL-depleted mice fail to clear $LCMV_{Arm}$ infection and become persistently infected, demonstrating their crucial role in eliminating the virus [60, 62, 67]. Interestingly, while the anti-viral antibody response is greatly suppressed in the absence of $CD4^+$ T cells, the induction of LCMV-specific CTL responses and the ability to resolve the infection is $CD4^+$ T cell-independent [67, 73].

Notably, LCMV is a noncytopathic virus. The destruction of lymphoid organs and the hepatic damage observed during LCMV infection has been described to be induced by $CD4^+$ and

cytotoxic $CD8^+$ T cell responses that destroy virus-infected cells rather than by the virus itself [74, 75].

The number of Ag-specific $CD8^+$ T cells during LCMV infection has long been underestimated due to the absence of methods that precisely measure specific T cell responses [76]. The development of fluorescently labelled tetrameric peptide/MHC-I molecules (MHC-I tetramers) or adoptive cell transfer of $CD8^+$ T cells from LCMV-specific TCR transgenic mice (P14 mice), however, significantly improved the ability to analyse and quantify Ag-specific CTL responses [76-78]. By using either of these two methods, previous reports demonstrated that LCMV-specific $CD8^+$ T cell activation could be detected in the spleen within 3 days p.i. [78, 79]. At the peak of the immune response, which occurs 7-8 days after infection, the number of activated $CD8^+$ T cells in the spleen increases more than 10-fold and around 70 % of all $CD8^+$ T cells are LCMV-specific [78, 79]. In LCMV-infected C57BL/6 mice, virus-specific $CD8^+$ T cells recognise at least 28 different MHC class I-associated LCMV peptides [80]. However, $CD8^+$ T cells specific for the viral NP peptide (NP396-404 (33%)) and the GP peptide (GP33-41 (25%)), restricted by MHC class I alleles D^b or K^b, dominate the $CD8^+$ T cell immune response [78, 81].

Following the resolution of $LCMV_{Arm}$ infection, the number of LCMV-specific $CD8^+$ T cells decreases 10-20-fold by day 30 post-infection. Only 5-10 % of the activated $CD8^+$ T cells present at the peak of the immune response develop into surviving memory $CD8^+$ T cells that are stably maintained throughout the life of the mouse (> 1.5 years) [41, 49, 78]. These $CD8^+$ T cells are $CD127^+$ but express low levels of KLRG1. In contrast, the number of $KLRG1^{hi}CD127^{lo}$ $CD8^+$ T cells sharply decreased from day 8 to 30 and continuously decline afterwards with a $t_{1/2}$ ~ 65-80 days [42].

Interestingly, several studies demonstrate that memory precursor $CD8^+$ T cells already exist in the $CD8^+$ T cell effector population as early as 6-8 days post LCMV infection [41, 82]. However, at that time point, they have not fully acquired functional memory cell properties, such as homeostatic proliferation or rapid recall responses to Ag [82]. As demonstrated by transfer experiments, $CD127^{hi}$ cells gradually develop into functional long-lived memory cells when analysed 3-6 weeks after transfer [41].

In contrast to $CD8^+$ T cells, $CD4^+$ T cell responses peak on day 10 p.i. with 20 % of total $CD4^+$ T cells revealing virus specificity [49]. Although virus-specific $CD4^+$ T cells display a prolonged contraction phase, 5-10 % of Ag-specific $CD4^+$ T cells are stably maintained as memory pool [49].

Besides $LCMV_{Arm}$, many other strains have been isolated [reviewed in 83]. For example, LCMV Clone 13, a variant of the Armstrong strain, suppresses LCMV-specific CTL responses by inducing $CD8^+$ T cell exhaustion resulting in viral persistence [84].

3.6 Characteristics of apoptotic cell death

Besides the activation and differentiation of immune cells, cell death is central to every immune response. During infection, host cell death occurs by pathogens that destroy infected cells, during the cytotoxic killing of target cells by immune cells or during T cell contraction following pathogen clearance [reviewed in 85, 86].

Over the last few years, multiple forms and cell death pathways have been defined based on morphological, biochemical, and functional properties [reviewed in 87]. Each type of cell death is induced by certain stimuli and conducted through distinct, sometimes overlapping signalling pathways.

Apoptosis, the programmed cell death, is an active, highly regulated, and controlled form of cell death that does not induce inflammatory responses [reviewed in 87, 88]. It is an evolutionarily conserved cell death pathway essential for the immune system and crucial for eukaryotic development, tissue homeostasis maintenance, and prevention of cancer. Several conserved morphological hallmarks characterise apoptotic cell death, such as cell shrinking, plasma membrane blebbing, nuclear condensation and fragmentation. These changes lead to the activation of cysteine-aspartic proteases, the caspases that degrade cellular components resulting in cell death [reviewed in 88].

In mammals, two apoptosis pathways exist, the extrinsic and the intrinsic pathway. In short, the extrinsic pathway is activated by the binding of death molecules such as Fas ligand (FasL), TNF-α and TNF related apoptosis-inducing ligand (TRAIL) to their specific death receptors (Fas, TNFR1/2). Ligation results in receptor trimerisation, recruitment of adaptor proteins (such as FADD) and pro-caspase 8 to assemble the death-inducing signalling complex (DISC), where pro-caspase 8 oligomerises and is cleaved into its active form, caspase 8 [reviewed in 88].

The intrinsic pathway is regulated by the balance of pro- and anti-apoptotic proteins of the Bcl-2 protein family. Cellular stress or damage results in the expression or cleavage and activation of pro-apoptotic Bcl-2 proteins (Bim, Bid) that directly or by antagonising anti-apoptotic Bcl-2 or Bcl-XL, trigger Bcl-2 associated X protein (Bax) and/or Bcl-2 antagonist/killer (Bak) oligomerisation. The activation of Bax and Bak results in cytochrome c release from mitochondria. In the cytosol, cytochrome c interacts with apoptotic protease activating factor-

1 (Apaf-1), resulting in caspase 9 activation. Caspase 8 and caspase 9 from both apoptosis pathways cleave and activate caspase 3 to execute apoptosis [reviewed in 88].

Another central biochemical feature of apoptosis is the appearance of PS on the cell surface. The phospholipid PS is a component of eukaryotic cell membranes. In living cells, PS is predominantly confined to the inner leaflet by ATP-dependent flippases, whereas scamblases transport phospholipids between the leaflets in a non-specific and ATP-independent manner [89, 90]. However, in apoptotic cells, the inactivation of flippases and activation of scramblases by caspase 3 results in the translocation of PS to the outer leaflet of the plasma membrane [90-93].

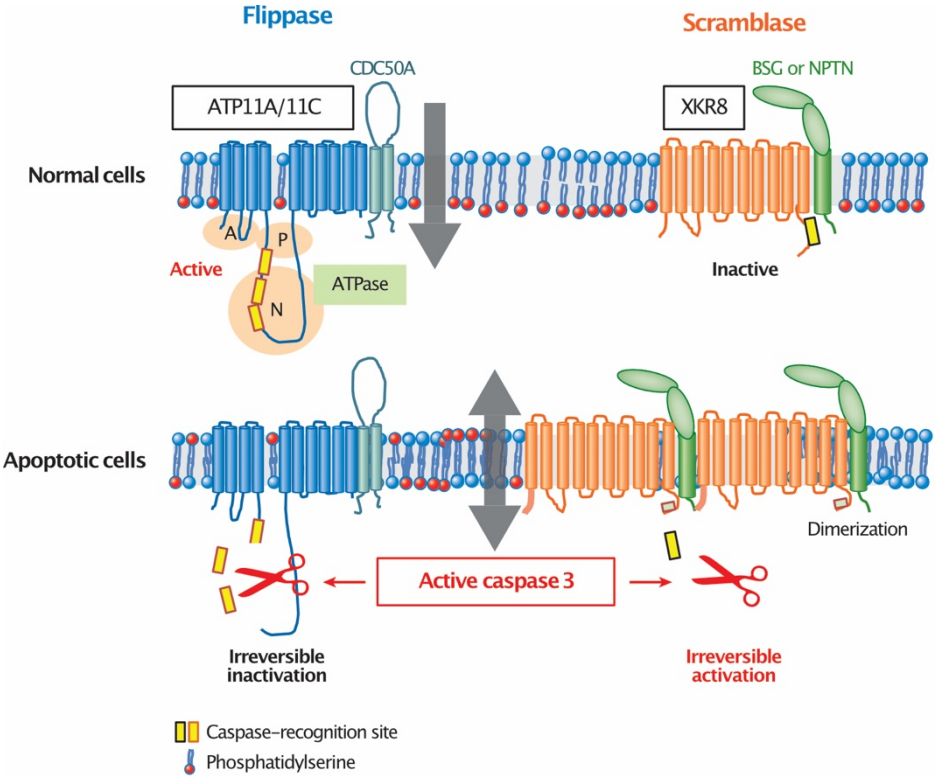

Figure 2: Molecular mechanisms of PS exposure during apoptosis.

In healthy living cells, the ATP-dependent flippases ATP11A/11C and the chaperone CDC50A continuously translocates PS from the outer to the inner leaflet of the plasma membrane. The scramblase XKR8 is inactive. In apoptotic cells, activated caspase 3 cleaves and irreversibly inactivates ATP11A/11C at the caspase-recognition sites. At the same time, caspase 3 activates the scramblase XKR8 by cleaving its C-terminal tail. In its cut form, XKR8 dimerises with basigin (BSG) or neuroplastin (NPTN) to form a complex, which non-specifically and bi-directionally exchanges phospholipids between the two lipid bilayers, resulting in the exposure of PS on the cell surface. Figure from [88].

On the cell surface, PS serves as an “eat-me” signal for the recruitment and engulfment of dying cells by macrophages in a process known as efferocytosis [reviewed in 88, 94]. This process

prevents the release of intracellular components, thereby avoiding inflammation and the activation of immune responses [95, 96].

PS exposure, however, is not a unique feature of apoptosis as other, non-apoptotic forms of cell death have been described to be associated with the translocation of PS to the outer leaflet of the plasma membrane [reviewed in 97].

Necrotic cell death is characterised by cytoplasmic swelling, plasma membrane rupture and the uncontrolled release of the cells' content into the extracellular environment, inducing inflammation and the activation of the immune system [reviewed in 98]. However, a programmed form of necrosis, called necroptosis, exists that is initiated by death receptors or pathogen recognition receptor pathways. These receptors induce the ubiquitinylation and activation of receptor-interacting serine/threonine-protein kinase 1 (RIPK1) [reviewed in 99]. Activated RIPK1 recruits RIPK3, which leads to their auto- and transphosphorylation and to the formation of a signalling complex, the necrosome. This complex phosphorylates the mixed lineage kinase domain-like (MLKL) protein, inducing its activation and oligomerisation. MLK trimers translocate to the plasma membrane, inducing plasma membrane rupture and consequently the release of immunostimulatory danger-associated molecular patterns (DAMPS).

Interestingly, PS exposure occurred during TNF-α and IFN-γ-induced necroptosis before membrane rupture [100, 101]. However, PS^+ necroptotic cells can be distinguished from PS^+ apoptotic cell death by morphological features. Cell shrinking and membrane blebbing are induced during apoptosis, while cell swelling and the permeabilisation of the plasma membrane are associated with necroptosis [102].

Furthermore, PS is transiently exposed before pyroptosis-associated cell lysis [103]. Pyroptosis is induced upon proinflammatory stimuli (such as intracellular infections) and requires inflammasome-dependent caspase 1 activation, which regulates the secretion of proinflammatory cytokines [reviewed in 99]. However, other caspases such as caspase 3, 5 or caspase 11 have been shown to trigger pyroptosis. When inflammatory caspases are activated beyond a specific threshold, they cleave members of the gasdermin protein family, such as gasdermin D (GSDMD), which in turn translocates to the plasma membrane, oligomerises to form a pore that causes cell lysis and the release of cytosolic content [reviewed in 99].

3.7 Apoptosis during infection

Apoptotic cell death of infected cells is a powerful mechanism to restrict the dissemination of intracellular pathogens as they strongly rely on living cells for their replication [reviewed in 85]. Pathogen-induced cell stress, cytoplasmic Ca^{2+} perturbation, and the recognition of invading infectious agents by pattern recognition receptors on the cell surface or in the cytoplasm can induce apoptosis [reviewed in 85, 104]. Additionally, infected cells are recognised by NK and CTLs, which, by releasing cytotoxic granzymes, induce apoptosis in target cells [reviewed in 105]. These apoptotic cells are then quickly engulfed by phagocytes, which in turn can present pathogen-derived components to other immune cells for their activation. As such, apoptosis of host cells is crucial for inducing immune responses [reviewed in 85].

Also, the anti-viral immune response against LCMV is associated with apoptotic events. During early LCMV infection, the splenic microarchitecture and infected APCs are destroyed by $CD8^+$ T cell-mediated cytotoxicity [74, 106]. Further IFN-induced apoptosis of memory $CD44^+CD8^+$ T cells has been described to occur two days after LCMV infection [107-109]. Even following viral clearance, apoptosis of LCMV-specific $CD8^+$ T cells is crucial for the termination of $CD8^+$ T cell responses and to restore T cell homeostasis [reviewed in 38]. However, the rapid and efficient uptake of apoptotic cells by macrophages, mediated by PS-binding proteins such as MFG-E8 (milk fat globule EGF factor 8), makes it challenging to analyse apoptotic cells *in vivo*, also in tissues with high cellular turnover rates [reviewed in 110].

3.8 Extracellular vesicles

Like apoptotic cells, several studies describe an enrichment of PS on the outer surface of extracellular vesicles (EVs) [reviewed in 111, 112]. EVs are a heterogeneous population of lipid-bilayer-enclosed structures that are secreted into the extracellular space. Virtually every cell produces EVs under physiological and pathological conditions, and the process of EV generation is highly conserved throughout evolution from bacteria, archaea to eukaryotes [113, reviewed in 114]. They contain distinct bioactive molecules, including proteins, metabolites, lipids, and nucleic acids, which largely depend on the parental cell's origin and the state. Although there is no current consensus regarding the classification of different vesicle types, EVs are roughly categorised into three main types based on their biogenesis, size, and cargo: exosomes, microvesicles (MVs) and apoptotic bodies [reviewed in 114, 115].

Exosomes are considered the smallest EVs, typically around 30-100 nm in diameter, produced within the endocytic pathway. Initially, they are generated as intra-luminal vesicles (ILVs) by inward budding of the membrane of multi-vesicular endosomes (MVEs). During the maturation of early into late endosomes, exosomes are released upon the fusion of MVEs with the plasma membrane [reviewed in 114, 115]. In contrast, outward budding releases MVs from the plasma membrane. MVs generally have a bigger size of approximately 100-1000 nm in diameter.

Apoptotic bodies are considered the largest EVs (1-5 µm) and are generated during the late stages of apoptotic cell death [reviewed in 115]. However, their impact on other cells is not well understood.

3.9 Biogenesis of exosomes and MVs

Several molecules are involved in the different steps of exosome generation and cargo sorting, including endosomal sorting complex for transport (ESCRT) proteins, syntenin or the tetraspanins [reviewed in 114] (Fig. 2). The loading of cargo into exosomes and the budding of ILVs from the limiting membrane of MVEs can occur through ESCRT-dependent or -independent mechanisms, which largely depends on the producing cell type and the cargo molecules [reviewed in 114, 116]. The ESCRT machinery consists of five subunits (-0, -I, -II, -III and Vps 4 complex (vacuolar protein sorting-associated protein 4) that mediate vesicle formation and cargo sorting in a stepwise fashion [reviewed in 117]. While ESCRT-0 and ESCRT-I recognise and accumulate ubiquitylated protein cargoes at specific lipid microdomains in the MVE membrane, recruited ESCRT-II and -III complexes exercise the bud formation and fission of ILVs using energy provided by the ATPase Vps4 [114, 118-123]. Besides, the ESCRT mechanism can also be initiated by syntenin and the ESCRT accessory protein ALG-2 interacting protein X (ALIX), which can recruit ESCRT-III and contribute to cargo selection [124].

In the absence of ESCRT, proteins of the tetraspanin family, including CD63 and CD9, participate in protein loading, and by forming tetraspanin-enriched microdomains induce an inward budding of the plasma membrane [116, 125, 126]. Additionally, ceramide, generated by neutral sphingomyelinase from sphingomyelin at membrane microdomains, induces negative membrane curvature, thereby promoting ILV budding [127, 128].

Besides proteins, exosome cargo includes nucleic acids, such as RNA species (mRNAs, micro RNAs (miRNAs), non-coding RNAs) and DNA [reviewed in 114]. Some miRNAs containing specific motifs were shown to be actively incorporated into exosomes [129, 130]. However, also passive incorporation of RNAs into exosomes has been described [131].

After their formation, MVEs either fuse with lysosomes for their degradation or are released as exosomes [reviewed in 114]. MVEs that are not destined for lysosomal degradation are transported to the plasma membrane via microtubules and actin filaments, a process that is regulated by various Rab (Ras-related in the brain) GTPases, including Rab27a and Rab27b [132-135]. The last step of plasma membrane docking and fusion is mediated by the controlled activity of Rab proteins, SNARE (Soluble NSF attachment protein receptor) proteins and members of the synaptotagmin family, finally resulting in the release of exosomes from the cell [132, 136].

The generation of MVs is associated with molecular changes of the peripheral cytoskeleton and rearrangements in the lipid composition of the plasma membrane that impact membrane curvature and fluidity [reviewed in 114]. An increase in intracellular Ca^{2+}, e.g. during activation, activates floppases, scramblases and calpain that induce random changes in the distribution of phospholipids and plasma membrane's detachment from the underlying cytoskeleton. These alterations result in the bending of the membrane and finally MV formation [reviewed in 114]. Like exosome generation, cholesterol and ceramide contribute to MV biogenesis by inducing membrane curvature and MV shedding [128, 137, 138].

Additionally, the cytoskeleton and proteins regulating its organisation are crucial for MV formation [reviewed in 114]. For example, members of the Rho family of GTPases and the RHO-associated protein kinase (ROCK), which coordinate actin reorganisation and myosin contractility, have been described to be involved in MV generation in tumour cells [139].

Contrary to the cargo loading of exosomes, the targeting and selection of MV cargo are less well characterised. For the loading into MVs, binding of lipid rafts and oligomerisation were shown to be sufficient to target lipids and cytosolic proteins to sites of MV budding [140-142]. The binding of highly oligomeric cytosolic proteins to the inner leaflet of the membrane is mediated by plasma membrane anchors such as acylation, myristoylation or palmitoylation, resulting in the concentration of proteins at membrane microdomains where MV form [140, 142]. The mechanisms that guide nucleic acids into MVs are mainly unknown.

The release of MV from the plasma membrane is mediated by ATP-dependent actin-myosin contraction at the vesicle neck, which is regulated by the GTP-binding protein ADP ribosylation factor (ARF) 6, ARF1 and Rho A (Ras homolog family member A) [143-145]. Also, proteins of the ESCRT machinery can contribute to MV secretion [146].

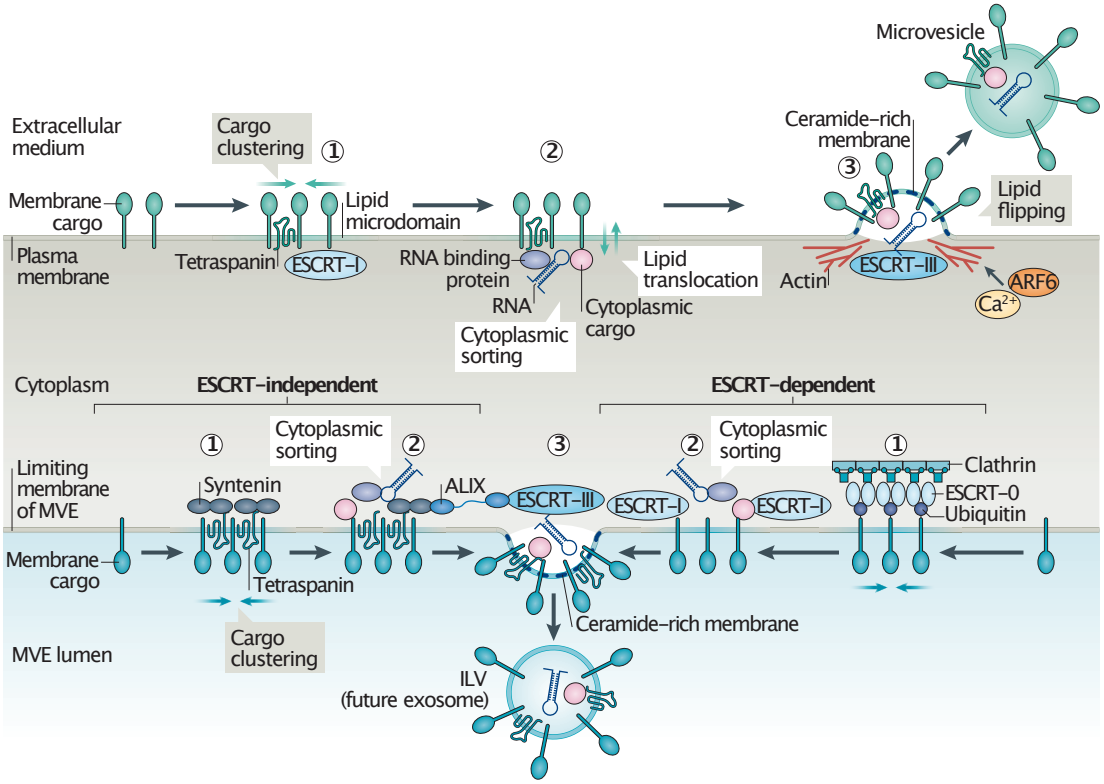

Figure 3: Biogenesis of exosomes and microvesicles.
The generation of exosomes and MVs occurs through several steps mediated by different sets of interacting proteins. In the first step, EV cargo such as lipids and proteins are clustered at specific microdomains of the plasma membrane or the membrane of MVEs to form MVs or exosomes, respectively. Cargo recruitment is carried out by several proteins (e.g. ESCRT proteins, tetraspanins, ALIX, synthenin) but also lipids (cholesterol, ceramide) within these microdomains. The formation of ceramide-rich microdomains together with GTP-binding proteins, cytoskeletal proteins, and ESCRT-III induce membrane curvature, budding and fission from the plasma membrane (MVs) or the MVE membrane (exosomes). While cargo sorting and membrane budding can occur through ESCRT-dependent and -independent mechanisms, ESCRT-III is required for the scission of ILVs. Many processes are shared between the biogenesis of exosomes and MVs (including those involving ESCRT proteins or ceramide). However, rearrangements of lipids in the plasma membrane have only been reported during the generation of MVs. Figure from [114].

3.10 Isolation and analysis of EVs

As EVs are secreted into the extracellular space and can be easily collected from cell culture supernatant or biofluids, including blood, urine, and saliva [reviewed in 115, 147]. The current gold standard for isolating EVs are methods based on ultracentrifugation, including differential ultracentrifugation or density gradient ultracentrifugation [reviewed in 115]. Other techniques to recover EVs include precipitation, size exclusion chromatography and immunoaffinity capture by Ab-coated magnet beads [reviewed in 115]. These isolation procedures are based on the size, density and composition of vesicles and, when combined, enable the separation of EVs from protein aggregates, viruses and cell debris [reviewed in 114]. Following purification,

analytical methods such as Western Blot analysis, nanoparticle tracking, electron microscopy, mass spectrometry (MS)-based proteomics, lipidomics and RNA or DNA sequencing are commonly used to determine the concentration, composition, and morphology of vesicles [reviewed in 115].

The cargo of EVs has been described as highly dependent on the molecular mechanisms involved in their biogenesis. However, as mentioned before, these mechanisms are largely shared by exosomes and MVs [reviewed in 114]. Furthermore, cells have been demonstrated to release distinct subpopulations of EV types, which are highly heterogeneous in size and composition [148-150]. Consequently, typical "exosome markers" such as MHC molecules, heat shock proteins or flotillin 1 were shown to be present on several isolated DC-derived EVs of varying sizes [150]. Though CD63, CD81, syntenin I and TSG101 were more enriched in small-sized vesicles (50-150 nm), comprising exosomes [150].

Due to their overlapping physical and biochemical characteristics, the isolation methods mentioned above fail to isolate EV subtypes exclusively and result in a mixed population of vesicles [reviewed in 115, 151]. Consequently, analytical methods are performed on EV populations of unknown origin, which prevents an exact assignment of molecular properties to a specific EV subtype [reviewed in 151]. Additionally, the clear cell origin of EVs purified from biological fluids cannot be determined. The heterogeneity and the absence of selective molecular markers hinder a reliable nomenclature of EVs [150, 152]. Therefore, at present, the International Society for Extracellular Vesicles (ISEV) recommends using "extracellular vesicle" as the best generic terminology "for particles naturally released from the cell that are delimited by a lipid bilayer and cannot replicate,.i.e. do not contain a functional nucleus" [153].

3.11 EVs as biomarkers

In addition to their biogenesis pathway, EV cargo strongly reflects the molecular phenotype of the producing cell [114, 154, 155]. Therefore, differences in the molecular content of EVs may represent changes in the physiological state of the parental cell, such as activation or pathology [reviewed in 156]. Besides, EVs can be easily, non-invasively collected from all kinds of body fluids [156]. For these reasons, EVs and their cargo are regarded as promising biomarkers for the diagnosis, prognosis, and monitoring of several diseases, including infections, tumours, metabolic, and neurological disorders [reviewed in 156]. Multiple studies revealed differences in the abundance of several RNA species and proteins between EVs from cancer patients and EVs from healthy individuals [reviewed in 157]. Furthermore, *Mycobacterium tuberculosis* (*M.*

tuberculosis)-derived peptides could be detected in EVs secreted from infected macrophages *in vitro*, and in EVs recovered from the serum of patients with *M. tuberculosis* infection, demonstrating the potential of EVs in the diagnosis of bacterial infection [158, 159].

Moreover, the number of secreted EVs was significantly increased in serum upon *M. bovis* infection in mice and cancer patients and *Plasmodium*-infected individuals compared to healthy controls [160-162]. To sum up, these studies suggest that, in addition to the composition of EVs, the amount of secreted EVs may possess great potential as a diagnostic marker for human diseases.

3.12 Interaction of EVs with target cells

EVs have long been regarded as cellular debris without functional relevance [163]. However, several studies have demonstrated that EVs can mediate cell-to-cell communication by transferring biologically active molecules between cells that induce phenotypic changes in recipient cells [164-167]. Once released, EVs can interact with specific target cells in the proximity or at distant sites through different means. Notably, the binding of EVs to cells is not random but largely depends on specific surface interactions between molecules on recipient cells and those enriched on the EV surface [168-171]. Molecules involved in selective targeting, docking, and the cellular uptake of EVs include integrins [171, 172], tetraspanins [173, 174], lipids, proteoglycans and components of the extracellular matrix (ECM) [175, 176]. For example, DC-derived EVs are targeted to activated $CD4^+$ T cells via CD54-LFA-1 interactions [169, 177]. Furthermore, EV capture by DCs was partially inhibited by blocking antibodies against LFA-1, ICAM-1, integrins, or CD9 and CD81 [169, 174]. Besides, CD44 contributes to EV docking and regulates EV uptake [178-180].

Cell-bound EVs have several different fates: EVs may fuse with the plasma membrane, thereby transferring EV surface molecules and their content to recipient cells [reviewed in 114]. Alternatively, intact EVs can also be internalised by different mechanisms such as endocytosis or phagocytosis [reviewed in 114]. Following their uptake, EVs are transported to endocytic compartments, where they can fuse with the MVE membrane transferring their content into the cytoplasm [reviewed in 114, 181]. Here, EV cargo was described to elicit or suppress various responses in recipient cells. In DCs, peptides from internalised exosomes were processed in endosomal compartments and loaded onto MHC-II molecules for presentation to $CD4^+$ T cells, thereby enhancing Ag presentation [174]. Furthermore, functional mRNAs and miRNAs have been reported to be directly transferred between cells via EVs, which after their release into

the cytoplasm, are translated and able to modulate gene expression in recipient cells [164, 167, 182].

In addition, the binding of ligands on EVs to particular surface receptors on target cells without EV uptake can be sufficient to trigger intracellular signal cascades that induce phenotypic and functional changes [reviewed in 114, 163, 183]. As a first example, MHC-II-carrying exosomes derived from B cells were shown to cause Ag-specific MHC class-restricted T cell activation [165]. Conversely, FasL on EVs from activated and EBV-transformed B cells were shown to induce apoptosis of Ag-specific $CD4^+$ T cells, thereby curtailing T cell responses [184, 185]. Several other reports followed demonstrating that EVs represent a mechanism of intercellular communication and participate in multiple physiological processes, including tissue regeneration, immune responses, tumour progression, inflammation, and infection [reviewed in 183, 186, 187].

3.13 Regulation of T cells responses by EVs

Recently, EVs attracted a lot of attention due to their potential usage as delivery vehicles for therapeutic agents [reviewed in 188], as diagnostic biomarkers for cancers [reviewed in 157] and to regulate immune responses [reviewed in 183]. B cell-derived EVs were shown to effectively present pMHC-II and co-stimulatory molecules to $CD4^+$ T cells, resulting in their Ag-dependent activation both *in vitro* and *in vivo* [165, 189]. Furthermore, the injection of pMHC and CD86-carrying EVs derived from DCs loaded with tumour-specific peptides induced potent $CD8^+$ T cell responses resulting in the delay of tumour growth or even eradication [166]. Also, *M. bovis*-infected macrophages were shown to release increased levels of EVs that contain mycobacterial components and could stimulate both specific $CD4^+$ and $CD8^+$ T cell responses *in vitro* and *in vivo* [158, 190]. Likewise, EVs from human cytomegalovirus-infected endothelial cells could trigger the proliferation of allogenic memory $CD4^+$ T cells *in vitro* [191]. These findings strongly suggest that APC-derived EVs can serve as a source of Ag that may promote T cell responses and consequently led to an array of studies investigating the immune-modulatory properties of EVs [reviewed in 183].

Both immature and activated DCs have been described to release EVs; however, DCs, that were activated by lipopolysaccharide secreted significantly more EVs with increased stimulatory capacity than immature DCs [155, 192-194]. Particularly, EVs from mature DCs, that are enriched for MHC class I and II complexes and co-stimulatory molecules (CD86 and ICAM-1)

were shown to effectively induce T cell proliferation, memory development and anti-tumour responses *in vitro* and *in* vivo [123, 155, 166, 169, 177, 193, 195, 196].

However, in most experiments, the activation of naïve $CD8^+$ and $CD4^+$ T cells was greatly supported by bystander DCs [155, 189, 197]. Hence, the stimulation of T cells has been suggested to occur by the transfer of released EVs to neighbouring DCs, which either directly present entire EV-derived pMHC complexes on their surface (cross-dressing) or present Ags associated with bound EVs on their own MHC molecules (cross-presentation) [174, 183, 189, 198-200]. Besides, released EVs may be recaptured by the parental cell, thereby directly presenting EV-associated molecules to T cells [reviewed in 183].

Conversely, several *in vitro* experiments demonstrated a direct activation of naïve and Ag-experienced $CD4^+$ and $CD8^+$ T cells by isolated APC-derived EVs loaded with peptides from pathogens [169, 194, 196, 201]. However, given the fact that EVs are less efficient than APCs in activating T cells [165, 199], EVs may not directly prime naïve T cells but rather stimulate activated or memory T cells *in vivo* [183, 188, 197]. Consistent with that, APCs were shown to release pMHC-carrying EVs during cognate immune cell interactions, which can be directly taken up by $CD4^+$ T cells at the immunological synapse [125, 197, 202, 203]. As EV-binding was associated with an activated T cell phenotype, APC-derived EVs were suggested to maintain the T cell activation status following APC interaction [169, 197]. However, EV-binding to activated T cells may also reduce an ongoing immune response, as FasL-carrying EVs secreted by human cancer cells or activated lymphocytes were shown to induce apoptosis of activated T cells [185, 204-207]. Currently, it is unclear whether interactions of T cells with free EVs exist *in vivo.* Furthermore, the contribution of EV-T cell interactions to the inhibition or activation of T cell responses *in vivo* has not been clarified yet.

3.14 DC-derived EVs in clinical trials

Due to their ability to induce $CD8^+$ T cell responses, DC-derived EVs have been tested clinically as cancer vaccines [208-210]. Two phase I clinical trials and one phase II trial have been conducted in patients suffering from melanoma or advanced non-small cell lung cancer [208-210]. In both phase I trials, EVs were obtained from autologous DCs (dendritic cell-derived EVs, Dex) pulsed with tumour antigens and then injected. The studies demonstrated that the administration of EVs to patients is safe and feasible. However, the treatment triggered only low T cell responses that caused long term disease stability in only some patients.

Consequently, a second-generation of Dex from IFN-γ -stimulated, tumour antigen peptide-pulsed DCs, with increased immunostimulatory properties, have been developed to improve their therapeutic efficacy [211]. However, this approach resulted in only limited T cell activity but induced NK cell function that correlated with a longer rate of progression-free survival (PFS) in a phase II clinical trial [210]. The limited efficacy of these clinical trials may be due to MHC-restricted peptides on Dex that were not able to induce T cell clones targeting tumour cells or due to the presence of inhibitory molecules on Dex, such as CD274/CD273, that suppress $CD8^+$ T cell responses [reviewed in 212]. Furthermore, the spatio-temporal kinetics of EV *in vivo* are unknown, and it remains to be determined whether injected EV reach lymphoid organs for Ag-presentation or are removed from the circulation by macrophages [213, 214]. To improve and develop new EV-based therapeutic approaches, a better understanding of the complex role of EVs in the immune system, such as their behaviour and function in living organisms, is necessary.

To elucidate the EV biogenesis, biodistribution, and uptake, isolated EVs have been labelled (lipophilic dyes) or tumour cells expressing reporter molecules that are fused to EV components (such as CD63, palmitoylation signal, MFG-E8) have been employed [114, 167, 215, 216]. Labelled EVs directly injected or secreted from implanted tumour cells were successfully visualised and tracked in cell culture and *in vivo* [167, 214, 216-218]. Undoubtedly, these studies provided crucial insights into the behaviour and nature of EVs *in vivo*. However, the injection of high concentrations of *in vitro* generated, genetically manipulated or fluorescently labelled EVs or the analysis of labelled EVs under artificial conditions might not reflect their behaviour in their natural environment [reviewed in 163, 219]. To understand their natural origin, properties, kinetics and to identify target cells in complex and dynamic *in vivo* settings, the investigation of naturally produced EVs *in vivo* is necessary. However, currently, *in vivo* studies on the role of endogenous EVs are hindered by the lack of suitable molecular detection methods.

3.15 Detection of PS^+EV and apoptotic cells by MFG-E8

To analyse PS^+ EVs and apoptotic cells, fluorescently labelled PS-binding Annexin V has been commonly used [220]. Unfortunately, for its optimal binding to PS, Annexin V requires high Ca^{2+} concentrations (>2 mM) [221], which preventing its *in vivo* application. Furthermore, Ca^{2+} was shown to form calcium-phosphate microprecipitates in the commonly used phosphate-

buffered saline (PBS) buffer, which strongly resemble EVs and might, therefore, lead to false-positive results upon analysis [222].

Another protein that binds PS is MFG-E8, a 53-66 kDa secreted glycoprotein initially discovered as a crucial component of milk fat globules. MFG-E8 has been shown to contribute to various physiological and pathological processes such as angiogenesis, arteriosclerosis, coagulation, and phagocytosis [reviewed in 223]. MFG-E8 plays an essential role in the recognition and clearance of dying cells [224]. In mice, MFG-E8-deficiency resulted in the accumulation of apoptotic material in the germinal centres (GCs), resulting in the development of systemic lupus erythematosus (SLE)-type autoimmune diseases [224]. MFG-E8 carries two epidermal growth factor (EGF) domains at its N-terminus and two factor VIII-homologous domains (C1 and C2) at its C terminus [225]. Furthermore, the N-terminus contains a signal peptide sequence, which directs MFG-E8 secretion into the extracellular space. Murine MFG-E8 comes in two different isoforms that are generated by alternative splicing [226]. The long splicing form contains proline/threonine-rich repeats (P/T) between the second EGF domain and the C1 domain and is primarily secreted by mammary epithelial cells [227], while these repeats are absent in the short isoform. The smaller isoform can be expressed in various cell types and tissues, including bone marrow-derived immature DCs [228], thioglycolate-activated peritoneal macrophages [229] and follicular DCs in GCs [224, 230]. The second EGF domain harbours a highly conserved arginine-glycine-aspartate (RGD) motif, which allows the binding of MFG-E8 to the integrins $\alpha_v\beta_3/\alpha_v\beta_5$ on phagocytes [229]. The C-terminal factor VIII-homologous domains mediate the recognition and binding of MFG-E8 to PS, e.g., on the surface of apoptotic cells. Therefore, MFG-E8 connects PS^+ apoptotic cells and integrin-expressing phagocytes, thereby promoting dead cells uptake [229, 231].

FITC-labelled MFG-E8 detects apoptotic cancer cell lines in a Ca^{2+}-independent manner *in vitro* [232, 233]. Interestingly, MFG-E8 has been shown to bind more effectively and sensitively to PS on early apoptotic cells than Annexin V [232-234]. Furthermore, radionuclide-labelled MFG-E8, which could be traced after i.v. injection has been suggested as a potential tool to detect apoptotic cells *in vivo* [235].

In addition to apoptotic cells, MFG-E8 has been shown to bind to highly curved PS^+ membranes and vesicles with high sensitivity [236, 237]. Consequently, FITC-labelled MFG-E8 has been successfully applied *in vitro* to detect different vesicle populations by flow cytometric analysis [238]. Takahashi et al. designed a fusion protein consisting of *Gaussia luciferase*, the N-terminal secretion signal, and the C1C2 domains of MFG-E8 (gLuc-LA) to monitor EVs *in vivo* [215].

Murine melanoma cells were transfected with gLuc-LA-expressing vectors, and secreted EVs were purified. Following i.v. injection, labelled EVs could be visualised *in vivo*, and their spatio-temporal tissue distribution could be determined [214, 215]. Together, these experiments suggest that labelled MFG-E8 can be suitable for detecting both PS^+ apoptotic cells and EVs *in vivo*.

To analyse endogenously produced EVs and circumvent the problem of detecting apoptotic cells or EVs generated during organ preparation, a PS-binding enhanced green fluorescent (eGFP)-tagged MFG-E8 version (MFG-E8-eGFP) was developed and successfully applied in mice in the present study. MFG-E8-eGFP injection allowed a reliable analysis and quantification of PS^+ EV and dead cells *in vivo* [239].

4 Aims of the thesis

The externalisation of PS on the outer leaflet of the plasma membrane is a common characteristic of apoptotic cell death, but also EVs expose PS on their surface. EVs have been described to mediate intercellular communication and participate in regulating $CD8^+$ T cell responses during infection and cancer. However, the analysis of apoptotic $CD8^+$ T cells and the function of naturally occurring EV-$CD8^+$ T cell interactions in complex *in vivo* settings remain elusive due to insufficient research.

This study aimed to investigate and visualise apoptotic and PS^+EV-bound $CD8^+$ T cells during LCMV infection *in vivo*. To detect and discriminate the two PS^+ populations, we used the PS-binding fusion protein MFG-E8-eGFP and imaging flow cytometry followed by a deep learning algorithm. By applying this approach, we aimed to get new insight into the origin, target cells and function of unmanipulated, endogenous EVs *in vivo*. With this study, we want to expand our knowledge about the contribution of apoptotic cells and EV-T cell interactions to the regulation of anti-viral $CD8^+$ T cell responses.

5 Material and methods

5.1 Materials

Materials are listed in alphabetical order.

5.1.1 Staining reagents

Table 1: Murine antibodies used for flow cytometry.

Reactivity/staining reagent	conjugate	clone	vendor	cat-#
Bcl-2	PE	BCL/10C4	BioLegend	633508
CD11c	PE/Cy7	N418	BioLegend	117318
CD127	PE	SB/199	BioLegend	121112
CD16/32 (Fc block)		93	BioLegend	101320
CD19	APC/eFluor780	eBio1D3	eBioscience	47-0193-82
CD19	PE/Cy7	6D5	BioLegend	115520
CD19	APC	1D3	BioLegend	152410
CD21/35	APC/Cy7	7E9	BioLegend	123418
CD23	PE/Cy7	B3B4	BioLegend	101614
CD28		37.51	BioXCell	BE0015-1
CD3		145-2C11	BioXcell	BE0001-1
CD31	AF647	MEC13.3	BioLegend	102516
CD4	APC	RM4-5	BioLegend	100516
CD44	APC/Cy7	IM7	BioLegend	103028
CD44	Pacific Blue	IM7	BioLegend	103028
CD44	APC/Fire750	IM7	BioLegend	103062
CD45	AF647	30-F11	BioLegend	103124
CD45.1	BV421	A20	BioLegend	10731
CD54	AF647	YN1/1.74	BioLegend	116114
CD62L	PE	MEL-14	eBioscience	12-0621-82
CD63	APC	NVG-2	BioLegend	143905
CD86	PE	GL1	eBioscience	12-0862-82
CD8a	PE/Cy7	53-6.7	BioLegend	100722
CD9	APC	eBioKMC8	eBioscience	17-0091-82
CD90.1	APC/Fire750	OX-7	BioLegend	202543
GFP	FITC	polyclonal	Acam	ab6662
KLRG1	PE/Cy7	2F1	eBioscience	25-5893-82

The table continues on the next page

Reactivity/staining reagent	conjugate	clone	supplier	cat-#
LCMV nucleoprotein		VL-4	BioXCell	BE0106
MHC-II (I-A/I-E)	PE/Cy7	M5/114.15.2	eBioscience	25-5321-82
NFATc1	PE	7A6	BioLegend	2649605
T-bet	PE	4B10	BioLegend	644810
TCRβ	APC/Cy7	H57-597	BioLegend	109219

Table 2: Human antibodies used for flow cytometry.

Reactivity/staining reagent	conjugate	clone	vendor	cat-#
CCR7	PE	G043H7	BioLegend	353204
CD3	PE/Cy7	UCHT1	eBioscience	25-0038-42
CD14	APC/Fire750	M5E2	Biolegend	301854
CD16	APC/Fire750	B73.1	Biolegend	360726
CD19	APC/Fire750	HIB19	Biolegend	302258
CD38	PE	HIT2	Biolegend	303506
CD4	PacificBlue	RPA-T4	BioLegend	300521
CD45RA	APCCy7	IV N906	BioLegend	304128
CD56	APC/Fire750	5.1H11	BioLegend	362554
CD8	AF647	SK1	BioLegend	344726
CD8a	BV421	RPA-T8	BioLegend	301008
HLA-DR	PE/Cy7	L243	eBioscience	25-9952-42

Table 3: Secondary antibody.

Reactivity/staining reagent	conjugate	supplier	cat-#	Local supplier
Goat anti-rabbit IgG (H+L)	Horseradish Peroxidase	Jackson ImmunoResearch	112-035-003	West, Grove, Pennsylvania

Table 4: Other reagents

Reactivity/staining reagent	conjugate	supplier	cat-#	Local supplier
DRAQ5		BioLegend	424101	San Diego, Kalifornia, US
FcR Blocking Reagent, human		Miltenyi Biotec	30-059-901	Bergisch Gladbach, Germany
Fixable Viability Dye	eFluor780	Thermo Scientific	#65-0865-18	Waltham, Massachusetts, US
LIVE/DEAD fixable violet dead cell stain kit	451 nm	Thermo Fisher	#L34955	Waltham, Massachusetts, US
MFG-E8-eGFP	eGFP	Home made		

The table continues on the next page

Reactivity/staining reagent	conjugate	supplier	cat-#	Local supplier
MHC tetramer H-2 D^b LCMV gp33-41	APC	NIH Tetramer core Facility		Atlanta, Georgia, US
Tetramer H-2 K^b LCMV gp34-43	APC	NIH Tetramer core Facility		Atlanta, Georgia, US

5.1.2 Chemicals and Consumables

Table 5: Chemicals and consumables used in this study.

Chemicals were purchased from Merck (Darmstadt, Germany), Roth (Karlsruhe, Germany) or Sigma-Aldrich (St. Louis, Missouri, US), if not stated otherwise.

Reagent	supplier	cat-#	Local supplier
10 µl graduated filter Tip (sterile)	Starlab	S1121-3810	Hamburg, Germany
10 µl graduated Tip	Starlab	S1111-3700	Hamburg, Germany
100 bp DNA ladder	New England BioLabs	N3231S	Ipswich, Massachusetts, US
100 x 20 mm CytoOne Dish, TC-treated	Starlab	CC7682-3394	Hamburg, Germany
1000 µl blue graduated Tip	Starlab	S1111-6701	Hamburg, Germany
1000 µl filter Tip (sterile)	Starlab	S1126-7810	Hamburg, Germany
14 mL round bottom polypropylene test tube	Corning Incorporated	352059	Corning, New York, US
15 mL tube PP 17/120 mm, conical bottom	Greiner bio-one	188271	Kremsmünster, Austria
2-Mercatpoethanol (50 mM)	Gibco	2198023	Carlsbad, Kalifornien, US
20 µl bevelled filter Tip (sterile)	Starlab	S1120-1810	Hamburg, Germany
200 µl graduated filter Tip (sterile)	Starlab	S1120-8810	Hamburg, Germany
200 µl yellow bevelled Tip	Starlab	S1111-1706	Hamburg, Germany
24-well clear flat bottom TC-treated multiwell cell culture plate	BD Biosciences	351147	Franklin Lakes, New Jersey, US
35 x 10 mm CytoOne dish, TC-treated	Starlab	CC7682-3340	Hamburg, Germany
50 mL reagent reservoir,	Kisker	713159	Steinfurt, Germany
50 mL tube PP 30/115 mm, conical bottom	Greiner bio-one	227261	Kremsmünster, Austria
Anti-FLAG M2 Affinity Gel	Sigma Aldrich	A4596	St. Louis, Missouri, US
$CD8a^+$ T cell isolation kit, mouse	Miltenyi Biotec	130-104-075	Bergisch Gladbach, Germany
Color coding cap insert for micrewtube tubes (green/red)	Roth	CK76.1/CK74.1	Karlruhe, Germany
Corning Erlenmeyer baffled cell culture flasks 1000 mL	Sigma-Aldrich	CLS431403	New York, US
Corning Erlenmeyer baffled cell culture flasks 250 mL	Sigma-Aldrich	CLS431407	St. Louis, Missouri, US
Corning Erlenmeyer baffled cell culture flasks 500 mL	Sigma-Aldrich	CLS431401	New York, US
Cryotube vial 1.0 mL	Thermo Scientific	375299	Waltham, Massachusetts, US
Disposable Glass Pasteur Pipette	VWR	612-1701	Radnor, Pennsylvania, US

The table continues on the next page

Reagent	supplier	cat-#	Local supplier
Dulbecco's modified Eagle's Media 2x	Merck	SLM-202-B	Darmstadt, Germany
Dulbecco's Phosphate Buffered Saline (500 mL)	Sigma-Aldrich	D8537	St. Louis, Missouri, US
EDTA disodium salt solution (100 mL)	Sigma-Aldrich	E7889	St. Louis, Missouri, US
Eppendorf tubes 5.0 mL	Eppendorf	0030119401	Hamburg, Germany
Ex-Cell 293 Serum-free medium for HEK 293 cells (1000 mL)	Sigma-Aldrich	14571C	St. Louis, Missouri, US
Falcon 5 mL round bottom polystyrene test tube	Corning	352008	Corning, New York, US
FBS	PanBiotech	P30-3306	Aidenbach, Germany
Flag-peptide	GenScript	RP10586	Piscataway Township, New Jersey, US
Foxp3 staining kit	ThermoFisher Scientific	00-5523-00	Waltham, Massachusetts, US
Gibco DMEM (1x) + GlutaMAX (500 mL)	Thermo Scientific	61965-026	Waltham, Massachusetts, US
Gibco L-Glutamine 200 mM	Thermo Scientific	25030-024	Waltham, Massachusetts, US
Gibco Pen Strep	Thermo Scientific	15140-122	Waltham, Massachusetts, US
Heparin Natrium	Ratiopharm GmbH		Ulm, Germany
HEPES solution 1 M, pH 7.0-7.6, sterile filtered (100 mL)	Sigma-Aldrich	H0887	St. Louis, Missouri, US
Injection syringe	Omnican-F	9161502	Melsungen, Germany
Intracellular Fixation & Permabilization Buffer set	ThermoFisher Scientific	88-8824-00	Waltham, Massachusetts, US
LS Columns	Miltenyi Biotec	130-042-401	Bergisch Gladbach, Germany
Lymphoprep™	AXIS-SHIELD	1114545	Oslo, Norway
Lysis Buffer	BD Biosciences	555899	Franklin Lakes, New Jersey, US
MACS Smart Strainer	Miltenyi Biotec	130-098-463	Bergisch Gladbach
MEM Eagle	PAN Biotech	P04-10500	Aidenbach, Germany
Microtest plate 96 well, round base	Starstedt	82.1582	Nürnbrecht, Germany
MyTaq DNA Polymerase + reaction buffer	Bioline	BIO-21106	Cincinnati, Ohio, US
Nitrile gloves	Starlab	SG-C	Hamburg, Germany
Nunc 96-well U bottom	ThermoFisher Scientific	163320	Waltham, Massachusetts, US
Pancoll, density: 1.0077 g/mL	PAN Biotech	P04-601000	Aidenbach, Germany
Parafilm	Bemis Company, Inc.	PM992	Neenah, Wisconsin, US
Pasteur-plastic pipets, 3.0 mL Macro	Ratiolab	2600111	Dreieich, Germany
PCR plastics single tubes with flat caps	Nippon Genetics, Europe GmbH	FG-021F	Dueren, Germany
PCR strip tubes with attached strip caps	VWR International	732-0546	Radnor, Pennsylvania, US
Pipette 10 mL, plastic	Greiner Bio-One	607160	Kremsmünster, Austria
Pipette 25 mL, plastic	Greiner Bio-One	760160	Kremsmünster, Austria

The table continues on the next page

Reagent	supplier	cat-#	Local supplier
Pipette 50 mL, plastic	Greiner Bio-One	768180	Kremsmünster, Austria
Polyamid mesh 40 µm	Klein & Wieler oHG	9068283	Königswinter, Germany
Polypropylene Bottle with screw-on cap, 250 mL	Beckman Coulter	356011	Brea, Kalifornien, US
Proteinase K 100 mg	Sigma-Aldrich	P2308	St. Louis, Missouri, US
QuadoMACS Separator	Miltenyi Biotec	130-091-051	Bergisch Gladbach, Germany
RPMI 1640 Medium GlutaMAX Suppplement	Gibco	61870-010	Carlsbad, Kalifornien, US
S-Pak-Filter 0,22 µm	Merck	RAWG047S6	Darmstadt, Germany
S-Pak-Filter 1,2 µm	Merck	RAWG047S6	Darmstadt, Germany
Safe-Lock tubes 2.0 mL	Eppendorf	0030120.094	Hamburg, Germany
SafeSeal reaction tube, 1.5 mL	Sarstedt	72.706	Nürnbrecht, Germany
Screw vials free-standing 1,5 mL	Roth	CK48.1	Karlruhe, Germany
Superdex^{TM} 200 Increase 5/150 GL	GE Lifersicences	289990945	Chicaco, Illinois, US
Vivaspin Turbo 15, 30000 MWCO PES	Sartoius	VS15T22	Göttingen, Germany

5.1.3 Devices

Table 6: Devices used in this study.

Device	Supplier	Local supplier
ÄKTA prime	GE Lifesciences	Chicago, Illinois, US
Analytic scale	Adventurer, Ohaus Corp.	New Jersey, US
BD FACSAriaFusion	BD Biosciences	New Jersey, US
CASY TT Cell Counter	OLS OMNI Life Science GmbH & Co KG	Bremen, Germany
Centrifuge 5415D	Eppendorf	Hamburg, Germany
Chemical scale	Kern	Albstadt, Germany
FacsCanto II Flow Cytometer	BD Biosciences	Franklin Lakes, New Jersey, US
Finnpipette Multipette	Thermo Scientific	Waltham, Massachusetts, US
Gel Doc XR+ Molecular Imager	Bio-Rad	Hercules, California, US
Heraeus Multifuge X3R	Thermo Scientific	Waltham, Massachusetts, US
HiLoad 26/600 Superdex 200 pg	GE Lifesciences	Chicago, Illinois, US
ImageStream MarkII	Luminex	Austin, Texas, US
Incubator CO_2 Galaxy 170R	Eppendorf New Brunswick	Hamburg, Germany
Incubator CO_2 Galaxy 170S	Eppendorf New Brunswick	Hamburg, Germany
Labfors 5 Bioreactor	Infors HT	Basel, Switzerland
Magnetic stirrer	Ika Labortechnik	Staufen, Germany
Mikro 220R cooling centrifuge	Hettich	Tuttlingen, Germany
Multifuge X3R	Thermo Scientific	Massachusetts, US
pH meter	Inolab	Weilheim, Germany
Safety cabinet FlowSafe B-[MaxPro]3-160	Berner International GmbH	Elmshorn, Germany

This table continues on the next page

Device	Supplier	Local supplier
Mikro 220R cooling centrifuge	Hettich	Tuttlingen, Germany
Multifuge X3R	Thermo Scientific	Massachusetts, US
pH meter	Inolab	Weilheim, Germany
Safety cabinet FlowSafe B-[MaxPro]3-160	Berner International GmbH	Elmshorn, Germany
Single channel pipettes, variable volume	Axygen Biosciences	Union City, New Jersey, USA
Sorval RC6, Avanti JXN-26	Beckman Coulter	Brea, California, US
Superdex 200 Increase 10/300 GL	GE Lifesciences	Chicago, Illinois, US
Table centrifuge	Eppendorf	Hamburg, Germany
Thermocycler PCR-machine	Biometra	Goettingen, Germany
Vortex-Genie 2	Scientific Industries	Bohemia, New York, US
Water bath	Grant Instruments Ltd.	Barrington Cambridge, UK

5.1.4 Media and Buffers

Table 7: Cell culture media and buffers used in this study.

All buffers and solutions were prepared using double destilled water (ddH_2O)

Media and buffers	Supplementing reagents
1 x PBS	150 mM NaCl
	10 mM Na_2HPO_4
	2 mM KH_2PO_4
	pH 7.4 adjusted with NaOH
FACS buffer	PBS
	2 % (v/v) FCS
MACS buffer	PBS
	2 % (v/v) FCS
	2 mM EDTA
10 x Gitocher buffer	670 mM Tris, pH 8.8
	166 mM ammnonium sulfate
	65 mM $MgCl_2$
	0.1 % Gelatin (w/v)
50 x TAE buffer	242 g Tris
	57.1 mL 100% acetic acid
	100 mL 0,5 EDTA (pH 8.0), H_2O at 1 L
T cell-medium	RPMI 1640
	10 % (v/v) FCS
	1% (v/v) Penicillin
	1% (v/v) Streptomycin
	5 µM 2-mercaptoethanol

This table continues on the next page

Media and buffers	Supplementing reagents
1x Gitocher buffer	5 µL 10x Gitocher buffer 2.5 µL 10% (v/v) Triton X-100 0.5 µl 2-mercaptoethanol 3 µL Proteinase K (10 mg/mL) 39 µL H_2O
Arg-Glu-Buffer	25 mM HEPES 200 mM L-ariginin 200 mM L-glutamic acid 150 mM NaCl 2% (v/v) Glycerol
OPD substrate	12.5 mL 0.2 M Na_2HPO_4 (Fluka 71645) 12.5 mL 0.1 M Citric acid (Fluka 27488) 25 mL ddH_2O 1 tablet DOP Ortho-Phenylendiamin 50 µL 30 % H_2O_2
4 % Paraformaldehyde solution	4 g EM grade paraformaldehyde 50 mL ddH_2O 1 mL NaOH 10 mL 10 x PBS H_2O at 100 mL

5.2 Mouse strains and human samples

5.2.1 Mouse strains

Wildtype mice or genetically modified mouse strains were either purchased from Javier or bred and kept at the Core facility Animal Models, Biomedizinisches Centrum, Ludwig-Maximilians-Universität München (LMU) according to federal guidelines. Animal experiments were approved by the Ethics Committee of LMU Munich, Germany.

P14/CD90.1 (Tg (TcrLCMV)327Sdz) mice

The P14 mice carry a transgenic TCR that is specific for a peptide (P14) from LCMV presented by the MHC class I molecule H2-D^b [77]. The transgenic TCR consists of the Vβ 8.1 and Vα2 segments and T cells can be analysed by FACS analysis using mAbs directed against these two segments.

OT-I/CD45.1 (Tg (TcraTcrb)1100Mjb) mice

This mouse strain carries a transgenic TCR (Vα2, Vβ5) recognizing the ovalbumin peptide SIINFEKL ($OVA_{257-264}$) that is presented in the context of H-$2K^b$ [240]. Transgenic mice are tested by FACS analysis by mAbs directed against Vα2 and Vβ5 segments.

Nur77 mice (C57BL/6-Tg (Nr4a1-EGFP/cre)820Khog/J)

These mice express an eGFP Cre recombinase fusion protein (eGFP-Cre) under control of the *Nr4a1* (Nur77) promoter within the BAC (bacterial artificial chromosome) transgene [241]. GFP expression is induced upon Ag receptor signalling in B and T cells and displays similar expression patterns as endogenous Nur77.

5.2.2 Human Studies

Yellow fever vaccination study was planned and conducted by Prof. Dr. Anne Krug and Prof. Dr. Rothenfusser and the selection of volunteers were approved by the ethics committee of the LMU Munich. Informed consent was obtained from all donors (age 22-35, non-smokers) without previous YF-17D vaccination. Donors were immunised with a single dose of YFV-17D-204 live-attenuated yellow fever vaccine strain (0.5 mL of Stamaril, Sanofi) subcutaneously. The immunisation of volunteers with Influvac (Mylan Health Care GmbH, Bad Homburg, Germany) or Vaxigrip (Sanofi, Paris, France) was performed by Prof. Dr. Anne Krug and PBMCs were kindly provided by Dr. Katharina Eisenächer.

5.3 Biochemical methods

5.3.1 Production of murine MFG-E8-eGFP from stably transfected HEK cells

Murine MFG-E8-eGFP (mMFG-E8-eGFP) and MFG-E8-mCherry were produced by HEK293 cells stably transfected cells (UniProtKB - P21956 (MFGM_MOUSE). Cells were adapted to medium without serum (Ex-Cell 293) supplemented with 1 % penicillin/streptomycin and 2 mM HEPES pH 7.0-7.6 and kept shaking in bottles at growing conditions. 2x 150 mL of shaking cell culture at a density of 1.5-2.5 x 10^6 cells/mL with a viability > 85% were used for inculation of the Labfors Bioreactor (Infors, Switzerland) and 1.5 L of medium without serum was added. Cells were grown for 5 days under growing conditions (pH 7.5, pO2 98 %, pCO2 5 %).

5.3.2 Purification of mMFG-E8-eGFP/mCherry

For protein harvesting, cells were centrifuged at 300 g for 10 min at 4 °C. To solubilise membrane and vesicles the supernatant was incubated 1 h at 4 °C in Arginine-Glutamate (Arg-Glu) buffer containing 0.1 % Triton-X100 under agitation on a magnetic stirrer. To remove debris the solution was spun (for 60 min at 40 000 g at 4 °C using an Avanti JXN-26 high speed centrifuge followed by filtration through 1.2 µm and then 0.22 µm membrane filters. As both, MFG-E8-eGFP/mCherry contain a C-terminal FLAG-tag, the purification of the proteins was

achieved by affinity chromatography using anti-FLAG M2-FLAG agarose beads. FLAG-columns were washed with PBS before usage and connected to an Äkta prime instrument and the filtered cell supernatant was loaded. The next day, the anti-FLAG-column was washed with 100 mL of Arg-Glu buffer and the column was removed from the Äkta. 5 mg of FLAG-peptide (GenScript) was dissolved in 30 mL of Arg-Glu buffer and mixed with the resin for 1 h at 4 °C while rotating to elute bound protein with an excess of FLAG-peptide. After incubation the resin was washed with Arg-Glu buffer and the eluted protein was concentrated using Vivapin columns (see Table 5) at 4200 rpm (Multifuge X3R, Thermo Scientific). Before protein was loaded the spinning, columns were pre-rinsed with 5 mL deionised water followed by 5 mL Arg-Glu buffer. After concentration, the protein was pooled and centrifuged on table centrifuge (Eppendorf) at max speed for 30 min at 4 °C to get rid of protein aggregates. The supernatant was transferred to a new 5 mL Eppendorf tube and the volume was determined. Protein concentration was determined by spectrometer at a wavelength of 488 nm for MFG-E8-eGFP (ε of GFP: 55000 M^{-1} cm^{-1}, MW: 81100 g/mol) and 587 nm for MFG-E8-mCherry (ε of mCherry: 7200 M^{-1} cm^{-1}, MW: 80619 g/mol).

Protein was aliquoted into screw cap tubes (200 µL per tube) and snap freesed in liquid N_2.

For injections into mice, 100 µg of MFG-E8 in a total volume of 200 µl Arg-Glu buffer was injected i.v. per mouse.

5.3.3 Genotyping NR4 mice

For genotyping genomic DNA was isolated. For this, 2-5 mm of mouse tail tips were cut and 50 µL of Gitocher buffer (see Table 7) was added. The mixture was incubated for 6 h and the proteinase K was inactivated in the following step at 95 °C for 5 min. For PCR genotyping 1 µL of isolated DNA was used and added to PCR master mix

Table 8: Mouse genotyping

The genotype of NR4 mice was determined by PCR on genomic DNA isolated from mouse tail tips.

Isolation of genomic DNA:	1 x Gitocher buffer (see Table 7) 0.5 % Triton-X 100 1% 2-mercaptoethanol 0.4 mg/mL proteinase K H_2O add to 50 µL 6 h at 55 °C and 5 min at 95 °C
PCR genotyping:	1 µL DNA 5 µL MyTaq Red Buffer 100 pM Primer for 100 pM Primer rev 5 U/mL MayTaq Polymerase H_2O add to 25 µL
Primer sequences for the two NR4 PCRs:	
RO 445	CGGGTCAGAAAGAATGGTGT
RO 446	CAGTTTCAGTCCCCATCCTC
RO 237	AGCTGACCCTGAAGTTCATCTG
RO 238	CATGATATAGACGTTGTGGCTGTT
PCR programm:	
Step 1: 95 °C	5 min
Step 2: 95 °C	30 sec
Step 3: 55 °C	30 sec
Step 4: 72 °C	45 sec - back to step 2 (35 x)
Step 5: 72 °C	5 min
Step 6: 4 °C	∞

5.3.4 Agarose gel electrophoresis

Gel electrophoresis on an agarose gel was performed to visualise and separate DNA fragments according to their size. For the preparation of the gel 1 % (w/v) agarose was dissolved in TAE buffer. 100 bp ladder were used to estimate the size of the DNA fragments. DNA samples were visualised using ethidium bromide (0.5 g/mL) that was added before the gel was solidified. Agarose gels were analysed on a Gel Doc XR+ Molecular Imager.

5.3.5 Proteome analysis

The proteome analysis was performed in collaboration with Jingyuan Cheng and PhD Felix Meissner from the Planck Institute for Biochemistry in Munich. In brief, 2 x 10^5 cells were lysed, proteins reduced and alkylated in 100 mM Tris (pH 7.6) lysis buffer containing 1 % sodium deoxycholate (SDC), 40 mM 2-Chloroacetamide (CAA). Cells were immediately heat-treated at 95 °C for 10 min and sonicated for 12 min with a Bipruptor Plus sonication device (Diagenode)

to shear DNA. The protein amount was determined by BCA assay. The enzymatic digest was carried out overnight at 37 °C using LysC and trypsin in a 1:100 (w/w) ratio and was stopped by adding isopropanol containing trifluoroacetic acid (TFA) at a final concentration of 1 % (v/v). The digested proteins were desalted using two discs of SDB-RPS material and resuspended in 80 % acetonitrile/ 0.1% TFA (v/v). LC-MS/MS was performed on an EASY-nLC 1200 ultra-high-pressure system (Thermo Fisher Scientific) via in-house packed columns (75 µm, 30 cm length and 1.9 µm C18) in a nonlinear 180 min gradient from 2 % acetonitrile, 0.5 % formic acid to 80 % acetonitrile, 0.5 % formic acid at 250 nL/min coupled to a quadrupole Orbitrap mass spectrometer (Q Exactive HFX, Thermo Fisher Scientific) via nano-electrospray ion source. Data were acquired using Xcalibur software (Thermo Fisher Scientific). Analysis of raw data was performed using the MaxQuant software (1.6.5.0) with a 1 % FDR at the peptide and protein level. Analysis of the data was performed by Dr. Tobias Straub from using R Studio v3.6.2.

5.4 Immunological methods

5.4.1 Preparation of single cell suspension

Animals were sacrificed by CO_2 and then desinfected with 70 % ethanol. Organs were removed using scissors and fine tweezers and put into FACS buffer. Single cell suspension of splenocytes was generated by pushing organs through a 40 µm cell strainer and washed with cold FACS buffer. Lymphocytes were purified by Pancoll (PAN Biotech) gradient centrifugation. For this, cells were taken up in 3 mL of FACS buffer and 3 mL of Pancoll was slowly and carefully added at the bottom of the tube by a plastic transfer pipette. The mixture was centrifuged for 10 min at 2000 rpm at 37 °C with an acceleration of 9 and a decceleration of 5. After the spin, the white layer containing mononuclear cells were collected and washed 2x with FACS buffer. Liiving cells were counted by a CASY cell counter (OMNI Life Sciences) and used for further analysis.

5.4.2 Preparation of single cell suspension for the analysis of nuclear NFATc1 translocation

Single cell suspension was prepared as described before (see 5.4.1). Cells were taken up in 2 mL cold FACS buffer and immediately fixed by adding 2 mL of 4 % PFA. Cells were incubated for 10 min at RT before cells were washed two times with FACS buffer and cells were counted on CASY. Cells were then permeabilised and stained (see 5.4.6).

5.4.3 Purification of peripheral mononuclear blood cells from murine blood

Blood was collected immediately from euthanised mice by cardiac puncture using a 1.0 mL syringe (Omnican-F) and directly transferred to a heparin (Ratiopharm GmbH) containing Eppendorf tube. Red blood cells were lysed using ACK buffer for 5 min at RT. Then cells were washed two times with FACS buffer and used for further analysis.

5.4.4 Preparation of human blood samples

PBMCs were purified from 7 mL of EDTA or Heparin anti-coagulated blood samples by mixing with equal amount of PBS. The mixture was layered onto 14 mL of Pancoll solution (PAN Biotech) and centrifuged at RT at 2100 rpm with an acceleration of 1 and a deceleration of 0 for 20 min. The PBMCs were collected at the interface, washed 3 times with PBS and stained with indicated antibodies.

5.4.5 Magnetic cell sorting

For the isolation of cell populations magnetic cell sorting (Miltenyi Biotec) has been used. This technique has been employed to purify $CD8^+$ T cells from spleen for adoptive transfer experiments ($CD8^+$ T cell Isolation kit, negative selection). All procedures were performed according to manufacturer instructions. Briefly, for negative selection splenocytes were first incubated 5 min with a biotinylated antibody mix on ice that do not bind to $CD8^+$ T cells. Then cells were incubated 10 min with anti-biotin microbeads, that bind to labelled cells. The cell mixture was then applied to a LS column placed in a paramagnetic field. Unlabelled $CD8^+$ T cells were washed through the column by rinsing three times with MACS buffer and eluted fraction was collected. Total cell number was determined by CASY.

5.4.6 Staining of cells with fluorescent reagent for flow cytometry

5 x 10^6 cells were incubated with Fc-Block and live/dead in PBS for 10 min at 4 °C and washed two times with FACS buffer. Antibody staining of cells was performed on ice for 25 min in FACS buffer in a volume of 100 µL and washed two times (180 g, 5min, 4°C) to remove unbound antibodies before analysis on an ImageStream^x MKII imaging flow cytometer (Luminex). For the analysis of LCMV-specific $CD8^+$ T cells splenocytes were stained with MHC-I tetramers (H-$2D^b$LCMVgp_{33-41} and H-$2K^b$LCMVgp_{34-43}, kindly provided by NIH tetramer facility with a dilution

of 1:100) in a volume of 100 µL for 30 min at RT and washed two times with FACS buffer, before cells were stained with the indicated antibodies.

For intracellular stainings cells were fixed and permeabilised in 100 µL of 1 x Fixation/Permeabilisation solution (eBioscience) for 20 min on RT in the dark, after they have been stained for surface markers. Cells were then washed twice with 1 x Permeabilisation Buffer (eBioscience) and then stained with specific antibodies in 100 µL of 1x Permeabilisation buffer for 30 min at 4 °C. Afterwards cells were washed and analysed using an ImageStream^x MKII flow cytometer or FACSCanto II. Cell sorting was performed at FACSAria using a 80 µm nozzle. Data analysis was performed using FlowJo version 10 (TreeStar, Ashland, OR, USA).

For intranuclear staining cells were permeabilised using the FoxP3 Permeabilisation buffer (eBiosceince) for 30 min at 4°C before after they have been stained for surface markers (goat alpha GFP-FITC, CD8-PECy7, CD44-PB (NFATc1 staining), CD44-APCCy7 (T-bet staining) (see). Cells were then washed two times with Permeabilisation buffer and then stained for NFATc1-PE/T-bet-PE and DRAQ5 in 100 µL of 1 x Permeabilisation buffer for 30 min at 4°C. Afterwards cells were washed two times and analysed using an ImageStream^x MK II.

5.4.7 *In vitro* stimulation and adoptive transfer

For the in vitro stimulation and adpotive transfer of transgenic P14 and OT-I CD8$^+$ T cells into C57BL/6 animals, spleens from transgenic mice were taken and CD8$^+$ T cells were magnetically enriched using the CD8$^+$ T cell isolation kit (see 5.4.5). Purity of isolated T cells was determined using anti-CD8, anti-CD90.1, anti-CD45.1 and the respective Vα2 antibodies by FACS analysis. 0.1 x 10^6 TCR transgenic CD8$^+$ T cells were cultured for two days in RPMI 1640-GlutaMAX medium (Thermo Fisher Scientific) supplemented with 10 % FCS, 1 % penecillin/streptomycin and 50 µM 2-Mercatpotheanol in 96-well round-bottom plates (Starstedt) precoated with 10 µg/mL anti-CD3 (BioXCell) and anti-CD28 mAb (BioXCell). Following *in vitro* stimulation 3.0-3.5 x 10^6 OT-I and P14 CD8$^+$ T cells were transferred i.v. into syngeneic and sex-matched mice that were infected two days earlier with $LCMV_{Arm}$. Recipient mice were scarified three days after transfer. Transferred T cells could be analysed by the congenic markers CD45.1 or CD90.1.

5.4.8 Sorting of MFG-E8-eGFP$^+$ splenocytes and TEM analysis

Single cell suspensions from mice infected with LCMV and injected with MFG-E8-eGFP were prepared as described (see section 5.4.1). Cells were labelled with anti-CD45-APC and anti-GFP-FITC antibodies in FACS buffer for 25 min at 4 °C after cells were incubated with live/dead violet

in PBS for 10 min on ice. After washing with FACS buffer cells were prefixed with freshly prepared 4% EM-grade PFA (Science Services) for 30 min. A FACSAriaIII (BD Biosciences) with a 130 µm nozzle was used to sort fixed cells into PBS containing 0.5 % BSA. Cells were washed 3 x with PBS for 10 min at 400 g and 4°C. Then wells were fixed with 2.5 % glutaraldehyde (Science Services) in 0.1 M cocadylate buffer (pH 7.4) for 15 min. Cells were washed (3x) with 0.1 M sodium cacodylate buffer for 10 min at 400 g and then fixed in reduced osmium (1 % osmium tetroxide (Science Services), 0.8 % potassium ferrcyanide in 0.1 M sodium cacodylate buffer. Further sample preparation and TEM analysis was performed by Dr. Martina Schifferer from the German Center for Neurodegenerative Diseases in Munich. Briefly, cells were contrasted in 0.5 % uranyl acetate in water (Science Services), then dehydrated through an ascending ethanol series. The pellet was embedded in epon resin and dried for 48 hours at 60 °C. Ulra-thin sections (50 nm) were cut and put onto formvar-coated grids (Plano) and again contrasted using 1 % uranyl acetate in water and Ultrostain (Leica). Images were acquired on a JEM 1400plus (JEOL).

5.4.9 Virus production

For LCMV propagation baby hamster kidney-21 cells (BHK-21) cells were used. On day 0, cells were seeded at a number of 3 x 10^5 cells in a 75 cm^3 flask in DMEM supplemented with 10 % of FCS. After 48 hours of growing, culture medium was removed, and cells were infected with a MOI of 0.08 in 3 mL of DMEM 10 % FCS and incubated 90 min at 37 °C with every 20 min tilting the flask. After infection period, 22 mL of warm DMEM 10 % FCS was added and virus infected cells were incubated 48 hours. The supernatant was collected in a 50 mL tube and cells and debris were spun down at 1300 rpm 5 min 4°C. 1 mL of supernatant containing virus particles were aliquoted into 2 mL Sarsteadt tubes and frozen in liquid nitrogen for long time storage at – 80 °C.

5.4.10 Quantification of LCMV by plaque forming unit assay

For determination of LCMV titers, Vero cells growing in DMEM 10 % FCS were used and resuspended in MEM 5 % FCS to a concentration of 8 x 10^5/mL when used for plaque assay. For quantification of virus forming units, prepared virus stocks were serially diluted 1:5 in 5 % FCS containing MEM 24-well plates and 200 µL of the dilutions were transferred into a 24-well plate. Then 200 µL of cell were added and incubated 3 hours at 37 °C. Then 400 µL of 2 x DMEM methylcellulose (1:1 ratio) were added without disturbing the attached cells. After 60 hours of

incubation at 37 °C, cells have formed a confluent monolayer. The supernatant was aspirated and 4 % of PFA was added for exactly 30 min at RT. The fixative was taken off and 200 µL of Triton-X in PBS (0.1 %) were added and incubated for 20 min at RT. The solution was discarded and 200 µL of PBS 5 % FCS were added for 20 min at RT to block non-specific binding. PBS was aspirated and 200 µL of 2.5 % FCS PBS containing VLA-4 antibody (1:100 BioXcell 1.8 mg/mL) was added and incubated 60 min at RT. The cells were washed 2x with PBS and the secondary peroxidase coupled goat anti-rat IgG HRP was added (1:100, Jackson ImmunoResearch Laboratories, Inc) and incubated for 60 min at RT. Cells were again washed 2 x with PBS and 400 µL of OPD substrate were added and incubated 15 min until a good colour is produced. Then the cells were washed again 2 x with 400 µL of PBS and plaques were counted to calculate PFU using the following formula:

$$\frac{\text{Average \# Plaques}}{D \times V} = \text{PFU/ml}$$

D = Dilution factor
V = Volume of diluted virus added

Formula from [242]

For infections, 2 x 10^5 PFU in PBS were injected intraperitonially (i.p) per mouse.

5.5 Data analysis

5.5.1 Analysis of apoptotic and EV$^+$ cells using the CAE-RF and IDEAS

The IDEAS software (Version 6.2, Luminex) was used to gate MFGe8-eGFP positive cells. TIF-Images (16-bit, raw) of MFGe8$^+$ cells were exported and apoptotic and EV$^+$ cells were identified by the CAE-RF using a graphical user interface as described before [239]. Three FCS files (encompassing EV-decorated, apoptotic or all cells) were created and analysed using FlowJo Version 10.

5.5.2 Co-localisation analysis

Nuclear localization of NFATc1 or T-bet was analysed using the 'similarity' feature on the IDEAS software. The similarity between the pixel intensities of the nuclear DRAQ5 and the NFATc1/T-bet fluorescence images of each individual cell was determined and enumerated as the similarity score (SS), which determines the correlation of pixel intensities between NFATc1/T-bet and DRAQ5 images. Peak masks for for MFG-E8-eGFP and the respective marker were created to assess the degree of co-localisation between MFG-E8$^+$ EVs and CD9/CD63, MHC-II,

CD86, CD54 and CD31 Both masks were combined, and co-localisation assessed using the BDS R3 feature of the IDEAS software.

5.5.3 Statistics

For statistical analysis the PRISM software (GraphPad software, La Jolla, CA, USA) was used. Significance was analysed using students t-test or one-way ANOVA-test, with *: $P< 0.05$**: $P < 0.01$ and ***: $P < 0.001$. Bar graphs show average ± standard deviation (SD).

6 Results

6.1 MFG-E8-eGFP detects apoptotic and PS$^+$EV-decorated cells *in vivo*

MFG-E8-eGFP stains apoptotic cells *in vivo* in irradiated mice [239]. We, therefore, aimed first to visualise and analyse cells that undergo apoptosis during viral infection by MFG-E8-eGFP *in vivo* application. For this, we used the acute LCMV$_{Arm}$ infection model as cell death is induced during the early phase of the infection [74, 106, 243]. Mice were infected with LCMV$_{Arm}$, MFG-E8-eGFP was injected i.v. on day 5 p.i., and splenocytes were analysed by imaging flow cytometry (IFC) (Fig. 4A).

In LCMV-infected mice, the frequency and the total number of MFG-E8-eGFP positive (MFG-E8$^+$) cells significantly increased compared to non-infected control mice (Fig. 4B, C). Importantly, no MFG-E8$^+$ cells were detected in non-injected mice, demonstrating the specificity of MFG-E8-eGFP *in vivo* staining. MFG-E8-eGFP negative (MFG-E8$^-$) cells showed a round morphology with an intact plasma membrane characteristic for living cells (Fig. 4D, left). In contrast, cells positively stained with MFG-E8-eGFP were heterogeneous, exhibiting two different staining patterns (Fig. 4D, right). *Bonafide* apoptotic cells displayed a bright plasma membrane staining with intensively stained apoptotic blebs. However, the second type of MFG-E8$^+$ cells we detected showed a more punctate MFG-E8-eGFP staining with one or a small number of intensely stained spots, whereas the rest of the cell body remained unstained. These MFG-E8$^+$ structures were of subcellular size, and therefore we assumed them to be PS$^+$ EVs attached to living cells.

To test this hypothesis, we sorted MFG-E8$^+$CD45$^+$ leukocytes from the spleen of LCMV-infected mice for transmission electron microscopy (TEM). Cells had a purity of around 90 % after sorting (Fig. 5A). We found vesicles attached to the surface of the sorted leukocytes (Fig. 5B). These particles were highly heterogeneous in size with about 30-200 nm in diameter, as typical for EVs [244]. Taken together, MFG-E8-eGFP injection enables the detection and analysis of both apoptotic and live PS$^+$EV-bound cells *in vivo* in LCMV$_{Arm}$-infected mice.

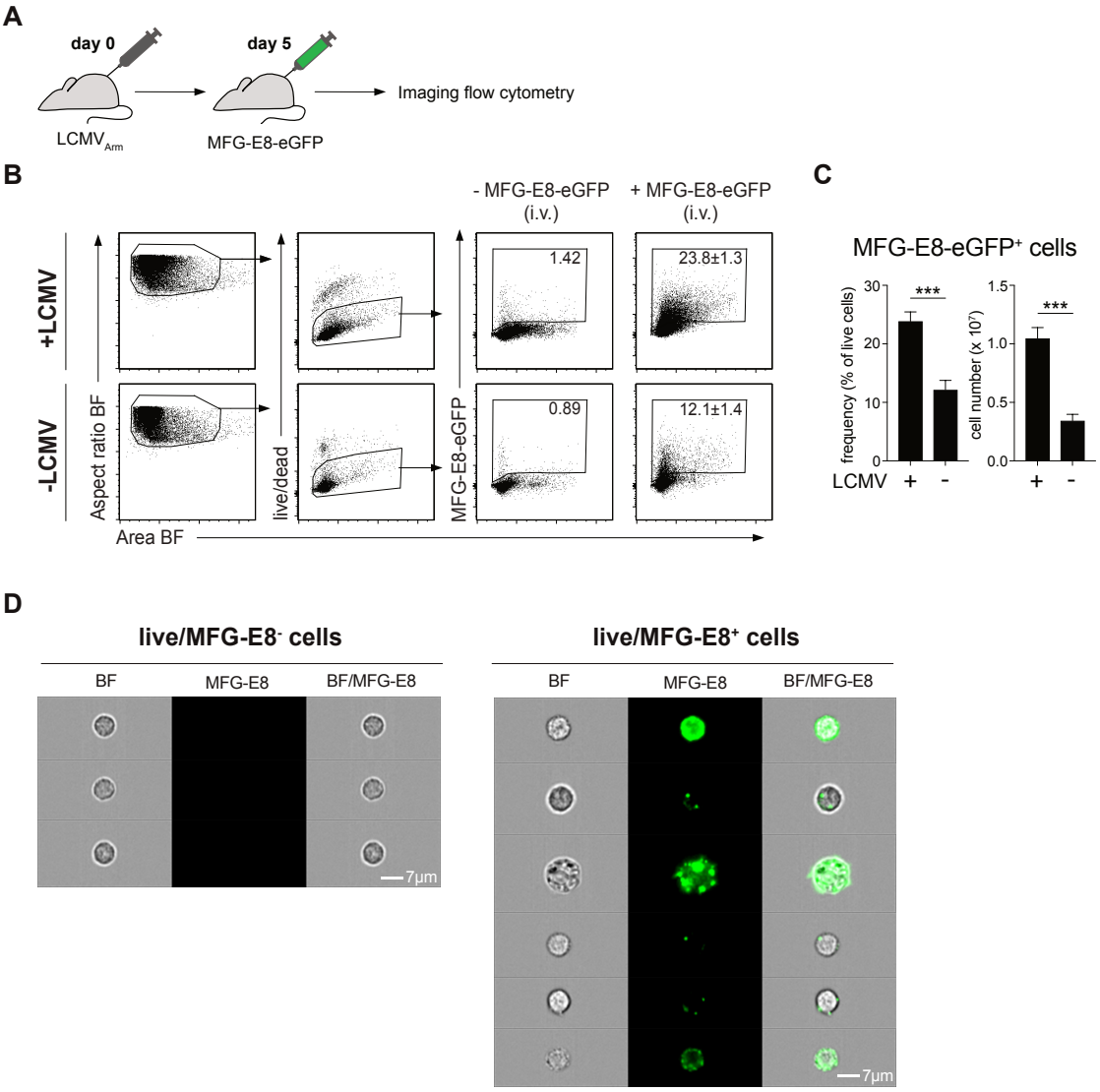

Figure 4: MFG-E8-eGFP detects apoptotic and EV-decorated cells *in vivo*.
(A) Illustration of the experimental setup. $LCMV_{Arm}$- and non-infected mice were injected i.v. with of MFG-E8-eGFP (100 µg/mouse) on day 5 post-infection to analyse PS^+ cells. After 1 h, the spleens were harvested, and splenocytes were analysed by IFC. (B) Dot plots display the gating strategy of live/dead$^-$MFG-E8-eGFP$^+$ cells from the spleens of non-infected and $LCMV_{Arm}$-infected mice. The area and aspect ratio of the bright field (BF) channel were used to identify single cells. Numbers in the gate indicate the mean percentages ± SD of MFG-E8$^+$ cells from $LCMV_{Arm}$-infected or non-infected, MFG-E8-eGFP-injected mice (n=3) and non-injected mice (n=1). (C) Bar graphs display the frequency (left) and total number (right) ± SD of MFG-E8-eGFP$^+$ cells in $LCMV_{Arm}$- and non-infected mice (n=3). (D) Representative images of BF, MFG-E8, and BF/MFG-E8 overlay channels of MFG-E8$^-$ and MFG-E8$^+$ cells are shown. Scale bar: 7 µm. Shown are representative results from 2 independent experiments. The unpaired Student's t-test was used to determine statistical significance, with *: $p< 0.05$, **: $p< 0.01$ and ***: $p< 0.001$. Figure shows data from [239] Figure 5. Figure 4C modified from [239] Figure 5.

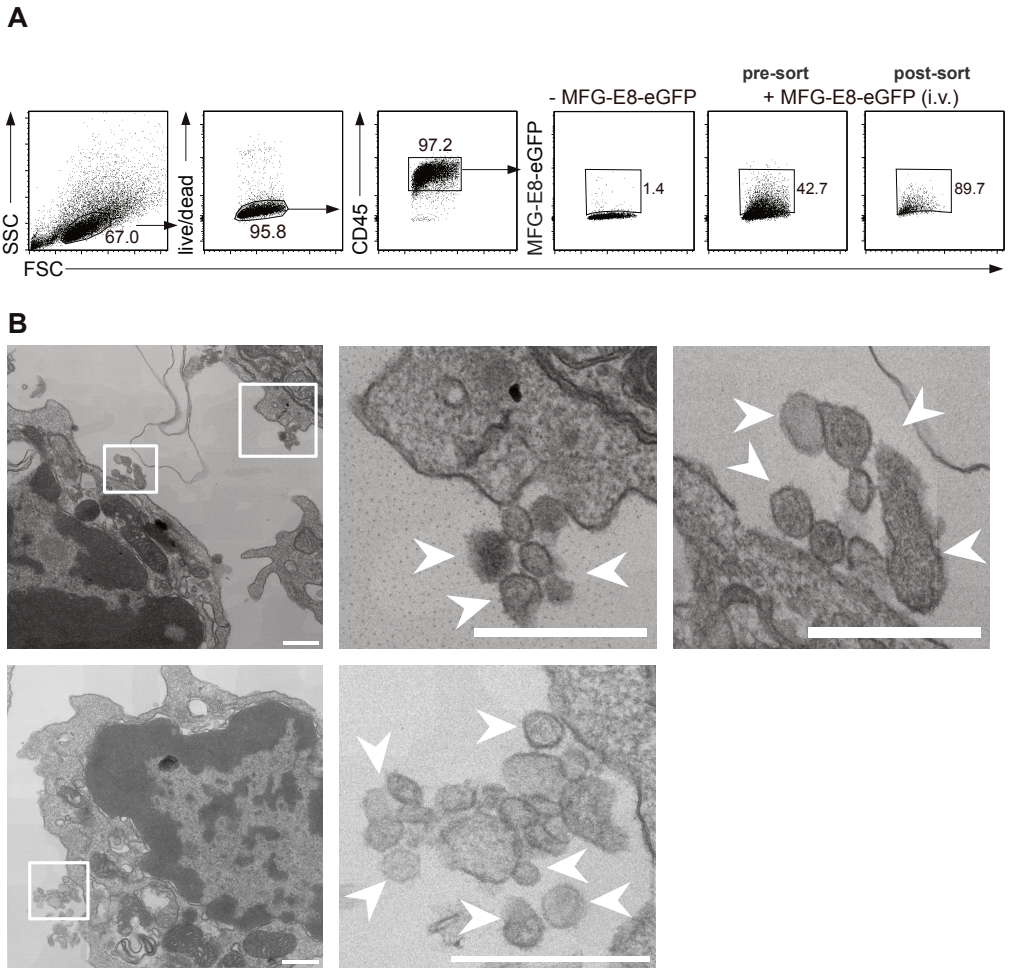

Figure 5: Transmission electron microscopy reveals the binding of EVs to leukocytes.
Mice were infected with $LCMV_{Arm}$, and MFG-E8-eGFP (100 μg/mouse) was injected on day 5 post-infection. Positive cells were FACS sorted on AriaFusion (BD) and visualised by TEM. (A) Sorting strategy of live/dead$^-$ CD45$^+$ MFG-E8$^+$ leukocytes from the spleen of LCMV-infected mice. Numbers next to the gate indicate the percentage of the respective population. (B) Representative images of sorted MFG-E8$^+$ leukocytes with EVs attached to their surface (indicated by white arrows). Scale bars: 500 nm. TEM analysis was performed by Dr. Martina Schifferer at the German Centre for Neurodegenerative Diseases in Munich. Figure 5 A from [239] Supplemental Figure 2 and B modified from [239] Figure 1.

6.2 EV-decoration of splenocytes is strongly induced upon LCMV infection

We next aimed to quantify apoptotic and EV-decorated (EV$^+$) cells in mice acutely infected with LCMV. Although IFC allowed the identification of apoptotic and EV$^+$ cells by visual inspection, we could not determine a distinguishing feature enabling their clear separation by flow cytometry. Therefore, we used a deep learning approach based on a convolutional autoencoder followed by a random forest classifier (CAE-RF) developed by Nikolaos Kosmas-Chlis and Jan Kranich [239]. This approach allows the identification and discrimination of apoptotic and EV-decorated cells in an automated fashion. To analyse apoptotic and EV$^+$ cells, TIF-images of MFG-E8$^+$ cells from $LCMV_{Arm}$-infected and non-infected mice were exported from the IDEAS software and sorted by the CAE-RF (Fig. 6A). Using this method, we reliably classified

MFG-E8$^+$ cells into apoptotic and live EV-bound cells. Generally, apoptotic cells displayed a higher median fluorescence intensity (MFI) for MFG-E8-eGFP than EV$^+$ cells (Fig. 6A). We detected a robust and significant increase of EV-decoration and apoptosis upon $LCMV_{Arm}$ infection (Fig. 6B, C). Surprisingly, after CAE-RF-sorting, we found the majority of all MFG-E8$^+$ cells to be live EV$^+$ cells, and only a minor fraction of around 2 % (LCMV-infected) and 1 % (non-infected) of all MFG-E8$^+$ cells were *bona fide* apoptotic cells (Fig. 6B). We detected 2 x 10^5 apoptotic cells in the spleens of non-infected control mice, and this number increased to around 1 x 10^6 in infected animals. However, the frequency and the total number of EV$^+$ cells exceeded that of apoptotic cells by a factor of 10 (Fig. 6B, C).

To determine, which specific cell types undergo apoptosis or display EV-decoration in more detail, $LCMV_{Arm}$-infected and non-infected control mice were injected with MFG-E8-eGFP and MFG-E8$^+$ non-B/non-T (CD19$^-$TCRβ$^-$) cells, T cells and B cells were analysed by IFC and the CAE-RF.

Apoptosis mainly occurred among CD19$^+$ B cells both in non-infected and LCMV-infected mice (Fig. 6C). However, the number of apoptotic cells was significantly higher upon LCMV infection. Apoptosis of non-B/non-T cells and CD8$^+$ T cells was only induced in infected animals (Fig. 6C). EV-decorated CD19$^+$ B cells and non-B/non-T cells were detected in non-infected and LCMV-infected mice, but again the number of EV$^+$ cells was further elevated in LCMV-infected animals (Fig. 6C). Whereas EV-decoration increased only slightly among CD4$^+$ T cells, we found a massive rise in the number of EV$^+$CD8$^+$ T cells during LCMV infection (Fig. 6C).

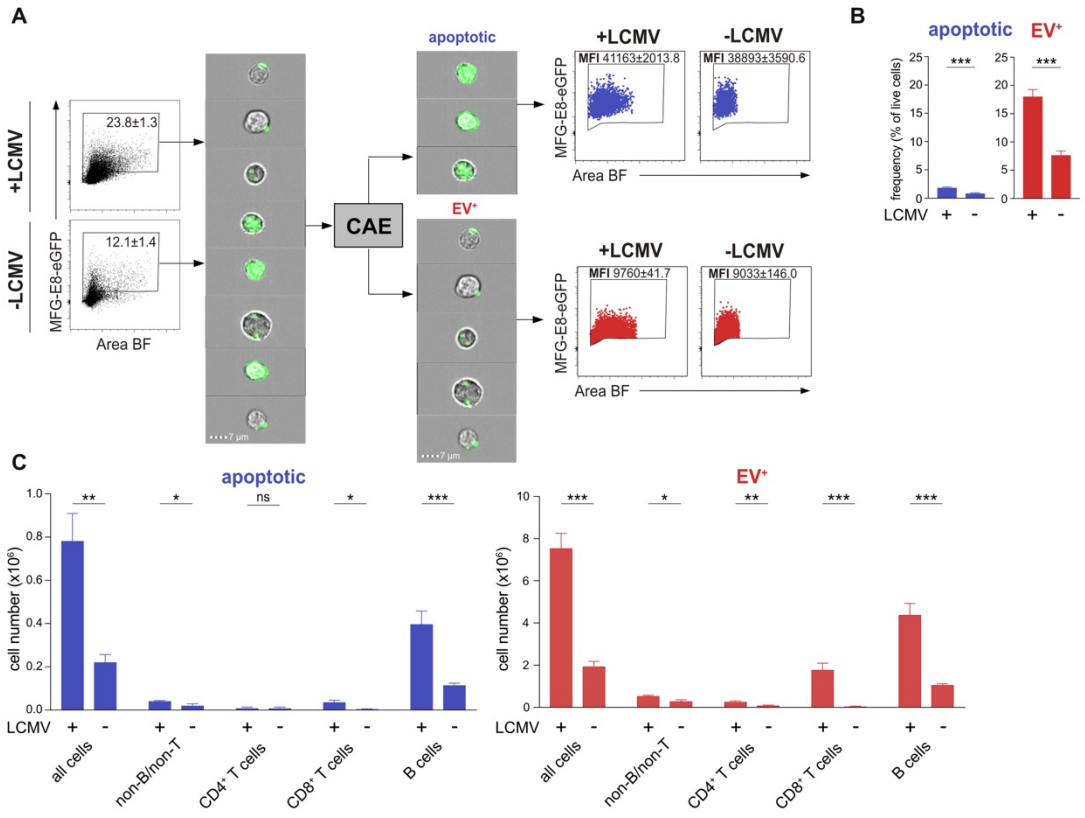

Figure 6: Analysis of EV$^+$ and apoptotic cells during LCMV-infection by a CAE-RF.
To examine apoptotic and EV$^+$ cells during LCMV infection, 100 µg of MFG-E8-eGFP were injected into non-infected and LCMV-infected mice (n=3) on day 5 p.i. and live/dead$^-$ splenocytes were quantified by IFC. (A) TIF images of the gated MFG-E8$^+$ population were exported from the IDEAS software, EV$^+$ and apoptotic cells were identified by the CAE and discriminated by a trained RF classifier [239]. The files of the sorted PS$^+$ cells were re-imported into IDEAS and analysed separately. Dot plots show the frequency ± SD of all MFG-E8$^+$ live/dead$^-$ splenocytes (black) and the MFIs ± SD of the MFG-E8-eGFP fluorescence of CAE-RF sorted apoptotic (blue) and EV$^+$ (red) splenocytes in LCMV-infected and non-infected mice. (B) Bar graphs display apoptotic (blue) and EV-decorated (red) cells as frequencies ± SD of live cells in LCMV-infected and non-infected mice quantified by CAE-RF. (C) Bar graph showing the absolute number ± SD of CAE-RF-sorted live/dead$^-$ apoptotic (blue) and EV$^+$ (red) cells of total live/dead$^-$ (all cells), non-B/non-T cells (CD19$^-$TCRβ$^-$), CD19$^+$ B cells, CD4$^+$ and CD8$^+$ T cells. Shown are results from 3 independent experiments. The unpaired Student's t-test was used to determine statistical significance, with *: p< 0.05, **: p< 0.01 and ***: p< 0.001. Figure shows data from [239] Figure 5. Figures 5B,C modified from [239].

LCMV infection elicits robust B cell responses [245].We therefore, analysed apoptosis and EV-decoration of different B cell subsets more specifically (Fig. 7A, B). Follicular (FO, CD19$^+$CD21$^+$CD23^{hi}) and immature (IM, CD19$^+$CD21$^-$CD23$^-$) B cells show increased EV-decoration and apoptosis upon LCMV infection (Fig. 7B). In contrast, marginal zone (MZ, CD19$^+$CD21^{hi}CD23^{lo}) B cells exhibited a high frequency of EV-decoration independently of infection. Furthermore, the frequency of EV$^+$ and apoptotic MZ B cells detected was generally higher than that of FO and IM B cells in mice infected with LCMV$_{Arm}$ and non-infected animals.

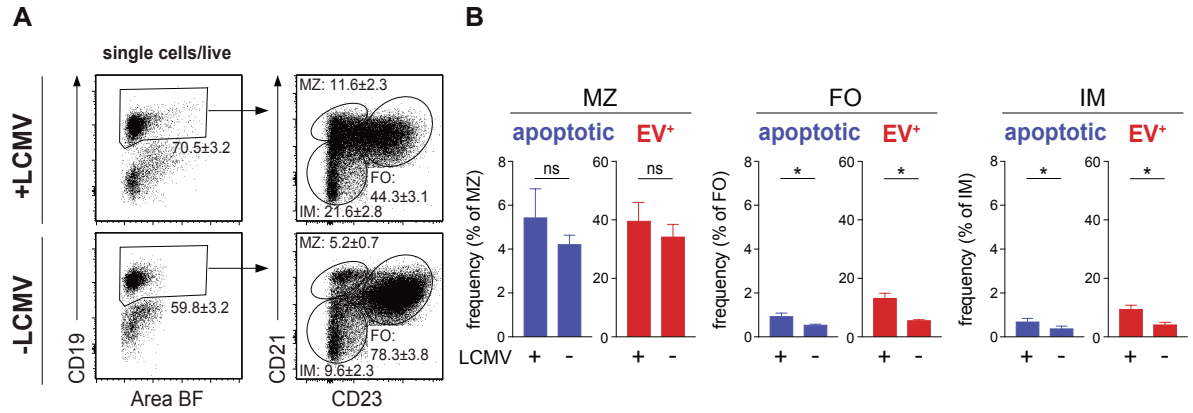

Figure 7: Analysis of EV-decoration and apoptosis of B cell subsets during LCMV infection.
MFG-E8-eGFP (100 μg/mouse) was injected into LCMV-infected and non-infected mice (n=3), and B cells were examined by IFC. EV^+ and apoptotic cells were separated using the CAE-RF. (A) Gating strategy to investigate apoptosis and EV-decoration of live/$dead^-$ FO ($CD19^+CD21^+CD23^{hi}$), MZ ($CD19^+CD21^{hi}CD23^{lo}$) and IM ($CD19^+CD21^-CD23^-$) B cells in LCMV- and non-infected animals. Percentages ± SD of the respective population are indicated. (B) Bar graphs display apoptotic (blue) and EV^+ (red) cells as average frequencies ± SD of the respective B cells subset (from left to right, MZ, FO, IM) in LCMV- and non-infected mice. Shown are representative results from 3 independent experiments. The unpaired Student's t-test was used to determine statistical significance, with *: p< 0.05, **: p< 0.01 and ***: p< 0.001. Figure modified from [239] Figure 5.

$CD11c^+$ $MHC\text{-}II^+$ dendritic cells (DCs), which can be infected by $LCMV_{Arm}$ [106, 246], displayed a slight but significant increase in EV-decoration and apoptosis during LCMV infection compared to non-infected mice (Fig. 8A, B).

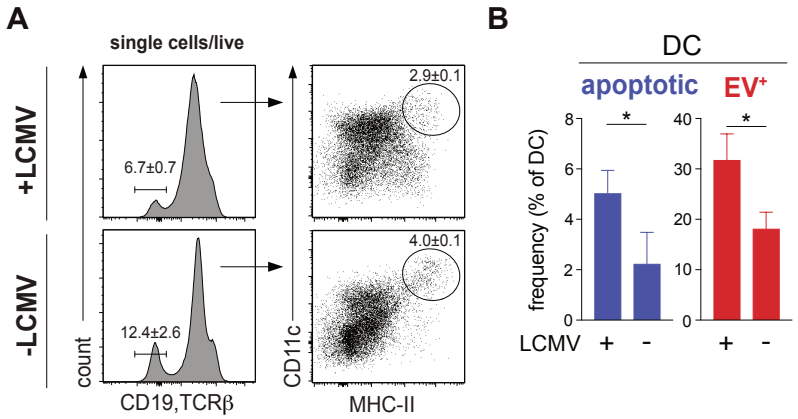

Figure 8: EV-decoration and apoptosis of DCs increase during LCMV infection.
LCMV-infected and non-infected mice (n=3) were injected with MFG-E8-eGFP (100 μg/mouse), and live/$dead^-$ $CD19^-TCR\beta^-$ $MHC\text{-}II^+$ $CD11c^+$ DCs were analysed by IFC. EV^+ and apoptotic cells were separated by the CAE-RF [239]. (A) Gating strategy to investigate apoptosis and EV-decoration of live/$dead^-$, $CD19^-TCR\beta^-$ $MHC\text{-}II^+$ $CD11c^+$ DCs in LCMV- and non-infected animals. Percentages ± SD of the respective populations are indicated. (B) Bar graphs display apoptotic (blue) and EV^+ (red) cells as average frequencies ± SD of the total live, DC population in LCMV- and non-infected mice. Shown are representative results from 3 independent experiments. The unpaired Student's t-test was used to determine statistical significance, with *: p< 0.05, **: p< 0.01 and ***: p< 0.001. Figure modified from [239] Figure 5.

Both $CD8^+$ and $CD4^+$ T cells responses are induced during acute LCMV infection [67]. When we looked at the frequencies of apoptotic $CD8^+$ and $CD4^+$ T cells, we found a significant increase in

CD8⁺ but not in CD4⁺ T cells upon LCMV infection (Fig. 9B). Although EV-decoration of CD4⁺ T cells slightly but significantly augmented during LCMV infection, it dramatically (8-fold) increased in CD8⁺ T cells with up to 45 % of CD8⁺ T cells being EV⁺. Due to the substantial binding of EVs to CD8⁺ T cells and the crucial role of cytotoxic T cells in eliminating LCMV infection, we next analysed different subsets of CD8⁺ T cells.

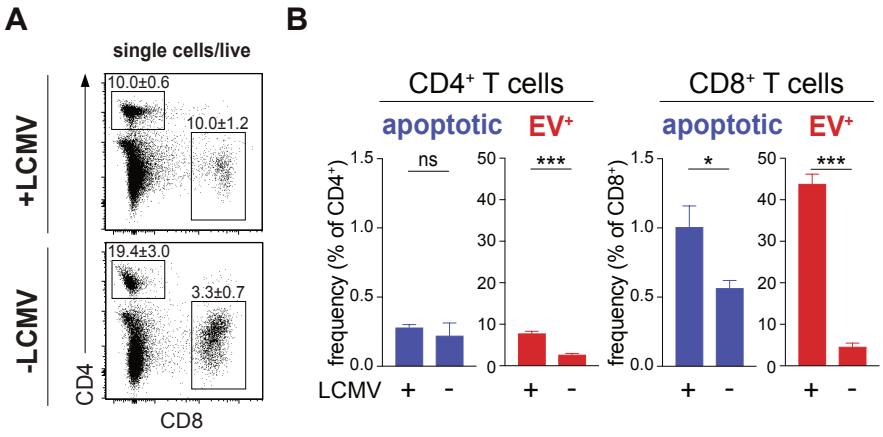

Figure 9: The frequency of EV-decorated T cells significantly increases during LCMV infection.
MFG-E8-eGFP (100 μg /mouse) was injected into LCMV-infected and non-infected mice (n=3), and live/dead⁻ CD4⁺ and CD8⁺ T cells were examined by IFC. EV⁺ and apoptotic cells were separated by the CAE-RF [239]. (A) Representative dot plots show the mean percentage ± SD of total live (black, live/dead⁻) CD4⁺ and CD8⁺ T cells in LCMV-infected and control animals. (B) Bar graphs display apoptotic (blue) and EV⁺ (red) cells as average frequencies ± SD of the respective CD4⁺ (left) or CD8⁺ (right) population in LCMV-infected and control mice. Shown are representative results from 3 independent experiments. The unpaired Student's t-test was used to determine statistical significance, with *: p< 0.05, **: p< 0.01 and ***: p< 0.001. Figure modified from [239] Figure 6.

6.3 EVs preferentially associate with Ag-experienced CD8⁺ T cells during LCMV-infection

We next aimed to assess if EVs preferentially bind to a specific T cell subset. In lymphoid organs, functionally different subsets are defined based on the expression of the L-selectin CD62L and the activation marker CD44 [247]. EV-decoration of naïve (T_N, CD62L^{lo}CD44^{hi}), central memory (T_{CM}, CD62L^{hi}CD44^{hi}), and effector (T_E, CD62L^{lo}CD44^{hi}) CD8⁺ T cells from control and LCMV-infected mice were analysed by MFG-E8-eGFP injection followed by IFC and CAE-RF-based sorting. In non-infected mice, we observed only a low frequency of EV⁺T_N and EV⁺T_{CM} CD8⁺ T cells, whereas around 20 % of T_E cells were EV-decorated (Fig. 10A). In contrast, during acute LCMV infection, EV-decoration significantly increased in all three subsets in terms of frequency and total number (Fig. 10A and B). However, we observed the most substantial increase in EV-decoration among activated CD44^{hi}CD8⁺ T cells compared to steady-state. While around 10 % of T_{CM} were associated with EVs, T_E displayed 55 % of EV-decoration, thus revealing a preferential binding of EVs to CD8⁺ T_E cells upon LCMV infection (Fig. 10B).

We further examined the frequencies of apoptotic $CD8^+$ T cell subsets in LCMV-infected and control mice. Apoptosis was not markedly induced in T_{CM} in the absence of infection. However, we found around 2 % of apoptotic T_E cells in non-infected animals (Fig. 10A). While apoptosis was increased in T_{CM} cells during early LCMV infection, the frequency of apoptotic T_E cells decreased. We detected apoptosis of T_N cells neither in LCMV-infected nor in non-infected animals. As shown before (Fig. 4), apoptotic and EV^+ $CD8^+$ T cells displayed different morphological staining patterns of MFG-E8 (Fig. 10C).

Considering the sharp increase of EV^+ cells on day 5 p.i., especially of $CD8^+$ T cells, we were interested in determining the kinetics of EV-decoration during LCMV infection. For this, apoptotic and EV-decorated splenocytes were quantified over the first fifteen days of LCMV infection by imaging flow cytometry and CAE-RF. We detected the highest frequency of EV^+ live cells and EV^+CD8^+ T cells on day 5 p.i. , which declined from day 10 to day 15 p.i. (Fig. 11). Similarly, apoptosis of total live and $CD8^+$ T cells reached its maximum on day 5. Notably, on day 15 p.i. EV-decoration and apoptosis dropped below the levels of non-infected mice. This data indicates that EV-decoration of $CD8^+$ T cells is transient and correlates with the published kinetics of LCMV-titers in the spleen, with a peak of the virus titer on day 5 p.i. and viral clearance 8 days after infection [248, 249].

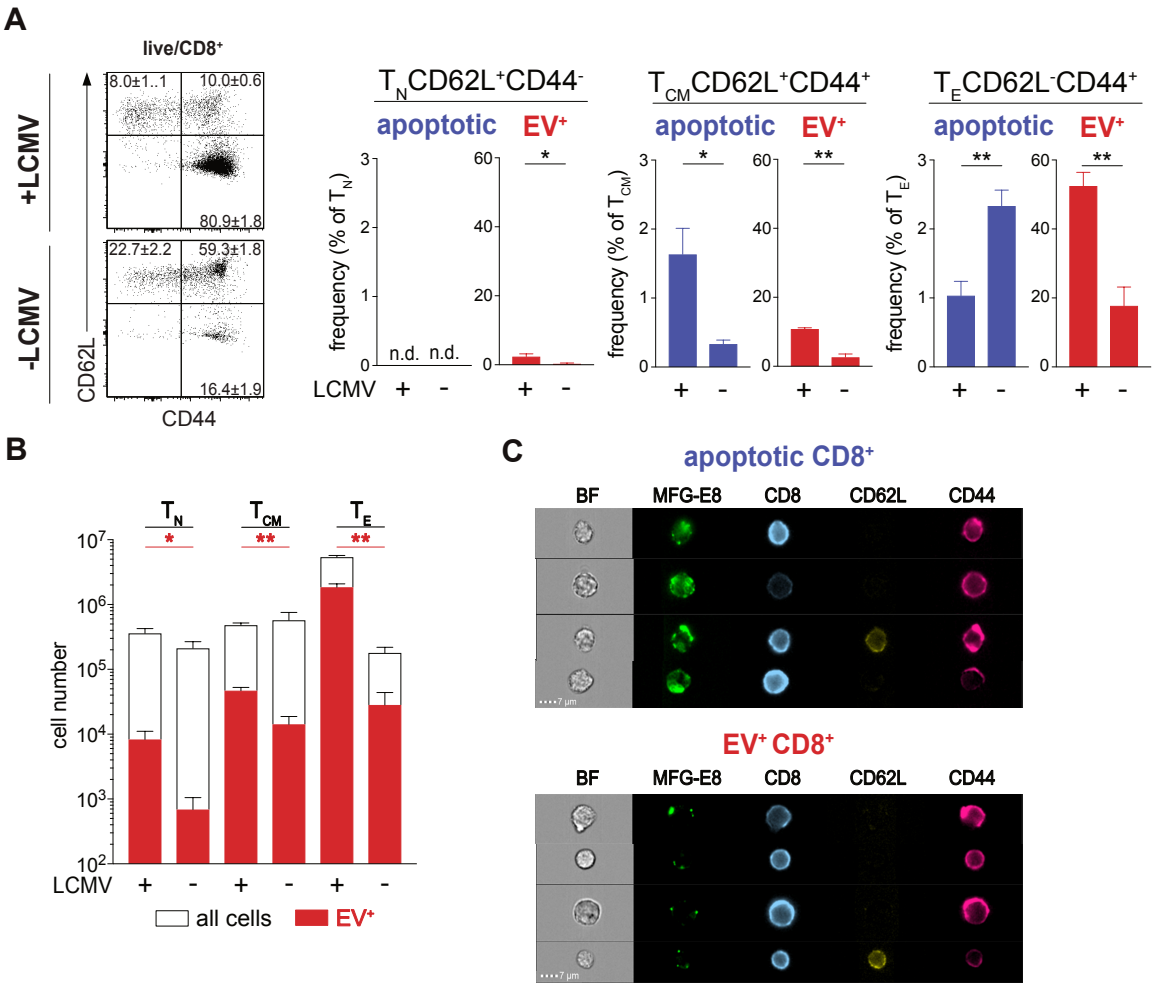

Figure 10: Effector CD8⁺ T cells strongly bind EVs during LCMV infection.

MFG-E8-eGFP (100 µg /mouse) was injected into LCMV-infected and non-infected mice (n=3), and different live/dead⁻ CD8⁺ T cell subsets were analysed by IFC. EV⁺ and apoptotic cells were separated using the CAE-RF [239]. (A) CD8⁺ T cell subsets were divided into naïve ($CD62L^+CD44^-$, T_N), central memory ($CD62L^+CD44^+$, T_{CM}), and effector ($CD62L^-CD44^+$, T_E) CD8⁺ T cells. Representative dot plots show the mean percentages ± SD of total live CD8⁺ T cells subsets in LCMV- and non-infected animals. Graphs display the frequencies ± SD of the respective MFG-E8⁺ apoptotic (blue) and EV⁺ (red) T_N, T_{CM} and T_E CD8⁺ T cell population in LCMV- and non-infected (mice. (B) Total numbers of all (white) and EV⁺ (red) T_N, T_{CM} and T_E CD8⁺ T cells are plotted in a bar graph. (C) Representative images of BF, MFG-E8, CD8, CD62L and CD44 of EV⁺ and apoptotic CD8⁺ T cells are shown. Scale bar 7 µm. Shown are representative results from 3 independent experiments. The unpaired Student's t-test was used to determine statistical significance, with *: $p< 0.05$, **: $p< 0.01$ and ***: $p< 0.001$. Figure modified from [239] Figure 6.

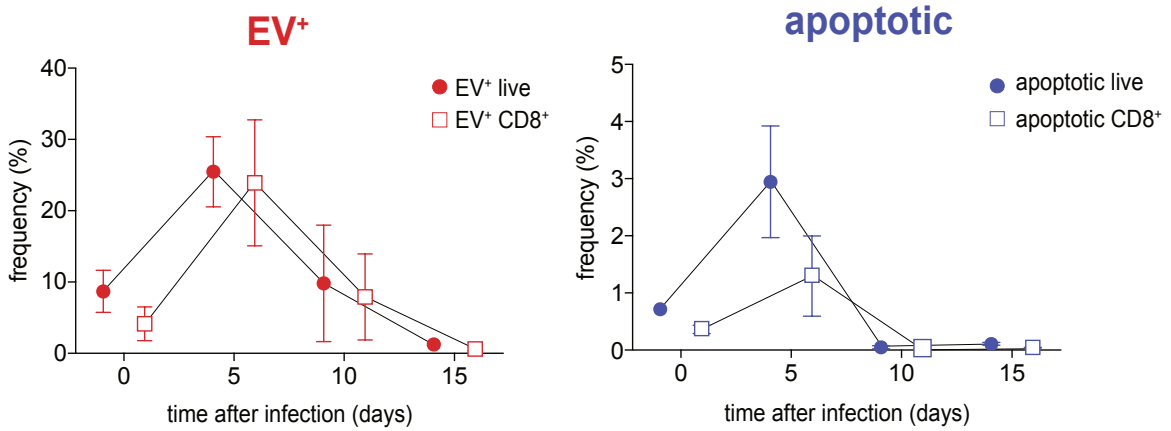

Figure 11: EV-decoration and apoptosis of CD8$^+$ T cells are transient.
Mice were infected with LCMV$_{Arm}$, and frequencies of EV$^+$ (red) and apoptotic (blue) total live cells and CD8$^+$ T cells were determined on day 5, 10 and day 15 p.i. by MFG-E8-eGFP-injection followed by imaging flow cytometry and CAE-RF. Representative results from 2 independent experiments are shown.

To investigate EV-decoration of Ag-specific CD8$^+$ T cells, we used two MHC-I-multimers (H-2D^b/LCMVgp$_{33-41}$-multimer (D^b/GP33) and H-2K^b/LCMVgp$_{34-43}$-multimers (K^b/GP34)) to detect LCMV-specific CD8$^+$ T cells in infected mice. MFG-E8-eGFP was injected into LCMV$_{Arm}$-infected mice on day 5 p.i., and multimer$^+$CD8$^+$ T cells were analysed for EV-decoration by IFC and the CAE-RF (Fig. 12 A and B). At that time point, MHC-I-multimer$^+$CD8$^+$ T cells made up 7 % (D^b/GP33$^+$) and 4 % (K^b/GP34$^+$) of all CD8$^+$ T cells in the spleen. We found around 20 to 30 % of these LCMV-specific CD8$^+$ T cells to be EV$^+$ (Fig. 12A and B). Compared to multimer$^+$ T cells, EV-decoration of D^b/GP33$^-$, K^b/GP34$^-$ and total (all) CD44$^+$CD8$^+$ T cells was slightly but significantly reduced. However, bystander T-cell activation plays no significant role in the polyclonal CD8$^+$ T cell response to acute LCMV infection [78, 80, 250]. Therefore, the multimer$^-$CD44$^+$CD8$^+$ T cell population probably contains T cell clones specific for other untested LCMV epitopes. These results show that a large fraction of Ag-specific CD8$^+$ T cells bind EVs. However, preferential binding of EVs to Ag-specific CD8$^+$ T cells cannot be concluded from this experiment. Consistent with previous experiments, CD44$^-$CD8$^+$ T cells did not bind EVs during LCMV infection, further supporting the idea that only Ag-experienced T cells bind EVs.

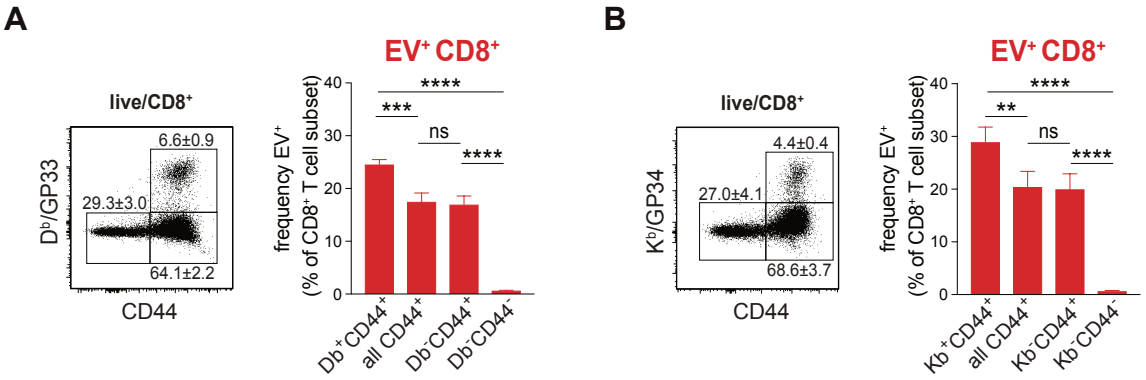

Figure 12: EVs bind to LCMV-specific effector CD8⁺ T cells.
To analyse EV-binding of LCMV-specific CD8⁺ T cells, MFG-E8-eGFP was injected and MHC-multimer H-2D^{b}LCMVgp$_{33\text{-}41}^{+}$ and H-2K^{b}LCMVgp$_{34\text{-}43}^{+}$ cells were quantified and analysed using the CAE-RF in day 5 LCMV-infected mice (n=3). Representative dot plots in A and B show the frequencies ± SD of total live/dead^{-} CD44^{+}multimer^{+}/CD44^{+}multimer^{-}/CD44^{-}multimer^{-} CD8^{+} T cells of both specificities. Bar graphs display the frequencies of ± SD of EV^{+} CD44^{+}multimer^{+}, EV^{+}CD44^{+}multimer^{-}, EV^{+}CD44^{-}multimer^{-} and total EV^{+}CD44^{+} (all) CD8^{+} T cells. Representative results from 2 independent experiments are shown. One-way ANOVA-test was used to determine statistical significance, with *: p< 0.05, **: p< 0.01 and ***: p< 0.001.

We next analysed EV-decoration of CD4^{+} T cell subsets during acute LCMV infection. Similar to CD8^{+} T cells, the frequency and the total number of EV-decorated T_N, T_{CM} and T_E CD4^{+} T cells raised upon LCMV infection (Fig. 13A, B). Again, the highest frequency of EV^{+} cells was observed in the CD44^{hi}CD62L^{-}CD4^{+} population. However, EV-decoration of effector CD4^{+} T cells (10-20 % EV^{+}CD44^{hi}CD62L^{-}CD4^{+}) was not as pronounced as that of CD44^{hi}CD62L^{-}CD8^{+} T cells (50-60 % EV^{+}CD44^{hi}CD62L^{-}CD8^{+}) (Fig. 10A). EV^{+}CD4^{+} T cells show a spot-like MFG-E8-eGFP staining (Fig. 13C).

Consistent with an increase in apoptosis, we found a reduction in the total number of T_{CM} CD4^{+} T cells during LCMV infection. We did not observe an increase in apoptotic T_N or T_E cells during the analysed phase of LCMV infection. In contrast to EV^{+} T cells, cells undergoing apoptosis display an almost entire MFG-E8-eGFP^{+} plasma membrane (Fig. 13C).

This data suggests that like CD8^{+} T cells, T_E CD4^{+} T cells tend to associate with EVs, although to a lesser extent.

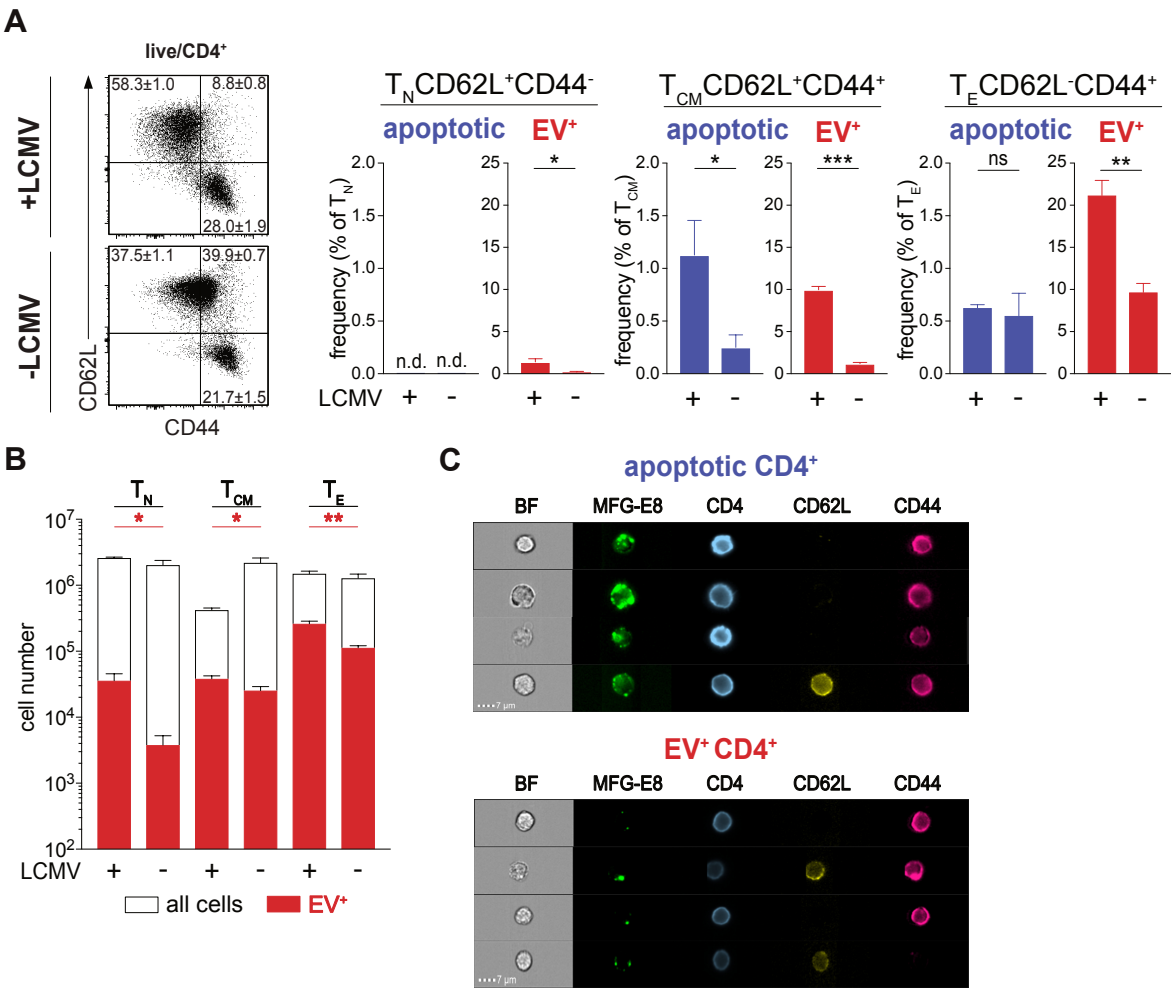

Figure 13: Effector CD4⁺ T cells display increased EV-decoration during LCMV infection.
MFG-E8-eGFP (100 µg /mouse) was injected into LCMV-infected and non-infected mice (n=3), and different subsets of CD4⁺ T cell were analysed by IFC and CAE-RF [239]. (A) CD4⁺ T cell subsets were subdivided into naïve ($CD62L^+CD44^-$, T_N), central memory ($CD62L^+CD44^+$, T_{CM}) and effector ($CD62L^-CD44^+$, T_E) CD4⁺ T cells. The mean percentages ± SD of total live CD4⁺ T cells subsets in LCMV- and non-infected animals are shown in representative dot plots. Bar graphs depict the frequencies ± SD of the respective MFG-E8⁺ apoptotic (blue) and EV⁺ (red) T_N, T_{CM} and T_E CD4⁺ T cell populations in LCMV-infected and control mice. (B) Bar graph displaying the absolute numbers ± SD of the total (white) and EV⁺ (red) T_N, T_{CM} and T_E CD4⁺ T cells. N =3. (C) Representative images of BF, MFG-E8, CD8, CD62L and CD44 of apoptotic and EV⁺ CD4⁺ T cells are shown. Scale bar 7 µm. Shown are results from 3 independent experiments. The unpaired Student's t-test was used to determine statistical significance, with *: $p< 0.05$, **: $p< 0.01$ and ***: $p< 0.001$. Figure modified from [239] Supplemental Figure 5.

EVs have been found in several bodily fluids, including saliva, urine and blood [reviewed in 115, 147]. To test whether EV-decoration of CD8⁺ T cells occurs not only in the spleen but also in the blood during infection, we compared the frequencies of EV⁺CD8⁺ T cells in the blood and spleen of LCMV-infected and control mice. For this, mice received MFG-E8-eGFP, and CD8⁺ T cells from the spleen and blood were analysed by IFC and CAE-RF. The frequency of live, MFG-E8⁺ cells but also apoptotic and EV⁺CD8⁺ T cells was significantly higher in the blood from LCMV-infected compared to non-infected mice, where we hardly detected EV-decoration or apoptosis of CD8⁺ T cells (Fig. 14A). Interestingly, we found significantly more MFG-E8⁺ cells, apoptotic and

EV^+CD8^+ in the blood than in the spleen within the same infected mice (Fig. 14A). On the one hand, this may indicate an enrichment of EV^+CD8^+ T cells in the blood during LCMV infection; on the other hand, EVs may be captured and filtered by splenic macrophages or MZ B cells, thereby reducing the local concentration of EVs in the spleen.

In addition, we also detected more apoptotic $CD8^+$ T cells in the blood compared to the spleen of LCMV-infected mice.

Next, we compared the frequencies of EV-decorated and apoptotic T cells subsets in the blood and spleen of LCMV-infected mice. Similar to the spleen, $CD62L^-CD44^+CD8^+$ T_E cells showed the highest level of EV-decoration in the blood upon infection (Fig. 14B). While there was no difference in the frequency of EV^+ T_E in the blood and spleen of LCMV-infected mice, EV-decoration of T_N and T_{CM} $CD8^+$ T cells was significantly elevated in the blood (Fig. 14B). These data reveal different EV-binding properties of $CD62L^+CD8^+$ T cells (T_{CM}, T_N) in the blood of LCMV-infected mice compared to those found in the spleen.

Furthermore, apoptosis of naïve and T_E $CD8^+$ T cells was slightly but significantly induced in the blood, while the frequencies of apoptotic T_{CM} were comparable.

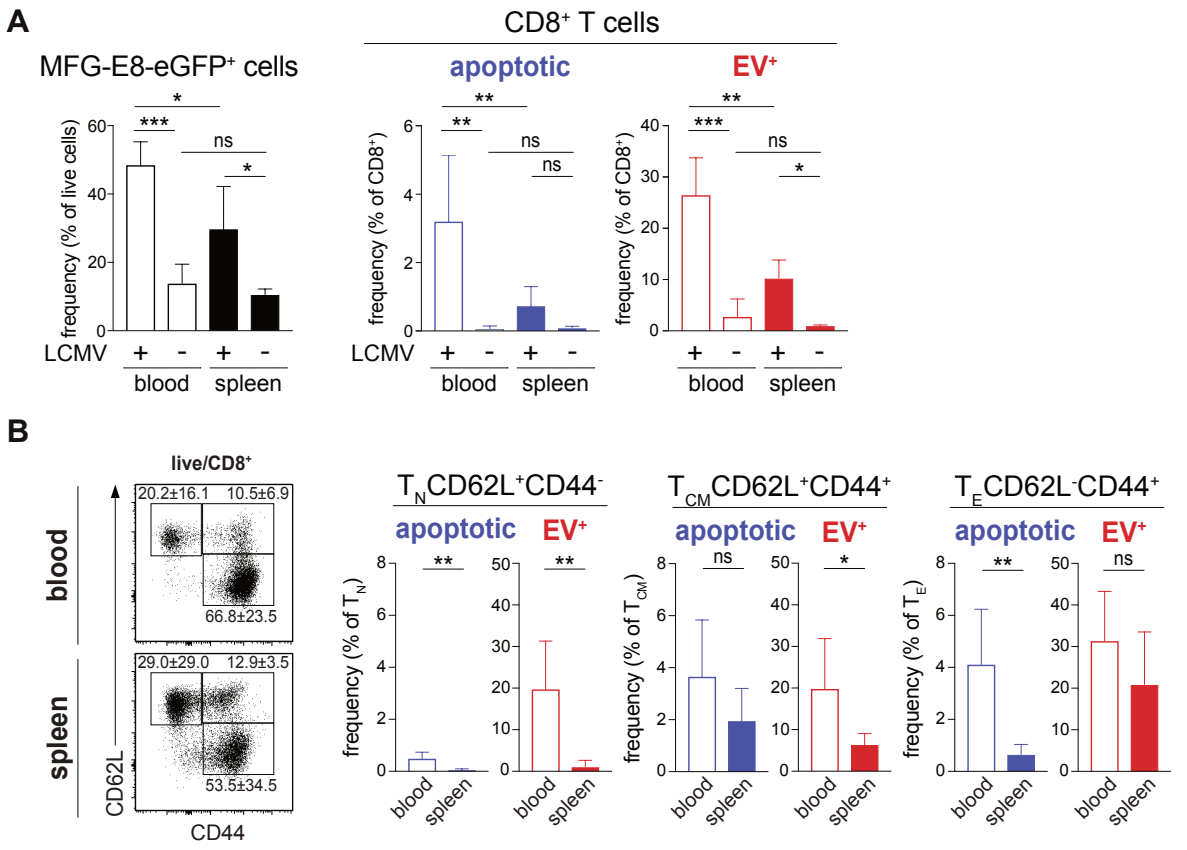

Figure 14: Increased frequencies of EV$^+$CD8$^+$ T cells in the blood of LCMV-infected mice.
LCMV- (n=5) and non-infected mice (n=3) received 100 µg of MFG-E8-eGFP on day 5 p.i., and live/dead$^-$CD8$^+$ T cells from the spleen and the blood were analysed by IFC. EV$^+$ and apoptotic CD8$^+$ T cells were quantified using the CAE-RF [239]. (A) Bar graph (left) shows the frequencies ± SD of MFG-E8$^+$ live cells in the blood (open) and spleen (black) of LCMV-infected and non-infected mice. Frequencies ± SD of apoptotic (blue) and EV$^+$ (red) CD8$^+$ T cells from blood and spleen of LCMV-infected and non-infected mice were quantified by CAE and plotted in bar graphs on the right. (B) Representative dot plots showing the frequencies ± SD of total T_N, T_{CM} and T_E CD8$^+$ T cells in the blood and spleen of LCMV-infected mice. Bar graphs visualise frequencies ± SD of apoptotic (blue) and EV$^+$ (red) T_N, T_{CM} and T_E CD8$^+$ T cells in the blood and spleen upon LCMV infection. Bar graphs show the results from 5 LCMV-infected mice pooled from 2 independent experiments (A, B) and the 3 non-infected mice from one experiment (A). One-way ANOVA-test (A) and the unpaired Student's t-test (B) were used to determine statistical significance, with *: p< 0.05, **: p< 0.01 and ***: p< 0.001.

6.4 Memory precursor cells preferentially bind EVs during LCMV infection

During acute LCMV infection, effector CD8$^+$ T cells differentiate into short-lived KLRG1^{hi}CD127^{low} terminal T_E cells or into KLRG1^{low}CD127^{hi} T_E cells which harbour the potential to differentiate into long-lived memory precursor cells [41-43]. To investigate EV-decoration of terminal effector and memory precursor CD8$^+$ T_E cells, we analysed multimer$^+$CD8$^+$ T cells for their expression of CD127 and KLRG1 and attached EVs on days 5, 10 and 15 p.i. by IFC and CAE-RF as described before.

CD127 expression levels of Ag-specific multimer$^+$CD8$^+$ T cells significantly increased from below 10 % to over 50 % during the time analysed (Fig. 15). Furthermore, while KLRG1$^+$CD127$^-$CD8$^+$ T cells gradually lost EV-decoration over time, the frequency of EV$^+$CD127$^+$ (KLRG1$^+$CD127$^+$,

KLRG1^{-}CD127^{+}) multimer^{+}CD8^{+} T cells increased. These results suggest that EVs are preferentially associated with KLRG1^{low}CD127^{hi} memory precursor cells during later time points of LCMV infection.

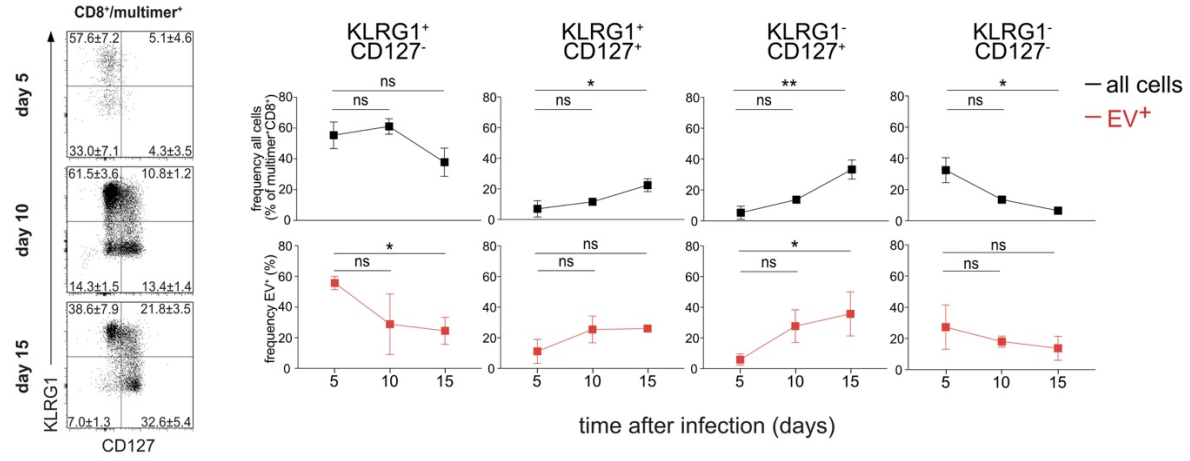

Figure 15: EVs preferentially associate with CD127^{+}CD8^{+} T cells throughout LCMV infection.
Mice were infected with LCMV$_{Arm}$ and injected with MFG-E8-eGFP (100 µg/mouse) on days 5, 10 or 15 post-infection. LCMV-specific (H-2K^{b}LCMVgp$_{34-43}$ and H-2D^{b}LCMVgp$_{33-41}$$^{+}$) live/dead^{-} CD8^{+} T cells were analysed for their expression of KLRG1, CD127 and their EV-decoration by imaging flow cytometry and CAE-RF. Representative dot plots showing the mean frequencies ± SD of KLRG1^{+}CD127^{-}, KLRG1^{+}CD127^{+}, KLRG1^{-}CD127^{+} and KLRG1^{-}CD127^{-} of total live (black) or EV^{+} (red) multimer^{+}CD8^{+} T cells on days 5, 10 or 15 post-infection. Black graphs display the frequencies ± SD of the different CD8^{+} T cell populations as determined by KLRG1 and CD127 expression on d5, d10, d15 p.i. as percentage of multimer^{+}CD8^{+} T cells. Red graphs display the frequencies ± SD of EV^{+} cells among the indicated KLRG1 and CD127 CD8^{+} T cells populations. N=3. Representative results from 2 independent experiments are shown. The unpaired Student's t-test was used to determine statistical significance, with *: p< 0.05, **: p< 0.01 and ***: p< 0.001.

CD127^{+} memory precursor cells have been detected as early as 8 days post LCMV infection [41, 50, 82]. At that time point, memory precursor cells show lower T-bet expression levels, whereas a high T-bet expression repress CD127 expression and promote terminal CD8^{+} T cell differentiation [42, 46]. As shown in Fig. 15, Ag-specific EV^{+}CD8^{+} T cells preferentially expressed the memory marker CD127 during later time points of LCMV infection. Therefore, to test whether EV-associated CD8^{+} T cells would also display a lower T-bet activity than MFG-E8^{-}CD8^{+} T cells, we compared T-bet expression and its subcellular localisation in EV^{+} and MFG-E8^{-}CD8^{+} T cells on day 8 after infection. For this, MFG-E8-eGFP was injected into LCMV-infected mice, stained for intracellular T-bet examined by IFC. However, when we analysed the images of permeabilised MFG-E8^{+} cells using the deep learning-based autoencoder [239], it was not possible to reliably discriminate apoptotic from EV^{+} cells. Permeabilisation buffers contain detergents such as Triton X-100 or NP-40, which lyse all membranes, including those of EVs [251, 252]. Although cells were previously fixed with 4 % PFA and MFG-E8^{+} cells could be readily

detected, small changes in the MFG-E8-eGFP staining pattern and cell morphology may cause the CAE-RF to classify MFG-E8$^+$ cells incorrectly. However, as previously demonstrated, only very few MFG-E8$^+$ apoptotic CD8$^+$ T cells (at maximum 1 %) were detected on days 5 and 10 post LCMV infection (Fig. 11). We regarded this low number as negligible; therefore, we investigated T-bet expression in the total MFG-E8$^+$CD8$^+$ T cell population for analysis. While T-bet expression increased in CD44$^+$CD8$^+$ T cells upon LCMV Infection, we detected significantly reduced T-bet expression levels in MFG-E8$^+$ compared to MFG-E8$^-$ effector CD8$^+$ T cells (Fig. 16A, B).

To quantify the extent of T-bet nuclear translocation, we used the 'Similarity' feature offered by the IDEAS software. Herein, the translocation of T-bet to the nucleus, as labelled by DRAQ5, is indicated by a median similarity score (SS) of > 1. We found a significantly lower nuclear translocation of T-bet in MFG-E8$^+$CD8$^+$ T cells than MFG-E8$^-$CD8$^+$ T cells, as evidenced by a lower SS and frequency of CD44$^+$CD8$^+$ T cells with nuclear T-bet (Fig. 16C). These results further suggest that EVs bind to cells displaying characteristics of memory precursor cells.

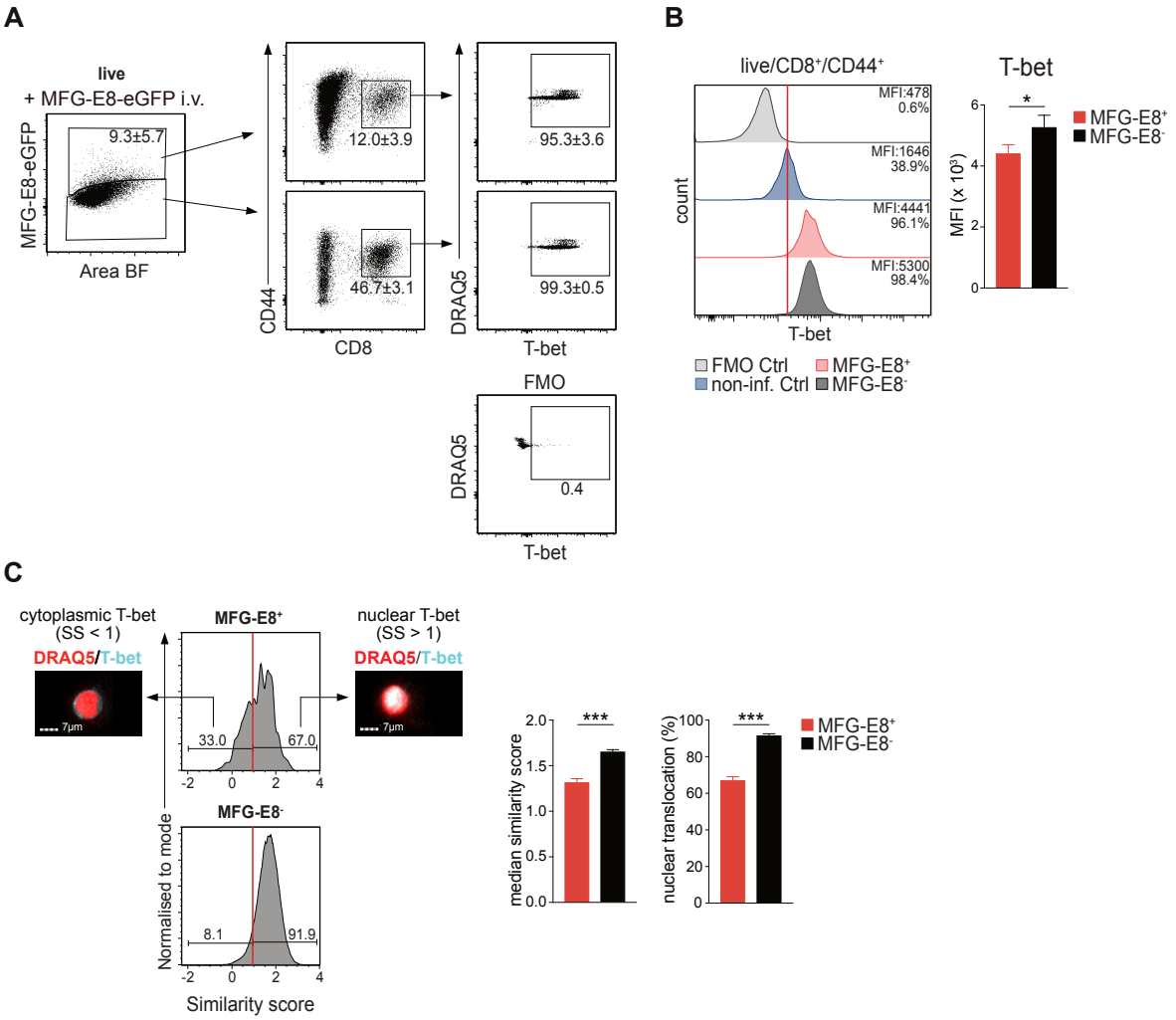

Figure 16: MFG-E8⁺CD44⁺CD8⁺ T cells display lower T-bet expression levels and nuclear translocation than MFG-E8⁻CD44⁺CD8⁺ T cells.

Mice were infected with $LCMV_{Arm}$, injected with MFG-E8-eGFP (100 µg/mouse) on day 8 p.i. and the expression and nuclear translocation of T-bet were compared in MFG-E8⁺ and MFG-E8⁻ CD44⁺CD8⁺ T cells by IFC. (A) Gating strategy used to analyse T-bet expression and nuclear translocation in live/dead⁻, MFG-E8⁺ and MFG-E8⁻ CD44⁺DRAQ5⁺T-bet⁺CD8⁺ T cells with frequencies± SD of the respective population. (B) Shown are representative histograms of the T-bet fluorescence intensity in unstained CD44⁺CD8⁺ from LCMV-infected mice (grey, n=1), CD44⁺CD8⁺ from non-infected mice (blue, n=1), MFG-E8⁺ (red) and MFG-E8⁻ (black) CD44⁺CD8⁺ from LCMV-infected mice (n=3). The frequencies and median fluorescence intensities (MFIs) ± SD of T-bet for each CD44⁺CD8⁺ T cell population is indicated. Bar graphs show the MFIs of T-bet expression ± SD for MFG-E8⁺ (red) and MFG-E8⁻ (black) CD44⁺CD8⁺ T cells. N =3. (C) Nuclear localisation of T-bet was analysed in splenic live/dead⁻MFG-E8⁺ and MFG-E8⁻CD44⁺CD8⁺ T cells from LCMV-infected mice on day 8 p.i. (n=3) using imaging flow cytometry. To quantify the extent of nuclear translocation, the co-localisation of nuclear DRAQ5 staining and T-bet staining was determined using the 'Similarity' feature provided by the IDEAS software. As determined by visual inspection, the translocation of T-bet to the nucleus is indicated by a median similarity score (SS) of > 1. Percentages of cells with SS >1 and <1 are shown in the histograms. The left bar graph depicts the median SS ± SD of the nuclear T-bet translocation. The right bar graph displays the frequencies ± SD of MFG-E8⁺ and MFG-E8⁻CD8⁺ T cells with nuclear T-bet. N=3. Shown are representative results of two independent experiments. Scale bar 7 µm. The unpaired Student's t-test was used to determine statistical significance, with *: p< 0.05, **: p< 0.01 and ***: p< 0.001.

The balance of the anti-apoptotic Bcl-2 family protein Bcl-2 and the pro-apoptotic Bcl-2 family protein Bim controls T cell homeostasis and cell death [253]. Surviving precursor memory CD8⁺ T cells have been shown to express higher levels of Bcl-2 compared to short-lived effector CD8⁺

T cells [254, 255]. To further test whether EV$^+$CD8$^+$ T cells belong to the surviving memory precursor pool, we determined Bcl-2 and Bim expression in MFG-E8$^+$ and MFG-E8$^-$CD8$^+$ T cells during LCMV infection by IFC on day 8 post-infection. MFG-E8$^+$CD8$^+$ T cells exhibited a higher expression of Bcl-2 compared to their MFG-E8$^-$ counterparts (Fig.17A). In contrast, there was no difference in the expression levels of Bim between the two populations analysed. The differential expression resulted in a higher Bcl-2/Bim ratio found in MFG-E8$^+$CD8$^+$ T cells, suggesting prolonged survival of EV-decorated CD8$^+$ T cells. Together with the results above, these data support the idea that surviving memory precursor cells preferentially bind EVs during LCMV infection.

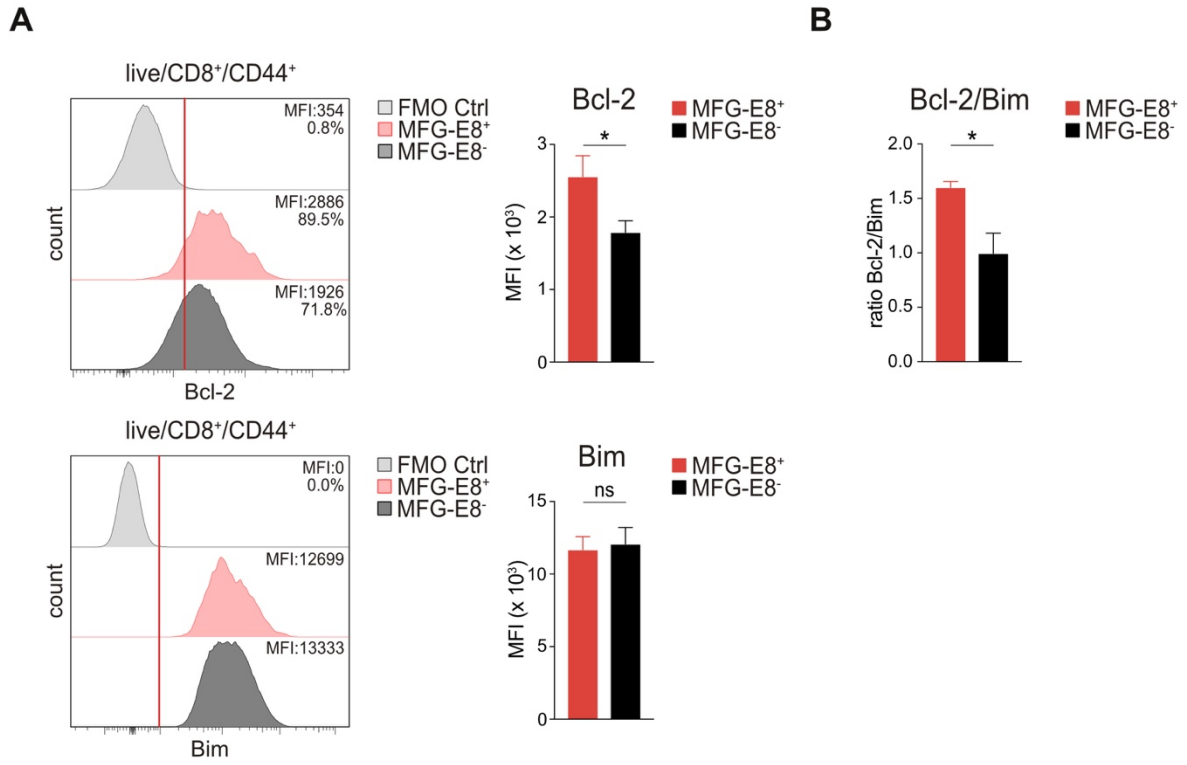

Figure 17: MFG-E8$^+$CD44$^+$CD8$^+$ T cells show a higher Bcl-2/Bim ratio compared to MFG-E8$^-$CD8$^+$ T cells.
To assess Bcl-2 and Bim expression in MFG-E8$^+$ and MFG-E8$^-$CD8$^+$ T cells in mice infected with LCMV$_{Arm}$, MFG-E8-eGFP (100 µg/mouse) was injected on day 8 post-infection. Splenic live/dead$^-$ MFG-E8$^+$ and MFG-E8$^-$CD44$^+$CD8$^+$ T cells were analysed for intracellular Bcl-2 and Bim expression using imaging flow cytometry (n=3). Flow cytometric histograms show the fluorescence intensity of Bcl-2 and Bim in unstained (grey, n=1), MFG-E8$^+$ (red) and MFG-E8$^-$ (black) CD44$^+$ CD8$^+$ T cells. MFI of Bcl-2 and Bim and the frequencies ± SD of cells expressing BCL-2 are indicated. Bar graphs show the MFI ± SD of Bcl-2 and Bim for MFG-E8$^+$ (red) and MFG-E8$^-$ (black) cells. (B) For each protein, the MFI obtained was normalised to the MFI of Bim of MFG-E8$^-$CD44$^+$ CD8$^+$ T cells and the Bcl-2/Bim expression ratios were calculated and presented on the graph. Shown are representative results from two independent experiments. The unpaired Student's t-test was used to determine statistical significance, with *: p< 0.05, **: p< 0.01 and ***: p< 0.001.

6.5 EVs attached to activated effector CD8$^+$ T cells originate from APCs

Having analysed the characteristics of CD8$^+$ T cells that bind EVs during LCMV infection, we next wanted to focus on the origin of EVs attached to these cells. In general, tetraspanins such as

CD63 and CD9 were described to be enriched in small EVs, including exosomes [125, 150, 166]. Furthermore, EVs secreted by APCs, such as DCs, contain MHC class II molecules and the activation markers CD86 and CD54 (ICAM-1) [166, 169, 177, 193, 196]. We, therefore, analysed $CD44^+CD8^+$ T cell-bound EVs for the presence of these APC and vesicles markers on day 5 post LCMV infection (Fig. 18A, B). $CD44^-CD62L^+T_N$ were used as EV^- control cells, as we have previously shown that these cells do not bind EVs *in vivo* during LCMV infection (Fig. 10). Consistent with that, T_N cells were negative for the EV markers CD9/CD63 (Fig. 18B).

EV^+CD8^+ T_E cells showed significantly higher MFIs of CD9/CD63, CD54, and MHC-II than their MFG-$E8^-$ counterparts and T_N $CD8^+$ T cells (Fig. 18B). Furthermore, the frequencies of cells positive for these markers were also increased in EV^+CD8^+ T_E cells. When we examined the images of CD9/CD63, CD54, and MHC-II positive $CD8^+$ T cells, we observed a spot-like staining pattern of the respective markers similar to the MFG-E8 staining (Fig. 18C). In contrast, while EV^+ T_E $CD8^+$ T cells displayed a significantly higher MFI of CD86 than MFG-$E8^-$ T_E cells, there was no difference in the signal intensity compared to T_N cells. Like the other tested APC/EV markers, T_E $CD8^+$ T cells showed punctate CD86 staining, while T_N cells revealed a uniform cell surface staining (Fig. 18C). Consistent with that, CD86 is expressed by resting T_N cells but downregulated in $CD44^+CD8^+$ T cells [256]. Together, these findings suggest that T_E cells acquired the tested surface molecules through EVs from APCs.

During early LCMV infection, the vascular endothelium is destroyed by T cell mediated-killing of $CD31^+$ endothelial cells [257]. To test whether activated $CD8^+$ T cells bind apoptotic bodies generated during LCMV infection, we assessed whether CD31 is present on MFG-$E8^+$EVs attached to $CD8^+$ T cells. However, almost no EV^+CD8^+ T cells were positively stained with CD31 (Fig. 18B). Thus, the majority of EVs attached to T_E $CD8^+$ T cells during LCMV infection are not derived from apoptotic cells but from activated APCs.

We also detected $marker^+$ EVs, which were not positively stained with MFG-E8-eGFP on $CD8^+$ T cells (Fig. 18B, C). It is possible that a small proportion of EVs falls below the detection limit of the injected MFG-E8-eGFP or that MFG-$E8^-$APC-$marker^+$ EVs were generated during organ preparation when MFG-E8-eGFP was absent.

To further confirm that EV^+T_E cells acquired the tested markers through APC-derived vesicles *in vivo*, we determine the co-localisation of MFG-E8-eGFP with the mentioned APC/EV markers on MFG-$E8^+CD8^+$ T_E cells. A spot mask was generated in the IDEAS software to identify MFG-$E8^+$ and $marker^+$ spots (Fig. 19A). Then, the IDEAS feature 'bright detail similarity' (BDS) was used to quantify the co-localisation of identified spots. A median BDS score of > 0.7 represents

co-localisation of the two markers analysed, whereas a BDS score < 0.7 indicates no or only weak co-localisation. MFG-E8-eGFP colocalised with CD9/CD63 on 73 % of EV$^+$CD8$^+$ T cells with a BDS score of 1.0 (Fig. 19B). Furthermore, high frequencies of EV$^+$CD8$^+$ T cells also showed co-localisation of MFG-E8-eGFP with CD54 (82 %, BDS score 1.1), CD86 (86 %, BDS score 1.2) and MHC-II (67 %, BDS score 0.9) on their bound EVs (Fig. 19B). Together, these results strongly suggest that the majority of EVs that bind to CD8$^+$ T cells *in vivo* during LCMV infection are derived from APCs.

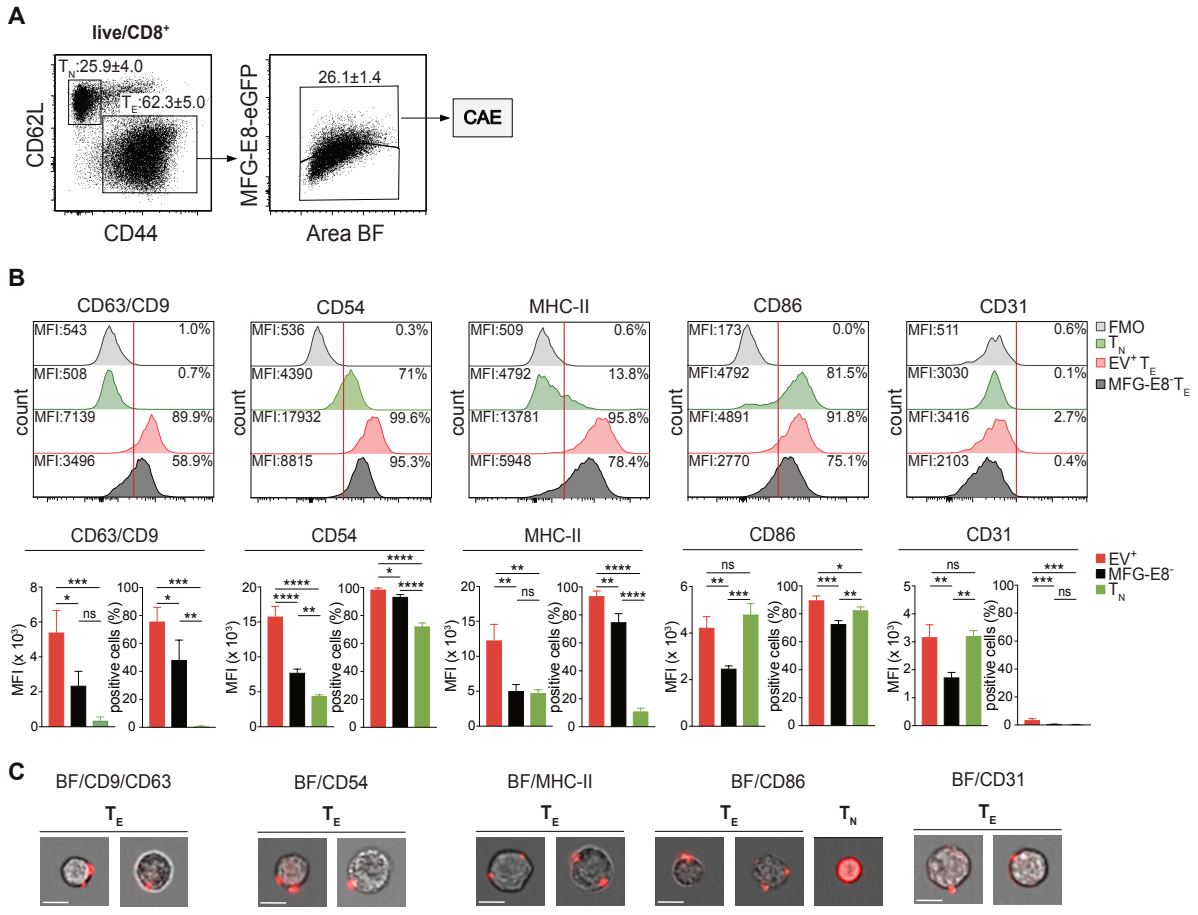

Figure 18: EVs attached to activated CD8$^+$ T cells carry APC markers.
Mice were infected with LCMV$_{Arm}$ and injected with MFG-E8-eGFP (100 µg/mouse) on day 5 p.i. (A) Gating strategy used to investigate APC and EV markers on live/dead$^-$, CD62L$^+$CD44$^-$ T$_N$ and EV$^+$ and MFG-E8$^-$CD62L$^-$CD44$^+$T$_E$ CD8$^+$ T cells. MFG-E8$^+$EV$^+$T$_E$ cells were identified by the CAE-RF. Shown are the frequencies ± SD of the respective population. (B) Surface proteins of live/dead$^-$ T$_N$, EV$^+$ and MFG-E8$^-$CD62L$^-$CD44$^+$CD8$^+$ T cells were detected by IFC with fluorescently labelled antibodies: anti-CD9/CD63 (combined staining), anti-CD54, anti-MHC-II, anti-CD86 and anti-CD31. Histograms indicate MFIs and frequencies ± SD of cells positively stained for these proteins. Shown are unstained CD62L$^-$CD44$^+$CD8$^+$ T cells (grey, n=1), T$_N$ CD8$^+$ T cells (green, n=3), EV$^+$ (red) and MFG-E8$^-$ (black) T$_E$ CD8$^+$ T cells (n=3). Shown are representative results from 2 independent experiments. Scale bar 7 µm. For statistical analysis, the unpaired Student's t-test was used with *: p< 0.05, **: p< 0.01 and ***: p< 0.001. Figure from [239] Figure 8 and Supplemental Figure 7.

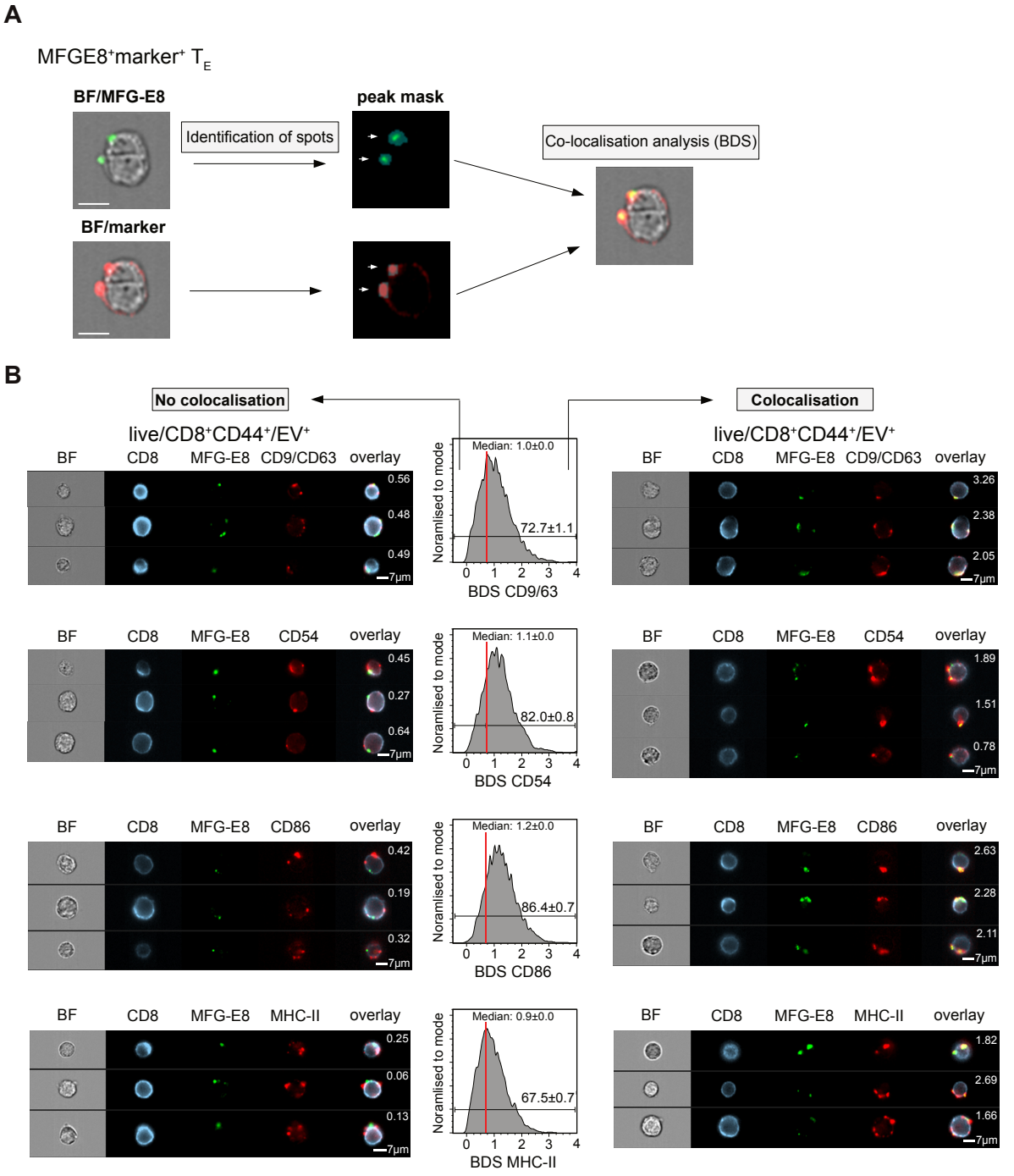

Figure 19: Substantial co-localisation of MFG-E8 and APC/EV markers on EV$^+$ T$_E$ CD8$^+$ T cells.
(A) The spot mask of the IDEAS software was used to identify and quantify MFG-E8-eGFP$^+$ and marker$^+$ spots on EV$^+$T$_E$ CD8$^+$ T cells, isolated from MFG-E8-eGFP injected, day 5-LCMV-infected mice (n=3). (B) The co-localisation of the EV-marker signal with the MFG-E8-eGFP signal on EV$^+$CD8$^+$ T$_E$ cells was calculated using the BDS feature available on IDEAS. The BDS score quantifies the overlap of MFG-E8-eGFP$^+$ and EV-marker$^+$ spots. We defined by visual inspection that cells having a BDS > 0.7 show a co-localisation of the fluorescence signal of MFG-E8-eGFP and the respective EV-marker in the same place. A BDS < 0.7 indicates no co-localisation of the two signals analysed. Median BDS scores and frequencies ± SD of EV$^+$ marker$^+$ T$_E$ CD8$^+$ T cells with co-localisation are shown in the histograms (n=3). Representative images display respective BDS scores. Scale bar 7 µm. Shown are representative results from 2 independent experiments. Figure modified from [239] Figure 8.

6.6 MFG-E8$^+$CD8$^+$ T cells display increased levels of nuclear NFATc1

APC-derived EVs that carry CD86, CD54 and MHC complexes have been demonstrated to activate T cells in an Ag-dependent manner *in vitro* [155, 165, 196]. Upon activation, TCR stimulation of CD8$^+$ T cells induces the rapid translocation of the transcription factor NFATc1 to the nucleus, which is crucial for CD8$^+$ T cell cytotoxicity during viral infection [27, 28]. To investigate whether EV$^+$CD8$^+$ T cell interactions influence TCR-signaling, we analysed the nuclear translocation of NFATc1 in MFG-E8$^+$ and MFG-E8$^-$CD8$^+$ T cells by MFG-E8-eGFP injection and IFC on day 5 post LCMV infection (Fig. 20A). We used the 'Similarity' feature provided by the IDEAS software to determine the extent of NFATc1 nuclear translocation. We found a significantly higher median SS score and an increased frequency of MFG-E8$^+$CD8$^+$ T cells with detectable nuclear NFATc1 translocation compared to MFG-E8$^-$ cells (Fig. 20B). As nuclear NFAT is rapidly exported after the termination of TCR-mediated signalling (nuclear halflife $t_{1/2} \sim 15$ min, [29]), our data indicate recent TCR stimulation, thus suggesting the contribution of EVs to CD8$^+$ T cell stimulation.

Next, we wanted to explore whether EV binding to CD8$^+$ T cells and the observed increase in nuclear NFATc1 in MFG-E8$^+$CD8$^+$ T cells is dependent on cognate T cell-DC interaction. For this, we transferred TCR-transgenic CD8$^+$ T cells that recognise LCMV gp_{33-34}/D^b MHC-I on DCs (P14 CD8$^+$ T cells) [77] side by side with TCR-transgenic CD8$^+$ T cells that do not recognise LCMV peptides but the ovalbumin peptide $OVA_{257-264}/K^b$ (OT-I CD8$^+$ T cells) [240] into LCMV-infected mice. In this case, OT-I cells should not get sustained DC contact and subsequent TCR stimulation in the same mouse. As only Ag-experienced T cells bind EVs (Fig. 10), we *in vitro* stimulated P14 and OT-I CD8$^+$ T cells for two days with anti-CD3/CD28 antibodies before their transfer into day 2-LCMV-infected mice. Three days after transfer, MFG-E8-eGFP was injected, and CD8$^+$ T cells were analysed for NFATc1 nuclear translocation by IFC (Fig. 21A). No significant difference regarding the EV-decoration of P14 and OT-I CD8$^+$ T cells were observed (Fig. 21B). However, we detected a lower frequency of MFG-E8$^+$OT-I cells compared to endogenous MFG-E8$^+$CD44$^+$CD8$^+$ T cells. Thus, EVs bind to activated CD44$^+$CD8$^+$ T cells independently of TCR-specificity, although to a slightly lesser extent.

We next compared nuclear translocation of NFATc1 in MFG-E8$^+$ and MFG-E8$^-$P14, OT-I and CD44$^+$ endogenous CD8$^+$ T cells. We found a significantly higher SS score and higher levels of nuclear NFATc1 in MFG-E8$^+$ P14 CD8$^+$ T cells compared to their MFG-E8$^-$ counterparts (Fig. 21C). Notably, the amount of nuclear NFATc1 of MFG-E8$^+$P14 CD8$^+$ T cells also exceeded that of *in*

vitro stimulated P14 cells. Similarly, endogenous MFG-E8^{+}CD8^{+} T cells exhibited elevated frequencies of cells with nuclear translocation of NFATc1 compared to MFG-E8^{-} endogenous CD8^{+} T cells. Although the frequency of OT-I cells with nuclear NFATc1 was much lower compared to that of P14 and endogenous CD44^{+}CD8^{+} T cells, MFG-E8^{+} OT-I T cells had slightly but significantly more NFATc1 in the nucleus than OT-I T cells without bound EVs (Fig. 21C). The elevated nuclear translocation of NFATc1 in MFG-E8^{+} OT-I cells, which do not recognise pMHC complexes on EVs generated during LCMV infection, may be explained by co-stimulatory molecules present on the EV surface. Together, these results further support the idea that EVs may promote the continuous stimulation of activated effector CD8^{+} T cells during acute LCMV infection.

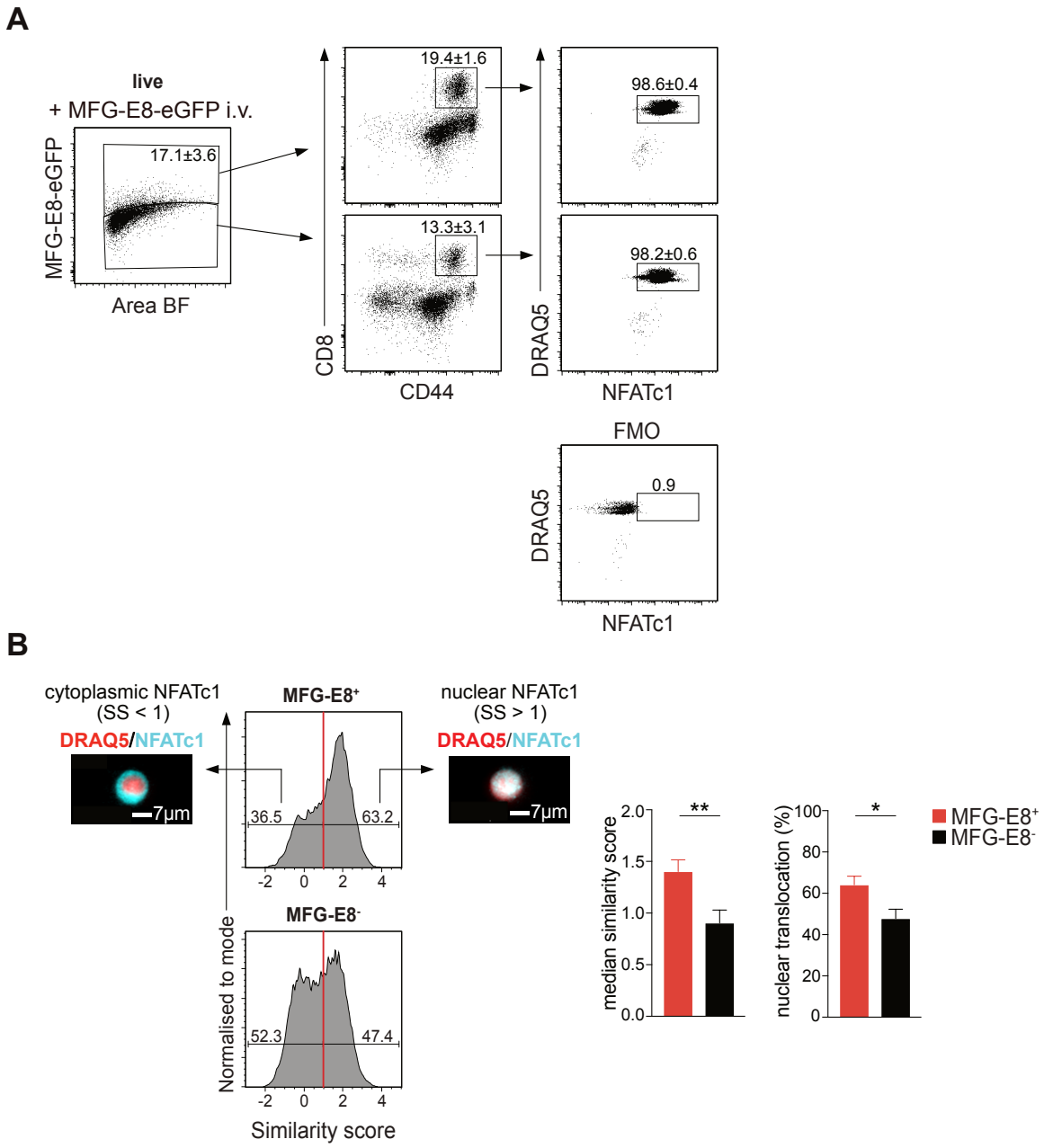

Figure 20: Increased nuclear translocation of NFATc1 in MFG-E8$^+$CD44$^+$CD8$^+$ T cells.

Mice were infected with LCMV$_{Arm}$ (n=3), MFG-E8-eGFP (100 µg/mouse) was injected on day 5 p.i., isolated splenocytes were immediately fixed with 4 % PFA and stained for surface markers before permeabilisation. Then permeablised cells were stained intracellularly and analysed by IFC. (A) Gating strategy to analyse nuclear translocation of NFATc1 in MFG-E8$^+$ and MFG-E8$^-$CD44$^+$CD8$^+$ T cells. Frequencies of the respective population are indicated. (B) To assess the nuclear translocation of NFATc1 in Draq5$^+$NFATc1$^+$MFG-E8$^+$ and MFG-E8$^-$CD44$^+$CD8$^+$ T cells, the co-localisation of the nuclear DRAQ5 (red) and NFATc1 (cyan) images was determined using the similarity feature of the IDEAS software. Cells with SS > 1 mainly display nuclear NFATc1, whereas cells with SS <1 show cytoplasmic NFATc1. Representative histograms of the SS of MFG-E8$^+$ and MFG-E8$^-$CD44$^+$CD8$^+$ T cells with frequencies of cells with cytoplasmic and nuclear NFATc1 are shown. Representative images next to the histogram display cells with cytoplasmic NFATc1 (left) and nuclear NFATc1 (right). Scale bar 7 µm. Bar graphs (left) show the median SS ± SD (left) and the frequencies ± SD (right) of MFG-E8$^+$ and MFG-E8$^-$CD44$^+$CD8$^+$ T cells. Shown are representative results from 4 independent experiments. For statistical significance unpaired Student's t-test was used with *: p< 0.05, **: p< 0.01 and ***: p< 0.001.

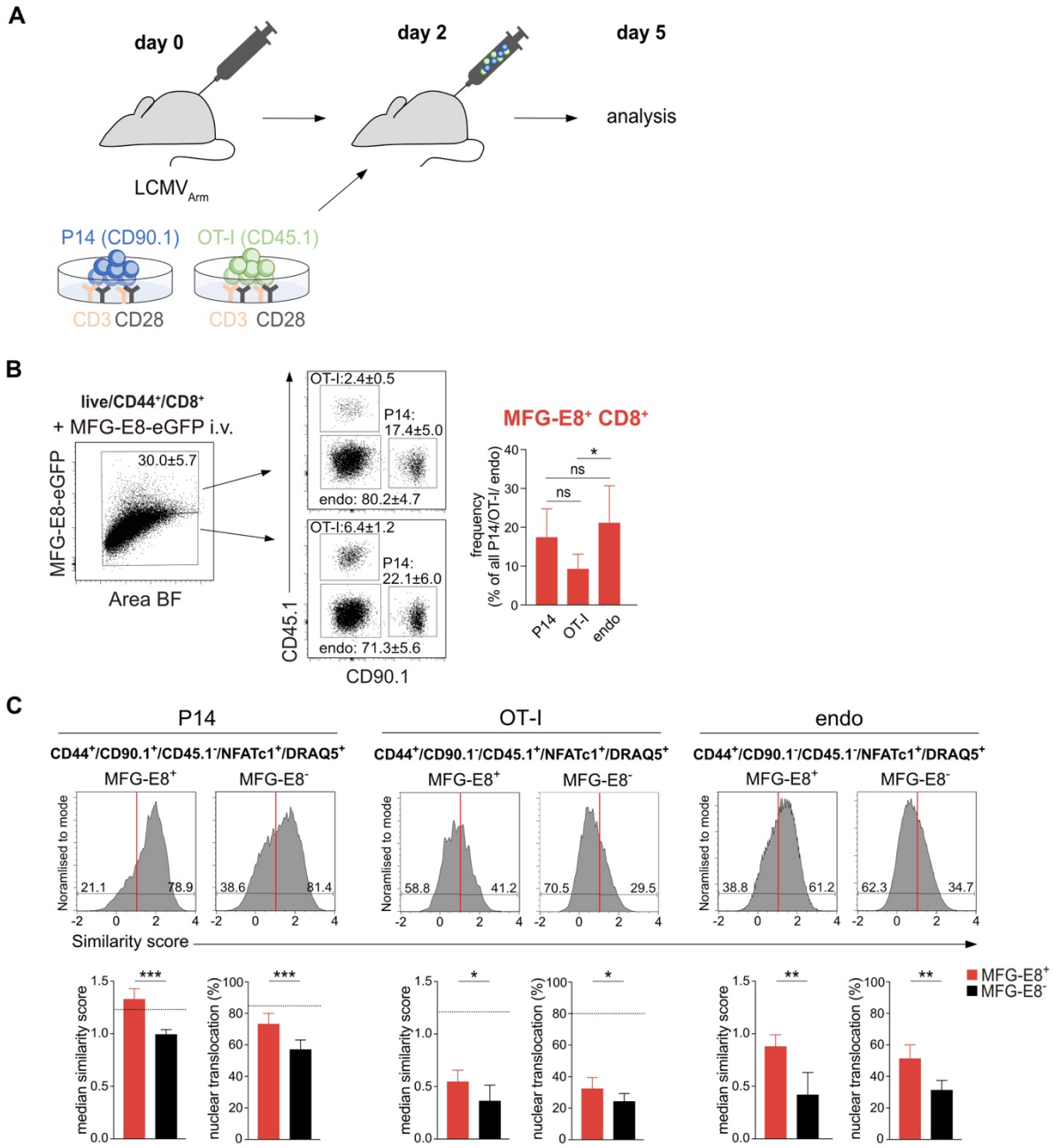

Figure 21: Ag-specific and non-specific MFG-E8$^+$CD44$^+$CD8$^+$ T cells display more nuclear NFATc1 than their MFG-E8$^-$ counterparts.

(A) Schematic of the experimental setup for analysing nuclear NFATc1 in transferred P14 and OT-I CD44$^+$CD8$^+$ T cells. Splenic P14 and OT-I CD8$^+$ T cells were stimulated *in vitro* with anti-CD3 and anti-CD28 antibodies for 48 hours and then transferred into day 2-LCMV-infected C57BL/6 mice. After three days, MFG-E8-eGFP (100 µg/mouse) was injected, and nuclear translocation of NFATc1 was analysed in MFG-E8$^+$ and MFG-E8$^-$CD44$^+$ P14, CD44$^+$ endogenous and CD44$^+$ OT-I CD8$^+$ T cells. (B) Dot plots show the gating of MFG-E8$^+$ and MFG-E8$^-$CD90.1$^+$ CD44$^+$ P14, CD45.1$^+$CD44$^+$ OT-I cells and CD90.1$^-$CD45.1$^-$ CD44$^+$ endogenous CD8$^+$ T cells (endo) with average percentages ± SD (n=6). The bar graph displays the average frequencies ± SD of MFG-E8$^+$CD44$^+$ P14, OT-I, or endogenous CD8$^+$ cells. (C) Representative histograms show the SS of MFG-E8$^-$ and MFG-E8$^+$ CD44$^+$ P14 (left), CD44$^+$ OT-I (middle), and endo (right) CD44$^+$CD8$^+$ T cells with frequencies of cells with a SS >1 and <1. The bar graphs show the frequencies and the median similarity scores ± SD of MFG-E8$^+$ and MFG-E8$^-$CD44$^+$P14 (left), CD44$^+$ OT-I (middle) and endo (right) CD44$^+$CD8$^+$ T cells. Results from 6 mice were pooled from 2 independent experiments. Dotted horizontal lines represent the SS of *in vitro*-activated P14 and OT-I right before their transfer into C57BL/6 mice (see A). For statistical significance one-way ANOVA (B) and unpaired Student's t-test (C) were used with *: p< 0.05, **: p< 0.01 and ***: p< 0.001.

6.7 No increased Nur77-eGFP expression in EV$^+$CD44$^+$CD8$^+$ T cells

TCR signalling in T cells rapidly induces the expression of *Nur77*, an immediate early gene [258, 259]. To further address whether EVs may stimulate TCR signalling, we made use of the Nur77-eGFP transgenic mouse where eGFP is under control of the *Nr4a1* (*Nur77*) promoter and can thereby be used as a reporter for antigen receptor signalling [258, 259]. Nur77-eGFP transgenic mice were infected with LCMV and injected with MFG-E8 C-terminally fused to mCherry (MFG-E8-mCherry) on day 5 after infection. Then, MFG-E8-mCherry$^+$CD8$^+$ T cells were quantified by IFC and the CAE-RF. *Nur77-eGFP* expression sharply increased upon LCMV infection compared to non-infected mice (Fig. 22, histogram) and was weakly, although not significantly, upregulated in activated EV$^+$CD44$^+$CD8$^+$ T cells in comparison to MFG-E8$^-$ CD44$^+$CD8$^+$ T cells in the same mouse (Fig. 22, bar graph). Nr4a1 has a short half-life (2-4 h), while the half-life of eGFP is up to 24 h [259]. Consequently, eGFP levels may accumulate over time, not reflecting recent TCR signalling, potentially induced by associated EVs. Therefore, the slight increase in the MFI of eGFP might still in hint towards an increased TCR-mediated activation of EV-decorated CD8$^+$ T cells.

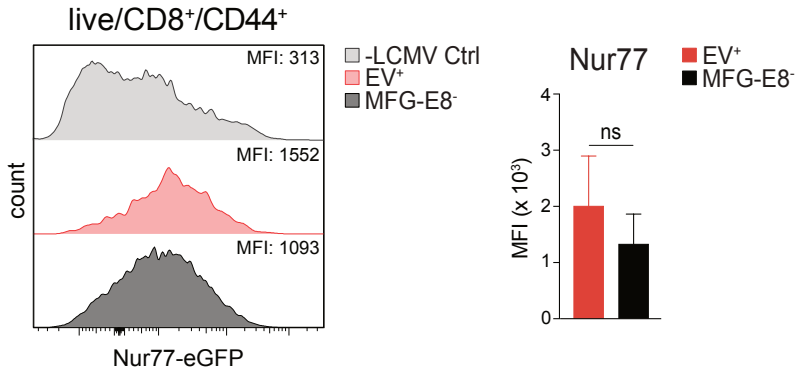

Figure 22: Comparable expression levels of the Nur77 transgenic reporter in MFG-E8$^+$ and MFG-E8$^-$CD44$^+$CD8$^+$ T cells in LCMV-infected mice.
MFG-E8-mCherry (100 µg/mouse) was injected into day 5-LCMV-infected mice, and live/dead$^-$MFG-E8$^+$ effector CD8$^+$ T cells were analysed by IFC and cells were sorted by the CAE-RF [239]. Representative histograms showing *Nur77-eGFP* expression in live/dead$^-$CD44$^+$CD8$^+$ T cells from non-infected mice (grey, n=1), of EV$^+$ (red) and MFG-E8$^-$ (black) CD44$^+$CD8$^+$ T cells from LCMV-infected mice (n=3). The bar graph shows the MFIs ± SD of Nur77-eGFP in EV$^+$ and MFG-E8$^-$CD44$^+$CD8$^+$ T cells. Shown are representative results from 2 independent experiments. For statistical significance, the unpaired Student's t-test was used with *: p< 0.05, **: p< 0.01 and ***: p< 0.001.

6.8 Proteomic analysis reveals differences in protein expression between MFG-E8$^+$ and MFG-E8$^-$CD8$^+$ T cells

To analyse whether EV binding induces changes in protein expression in activated CD8$^+$ T cells, we performed a proteome analysis of EV$^+$ and MFG-E8$^-$ T_E CD8$^+$ T cells. For this, mice were infected with $LCMV_{Arm}$, MFG-E8-eGFP was injected on day 5 p.i., and splenic MFG-E8$^+$ or MFG-

E8$^-$CD62L$^-$CD44$^+$CD8$^+$ T cells were FACS sorted. After sorting, purity ranged from 88 to 90 % (Fig. 23A). Sorted cells were lysed, peptides were identified and quantified by mass spectrometry (MS) followed by MaxQuant analysis. MS was performed by Jingyuan Cheng and Felix Meissner from the Max Planck Institute of Biochemistry in Munich and the analysis was performed by Tobias Straub from the LMU Munich. Using MS, 4481 proteins were detected in MFG-E8$^+$ and MFG-E8$^-$ effector CD8$^+$ T cells on day 5 after infection. Fig. 23B depicts two heat map presentations of 50 proteins with significantly different ($p \leq 0.05$) relative abundances in MFG-E8$^+$ and MFG-E8$^-$ effector CD8$^+$ T cells.

Generally, MFG-E8$^+$ CD8$^+$ T cells show a higher abundance of proteins involved in gene expression and DNA replication (Pwp1, Wdr43, Pole), protein synthesis and protein folding (Eif3f, Eif4a1,Cluh, Clpb) or proliferation (Grn, Cdk4, Hells) (Fig. 23B, left heat map) [252, 260]. When we next looked for proteins that play roles in CD8$^+$ T cell activation, we found a higher amount of Stx4 in MFG-E8$^+$ CD8$^+$ T cells, which is crucial for CD8$^+$ T cell-mediated cytotoxic killing of target cells [261]. At the immune synapse, Stx4 has been shown to mediate the exocytosis of lytic granules in CD8$^+$ T cells [261]

Conversely, in MFG-E8$^-$ CD8$^+$ T cells, we found an increased amount of Pdcd4, which inhibits cytoplasmic mRNA translation [262, 263] (Fig. 23B, right heat map). Furthermore, Pdcd4-deficient CD8$^+$ T cells display an increased production of effector molecules, including IFN-γ and show greater control of tumour growth *in vivo* [264]. Similarly, deficiency of Mst1, which was more abundant in MFG-E8$^-$CD8$^+$ T cells, results in enhanced cytotoxicity and suppression of tumour progression *in vivo* [265]. However, we also detected proteins involved in T cell activation more abundant in MFG-E8$^-$CD8$^+$ T cells. For example, protein levels of Plcg1, which is involved in TCR-mediated signalling [266], were enriched in MFG-E8$^-$ CD8$^+$ T cells.

Besides these examples, we detected several proteins with yet unknown function enriched in MFG-E8$^+$ or MFG-E8$^-$CD8$^+$ T cells. These results demonstrate that there are numerous proteins differentially regulated in MFG-E8$^+$ and MFG-E8$^-$CD8$^+$ T cells and suggest that they are not only phenotypically but also functionally different.

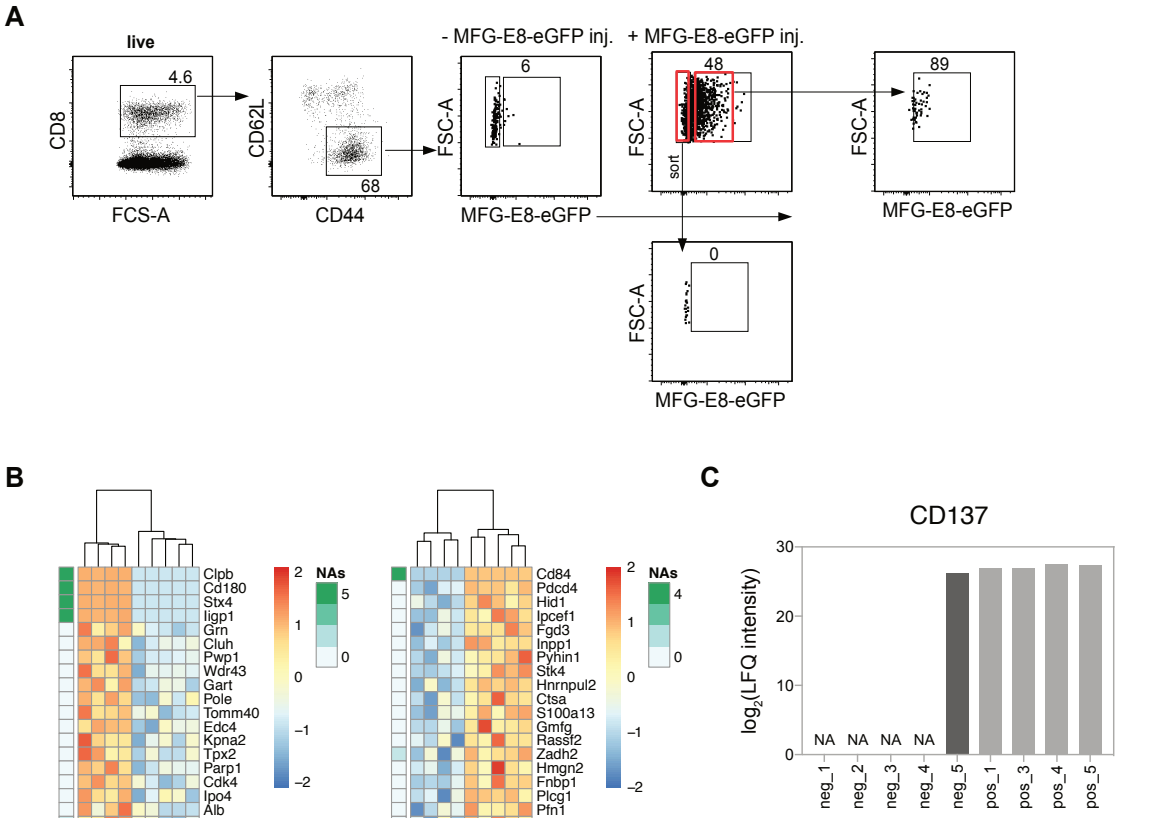

Figure 23: MFG-E8$^+$CD8$^+$ T cells show a high abundance of proteins driving proliferation and protein synthesis.

Day 5 LCMV-infected mice (n=3) were injected with MFG-E8-eGFP (100 µg/mouse) and MFG-E8$^+$/MFG-E8$^-$ live/dead$^-$CD62L$^-$CD44$^+$CD8$^+$ T cells were FACS sorted and subjected to proteome analysis. (A) Gating strategy and purity check of sorted MFG-E8$^+$ and MFG-E8$^-$ effector CD8$^+$ T cells. After the sort, MFG-E8$^+$ CD8$^+$ T cells had a purity of around 90 %. Numbers in the dot plots illustrate the frequencies of the respective cell population. (B) Heatmap presentation of 50 proteins that display significantly different relative abundances ($p \leq 0.05$) in MFG-E8$^+$ and MFG-E8$^-$ effector CD8$^+$ T cells on day 5 p.i., identified by MS-based proteomics. Shown are the replicates of MFG-E8$^+$ (pos_1, pos_3, pos_5, pos_5) (n=4) and MFG-E8$^-$ (neg_1, neg_2, neg_3, neg_4, neg_5) (n=5) CD8$^+$ T cells sorted from day 5 LCMV-infected mice. The relative abundance of each indicated protein in each sample is colour-coded based on the z-score of the normalised $\log_2$(LFQ (label free quantification) intensity) after imputation (Red= upregulated; blue =downregulated)[267]. The left heatmap shows proteins significantly enriched in MFG-E8$^+$CD8$^+$ T cells and the right heat map displays proteins significantly upregulated in MFG-E8$^-$CD8$^+$ T cells. The number of missing values (NA, not available) for each protein are indicated. (C) Bar graph showing original (raw) normalised $\log_2$ transformed LFQ intensities or missing values (NA) of CD137 in MFG-E8$^+$ (pos_1, pos_3, pos_4, pos_5) and MFG-E8$^-$ (neg_1, neg_2, neg_3, neg_4, neg_5) CD8$^+$ T cells. Data analysis was performed by Tobias Straub.

Although not significantly different abundant after missing-value correction (imputation) of the proteomic data, the protein CD137 (4-1BB) drew our attention. CD137 was found at similar levels in all MFG-E8$^+$CD8$^+$ T cells samples but could not be quantified in four of five MFG-E8$^-$CD8$^+$ T cell samples when we looked at the raw MS data (Fig. 23C). One reason for the missing values is that the abundance of a particular protein is below the detection limit in a specific sample, implying a low amount of CD137 in the majority of the MFG-E8$^-$CD8$^+$ T cell samples. CD137 is a co-stimulatory receptor, which is rapidly but transiently expressed after TCR-mediated cell activation [268, 269]. Furthermore, CD137 ligation was shown to positively regulate the proliferation and survival and to enhance effector functions of activated CD8$^+$ T cells, including IFN-γ secretion and cytotoxic killing [269-271]. To clarify whether CD137 is differentially expressed in EV$^+$ and MFG-E8$^-$CD8$^+$ T cells, mice were infected with LCMV$_{Arm}$, received MFG-E8-eGFP on day 5 p.i., and CD44$^+$CD8$^+$ T cells were analysed by IFC and the CAE-RF. We found a significantly higher MFI of CD137 in EV$^+$CD8$^+$ T cells than in MFG-E8$^-$CD8$^+$ T cells (Fig. 24A). Furthermore, a higher frequency of EV$^+$CD8$^+$ T cells was positively stained for CD137, suggesting that these cells received recent TCR stimulation, potentially by EVs. Representative images of EV$^+$ and MFG-E8$^-$CD44$^+$CD8$^+$ T cells show a surface expression of CD137, indicating that CD137 was not acquired by bound EVs (Fig. 24B).

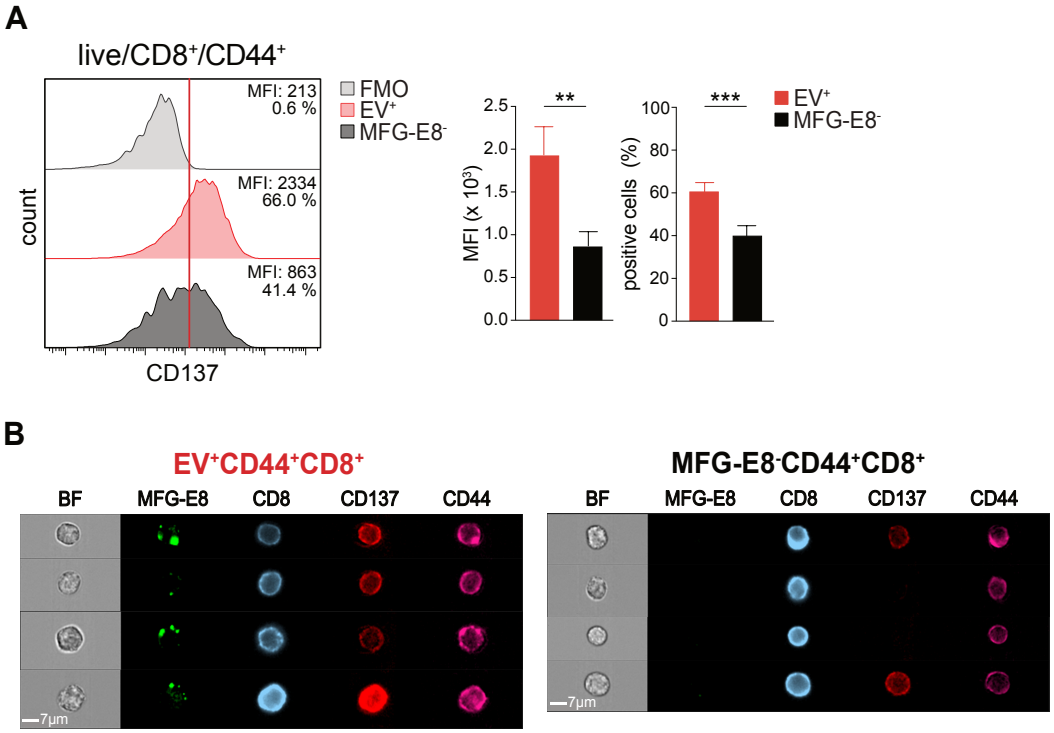

Figure 24: EV$^+$CD8$^+$ T cells display an increased expression of CD137 compared to MFG-E8$^-$ effector CD8$^+$ T cells. MFG-E8-eGFP (100 µg/mouse) was injected into mice (n=4) infected for 5 days with LCMV$_{Arm}$. CD44$^+$CD8$^+$ T cells were analysed by IFC and CAE-RF. (A) Representative histogram showing CD137 expression of live/dead$^-$ MFG-E8$^-$ (black), EV$^+$ (red), or unstained (grey) CD44$^+$CD8$^+$ T cells. Indicated are the MFI ± SD and the frequency ± SD of CD137$^+$ liveCD44$^+$CD8$^+$ cells. The bar graph shows the frequencies and MFIs ± SD in EV$^+$ (red) and MFG-E8$^-$ (black) CD44$^+$CD8$^+$ T cells (n=4). (B) Shown are representative images of BF, MFG-E8, CD8, CD137 and CD44 of EV$^+$ and MFG-E8$^-$CD8$^+$ T cells. Scale bar 7 µm. For statistical significance, unpaired Student's t-test was used with *: p< 0.05, **: p< 0.01 and ***: p< 0.001.

6.9 EV-decoration of human CD8$^+$ T cells increases following vaccination

Having demonstrated the occurrence and binding properties of EVs in a murine model of infection, we next wanted to test whether CD8$^+$ T cells from human peripheral blood also become EV-decorated during acute viral infection. For this, we prepared PBMCs from peripheral blood of six healthy volunteers who were immunised with a live attenuated yellow fever virus (YFV)-based vaccine (kindly provided by Prof. Dr Rothenfußer and Prof. Dr Krug from LMU Munich). Human PBMCs were analysed before and on days 7, 14, and 28 after vaccination and stained *in vitro* with MFG-E8-eGFP (Fig. 25A). While the frequency of CD8$^+$ T cells did not change over time, EV-decoration of CD8$^+$ T cells reached its maximum on day 14 after vaccination (Fig. 25B). Similarly, we detected the highest frequency of live, activated HLA-DR$^+$CD38$^+$ CD8$^+$ T cells on day 14 p.i., which then declined by day 28 after vaccination (Fig. 25C). Also, the highest level of EV-decorated activated HLA-DR$^+$CD38$^+$CD8$^+$ T cells occurred 2 weeks after immunisation (Fig. 25C, D). Similar to naïve CD8$^+$ T cells in the blood of LCMV-infected mice, non-activated HLA-DR$^-$CD38$^-$ CD8$^+$ T cells also displayed EV-decoration. Comparable to

activated $CD8^+$ T cells, the peak of EV^+ non-activated $CD8^+$ T cells occurred day 14 post-vaccination. However, EV-decoration of $HLA\text{-}DR^+CD38^+$ was greater than that of $HLA\text{-}DR^-CD38^-$ $CD8^+$ T cells, indicating that EVs generated during YFV vaccination tend to bind to activated $CD8^+$ T cells. To sum up, these data show that EV-decoration of $CD8^+$ T cells also occurs in human blood during acute viral infection, with a maximum of EV^+CD8^+ T cells at the peak of the $CD8^+$ T cell immune response [272, 273].

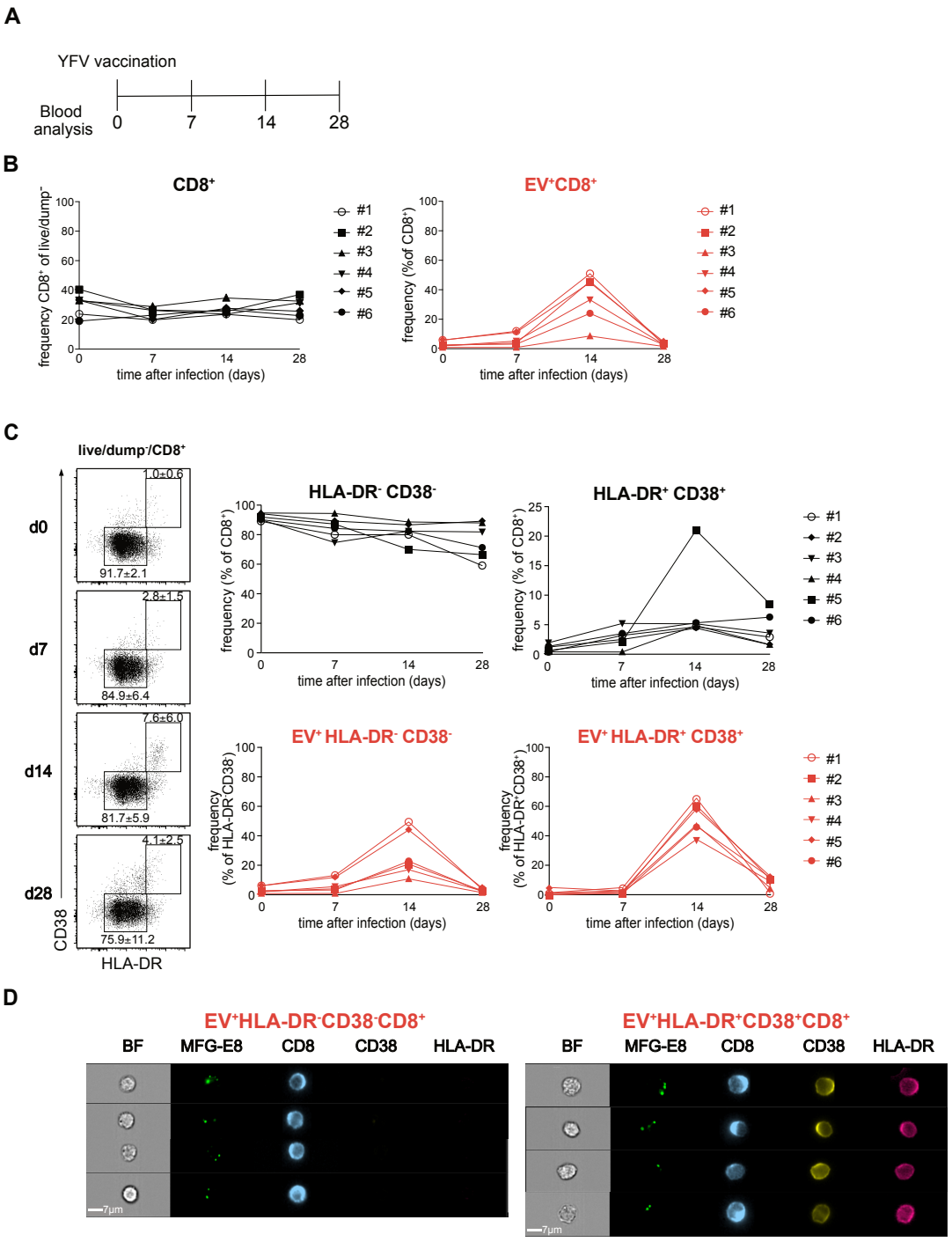

Figure 25: EV-decoration of human CD8⁺ T cells increases following yellow fever vaccination.
(A) Schematic experimental setup. Six healthy volunteers (#1-#6) were immunised with the live-attenuated yellow fever vaccine YFV-17D in a vaccine study planned and conducted by Prof. Dr Rothenfußer and Prof. Dr Krug at the LMU Munich. PBMCs were isolated from whole EDTA-blood samples before immunisation (0), and on days 7, 14 and 28 after vaccination and CD8⁺ T cells were analysed for their EV-decoration by MFG-E8-eGFP *in vitro* staining followed by IFC and CAE-RF. Non-CD8⁺ T cells were excluded from the analysis by gating on live/dead⁻CD19⁻CD14⁻ CD16⁻ CD56⁻ cells. (B) Graphs show the frequencies of CD8⁺ and EV⁺CD8⁺ T cells of each donor collected from peripheral blood before (d0) and on days 7, 14 and 28 after immunisation. (C) Representative dot blots showing total, live HLA-DR⁻CD38⁻ and HLA-DR⁺CD38⁺ human CD8⁺ T cells that were collected from peripheral blood before (d0) and on days 7, 14 and 28 after immunisation. Average frequencies of all donors ± SD of T cells subsets are indicated. Graphs show the frequencies of the total, live (black) and EV⁺ (red) HLA-DR⁻CD38⁻ and HLA-DR⁺CD38⁺ CD8⁺ T cells on days 0, 7, 14, 28 post-immunisation of each donor. (D) Shown are representative images of BF, MFG-E8, CD8, CD38 and HLA-DR of EV⁺CD38⁺HLA-DR⁺ and EV⁺CD38⁺HLA-DR⁺CD8⁺ T cells. Scale bar 7 µm.

YFV vaccination also elicits broad $CD4^+$ T cells responses [274]. Like $CD8^+$ T cells, we analysed $CD4^+$ T cells for their EV decoration and HLA-DR and CD38 expression before and on days 7, 14, and 28 post-immunisation. While the frequency of $CD4^+$ T cells did not change from day 0 to 28 after vaccination, EV-decoration of $CD4^+$ T cells was highest on day 14 (Fig. 26A). We observed an increase of activated HLA-DR^+CD38^+ $CD4^+$ T cells peaking around 2 weeks after vaccination, where 2 % of total $CD4^+$ T cells expressed these markers (Fig. 26B). In contrast to $CD8^+$ T cells, a large fraction of $CD4^+$ T cells became single positive for CD38 (HLA-DR^-CD38^+) after immunisation. In HIV-infected individuals, $CD38^+$ is highly expressed on HLA-DR^-CD4^+ T_{CM} cells, exhibiting a low expression of activation markers [275]. Despite their different activation status, EV-decoration of all $CD4^+$ T cell subsets peaked on day 14 after vaccination with a higher percentage of EV^+HLA-DR^-CD38^+ (T_{CM}) and activated EV^+HLA-DR^+CD38^+ $CD4^+$ T cells compared to non-activated EV^+HLA-DR^-CD38^- $CD4^+$ T cells (Fig. 26B, C). These results demonstrate that $CD8^+$ T cells and $CD4^+$ T cells become EV-decorated in the peripheral blood of YFV-immunized volunteers.

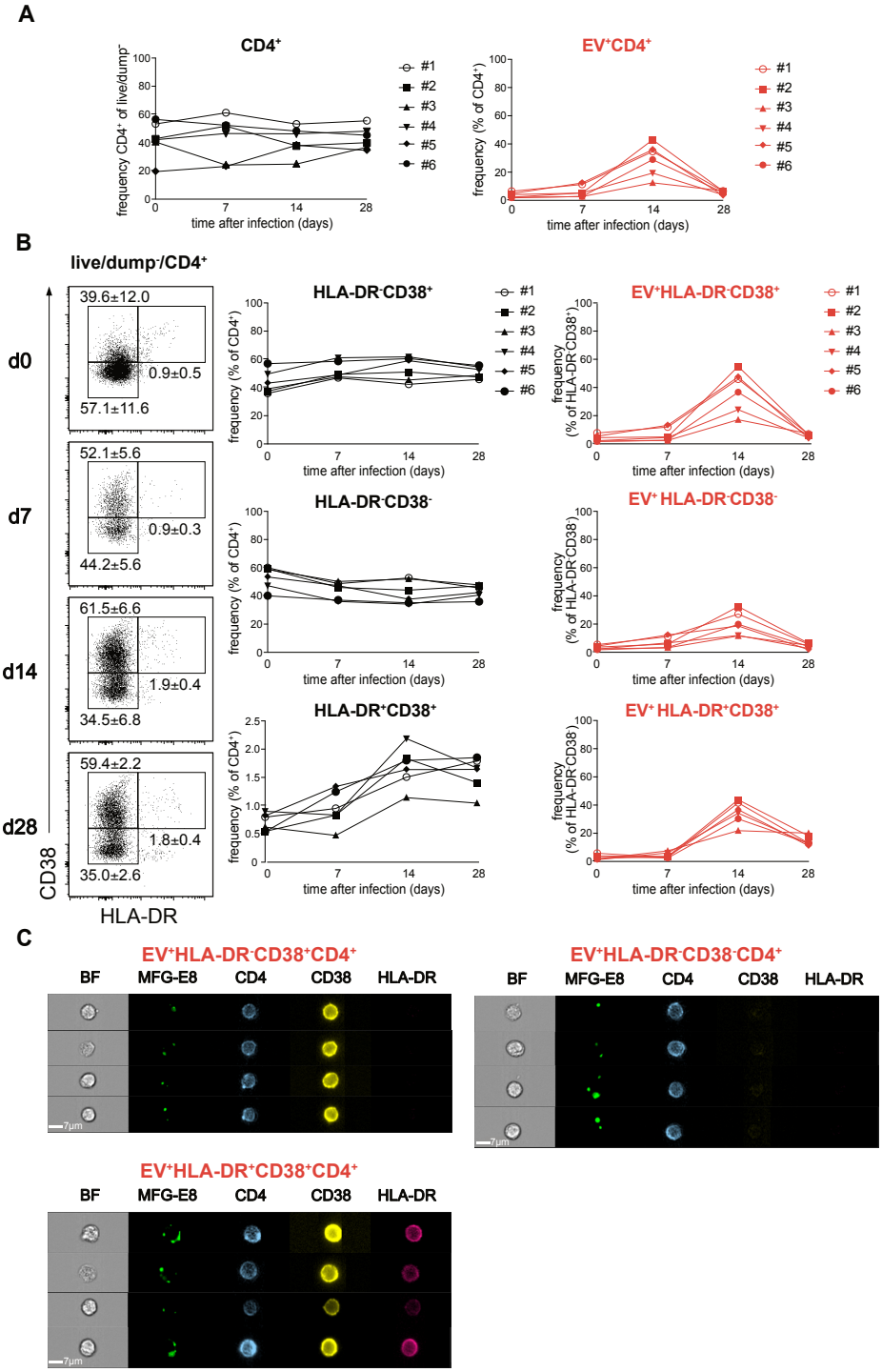

Figure 26: Human CD4⁺ T cells become EV-decorated following yellow fever vaccination.

Six healthy volunteers (#1- #6) were immunised with the yellow fever vaccine YFV-17D by Prof. Anne Krug at the LMU Munich. PBMCs were isolated from whole EDTA-blood samples before immunisation (0) and on days 7, 14 and 28 after vaccination. CD4⁺ T cells were purified and analysed for their EV-decoration by MFG-E8-eGFP *in vitro* staining, followed by IFC and CAE-RF. Non-CD4 T cells were excluded from the analysis by gating on live/dead⁻ CD19⁻CD14⁻CD16⁻CD56⁻ cells. (A) Graphs show the frequencies of total CD4⁺ (black) and EV⁺CD4⁺ (red) T cells of each donor collected from peripheral blood before (d0) and on days 7, 14 and 28 after immunisation. (B) Representative dot plots of total, live HLA-DR⁻CD38⁻, HLA-DR⁻CD38⁺ and HLA-DR⁺CD38⁺ human CD4⁺ T cells collected from peripheral blood before (d0) and from day 7, 14 and 28 after immunisation. Average frequencies of all donors ± SD of CD4⁺ T cells subsets are shown. Graphs show the frequencies ± SD of the total, live (black) and EV⁺ (red) HLA-DR⁻CD38⁻, HLA-DR⁻CD38⁺ and HLA-DR⁺CD38⁺CD4⁺ T cells for day 0, 7, 14, 28 post-immunisation of each donor. (C) Representative flow cytometry images of BF, MFG-E8, CD8, CD38 and HLA-DR of EV⁺HLA-DR⁻ CD38⁻, EV⁺HLA-DR⁻CD38⁺, and EV⁺HLA-DR⁺CD38⁺ CD4⁺ T cells on day 14 after vaccination. Scale bar 7 µm.

To test whether EV-decoration of T cells also occurs upon immunisation with subunit vaccines, we analysed PBMCs from two healthy volunteers that were immunised either with Vaxigrip (Sanofi Pasteur) or Influvac (Mylan), containing inactivated fragments of the viral surface protein haemagglutinin from different selected influenza virus strains (kindly provided by Dr. Katharina Eisenächer and Prof. Dr Anne Krug). PBMCs were isolated before and 7 days after immunisation and analysed for EV-decoration by *in vitro* straining with MFG-E8-eGFP. Although the percentage of the $CD8^+$ and $CD4^+$ T cell populations did not change over the time examined, the frequency of EV^+CD8^+ and EV^+CD4^+ ($CD3^+CD8^-$) T cells increased from day 0 to day 7 (Fig. 27A). In general, EV-decoration of $CD8^+$ T cells was more pronounced than that of $CD4^+$ T cells. To assess whether EVs bind to a specific $CD8^+$ or $CD4^+$ T cell subset, PBMCs were stained for CCR7 and CD45RA, which are established markers to discriminate naïve ($CCR7^+CD45RA^+$, T_N) and central memory ($CCR7^+CD45RA^-$, T_{CM}) from effector memory ($CCR7^-CD45RA^-$, T_{EM}) and $CD45RA^+$ effector memory ($CCR7^-CD45RA^+$, T_{EMRA}) T cell populations [276]. While the frequency of $CD8^+$ T_N cells increased after immunisation, it decreased for $CD8^+$ T_{EMRA} cells (Fig. 27B). We could not detect a clear trend regarding the frequencies of $CD4^+$ T cell subsets after immunisation (Fig. 27C). However, EV-decoration of all $CD8^+$ and $CD4^+$ T cell subsets increased after vaccination (Fig. 26B, C). Moreover, we did not observe a preferential binding of EVs to either of the subsets before or on day 7 after immunisation. These data demonstrate that EV-decoration of especially $CD8^+$ T cells occurs 7 days after immunisation with an inactivated subunit vaccine.

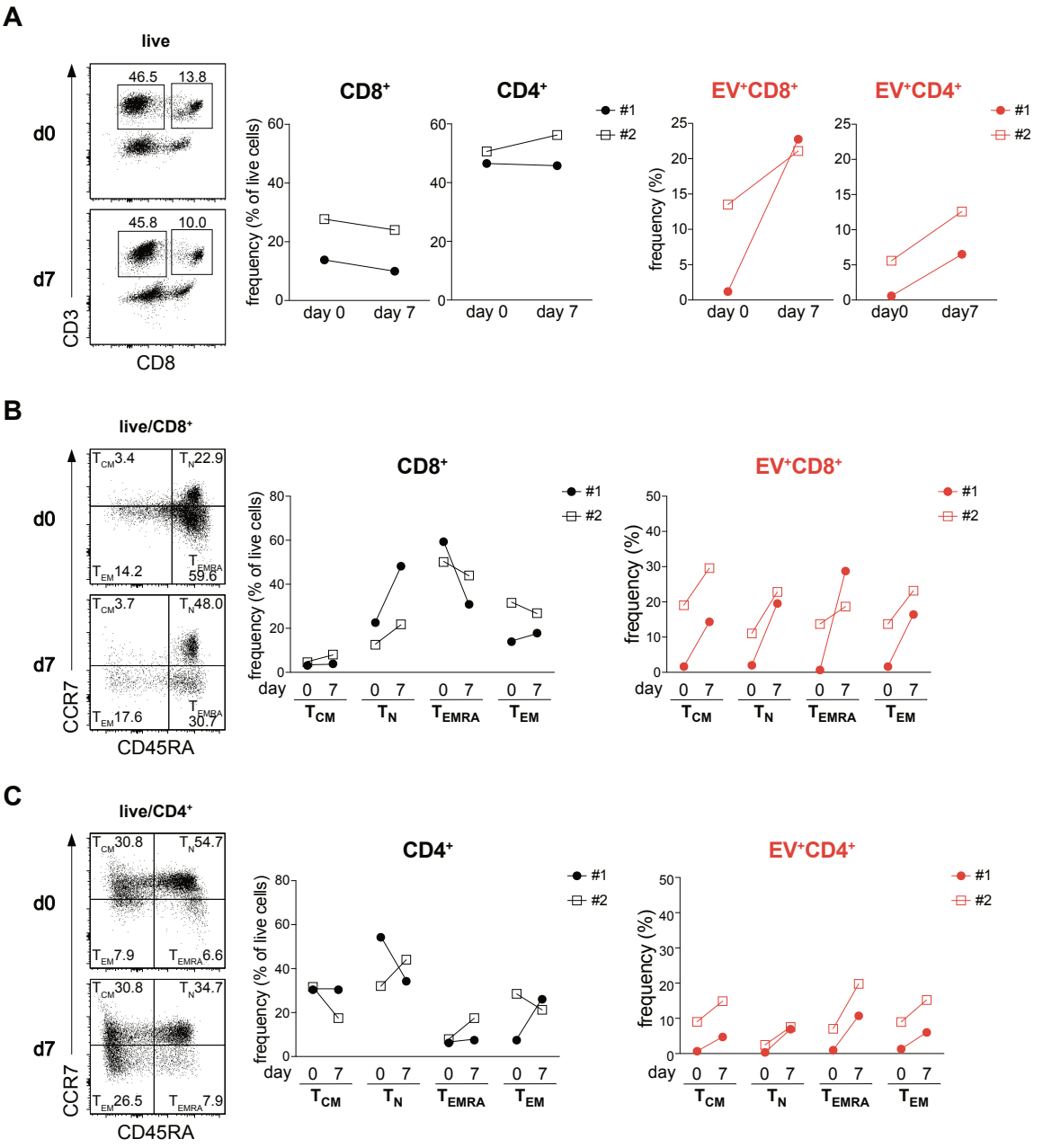

Figure 27: Human CD8⁺ and CD4⁺ T cells bind EVs following influenza vaccination.
Two healthy donors (#1 and #2) were immunised with subunit vaccines (Influvac, Vaxigrip) by Prof. Dr Anne Krug. Heparin blood was collected before and 7 days after immunisation, and PBMCs were isolated by Dr. Katharina Eisenächer. Live/dead⁻ CD8⁺ and CD4⁺ T cells were analysed for their EV-decoration by MFG-E8-eGFP *in vitro* staining followed by IFC and CAE-RF. (A) Representative dot plots display the frequencies of total, live/dead⁻ CD8⁺ ($CD3^+CD8^+$) and CD4⁺ ($CD3^+CD8^-$) T cells on day 0 and day 7 post-immunisation. Graphs show the frequencies of the total live (black) and EV⁺ (red) CD8⁺ and CD4⁺ T cells for each donor on day 0 and day 7 after vaccination. (B) Representative dot plots of total live, naïve ($CCR7^+CD45RA^+$, T_N), central memory ($CCR7^+CD45RA^-$, T_{CM}), effector memory ($CCR7^-CD45RA^-$, T_{EM}) and $CD45RA^+$ effector memory ($CCR7^-CD45RA^+$, T_{EMRA}) CD8⁺ collected from peripheral blood before (d0) or on day 7 after vaccination. Bar graphs show the frequencies of total live (black) and EV⁺ (red) T_N, T_{CM}, T_{EM}, T_{EMRA} CD8⁺ T cells before (d0) and day 7 post-immunisation of each donor. (C) Representative dot plots of total live, T_N, T_{CM}, T_{EM} and T_{EMRA} CD4⁺ collected from peripheral blood before (d0) or on day 7 after vaccination. Bar graphs show the frequencies of total live (black) and EV⁺ (red) CD4⁺ T cell subsets before (d0) and day 7 post-immunisation of each donor.

7 Discussion

The *in vivo* analysis of apoptotic and naturally produced EVs has remained a significant challenge. Here, upon injection of the PS-binding MFG-E8-eGFP reagent and the analysis of PS^+ cells by IFC and a CAE-RF, we successfully quantified EV^+ and apoptotic cells *in vivo* during acute LCMV infection.

7.1 Analysis of apoptotic cells *in vivo*

Virus-infected DCs, macrophages, and the splenic microarchitecture are destroyed by $CD8^+$ T cell-mediated killing of target cells during the early stages of LCMV infection [74, 106]. Consistent with that, the frequency and the total number of MFG-$E8^+$ apoptotic cells, including apoptotic DCs, significantly increased upon LCMV infection compared to non-infected mice. However, we unexpectedly identified the majority (90 %) of MFG-$E8^+$ cells not to be apoptotic but rather to be associated with PS^+EVs.

Apoptosis was induced in only 1- 2 % of B cells, $CD8^+$ T_{CM} and $CD4^+$ T_{CM} cells on day 5 post-LCMV-infection. The detection of apoptotic $CD8^+$ is consistent with reports describing IFN-induced attrition of $CD44^+CD8^+$ T_{CM} cells 2 to 4 days after $LCMV_{Arm}$ infection [107-109]. However, conversely to our data, around 25 % of Annexin $V^+CD44^{hi}CD8^+$ T cells were detected *in vitro* on day 2 p.i. [107]. Furthermore, following viral clearance, previous studies reported high frequencies of apoptotic virus-specific T cells in the spleen of LCMV-infected mice [277, 278], while we hardly observed apoptosis of $CD8^+$ T cells on day 10 post-infection. The generally low frequency of detected apoptotic cells in both non- and LCMV-infected mice is probably due to the rapid removal of dead cells by phagocytes *in vivo* [279]. Other reasons for these differences might be the time point of analysis and the method used to identify apoptotic cells. Analysis of apoptotic $CD8^+$ T cells was mostly performed *ex vivo* either by Annexin V staining or by TUNEL assay and active caspase 3 staining [107-109, 277, 278]. These methods require tissue dissociation, specific buffers or culturing of cells before analysis, thereby preventing their *in vivo* application and the detection of apoptotic cells *in situ*. As cells may die during organ preparation and cell incubation, the quantification of apoptotic cells *in vitro* might not reflect their numbers *in situ* in living organisms. Furthermore, Annexin V positivity of $CD44^{hi}CD8^+$ T cells from LCMV-infected mice, directly analysed *ex vivo* by flow cytometry, did not correlate with DNA fragmentation or caspase 3 activation [277, 278, 280]. These experiments show that

the flow cytometric analysis of PS^+ cells does not allow the discrimination of PS^+ apoptotic from PS^+ living cells.

Consequently, PS exposure on living cells was suggested to occur upon lymphocyte activation in the absence of apoptosis [277, 281, 282]. Consistent with that, Annexin V has been described to bind to viable T cells and B cells upon Ag-receptor engagement [282-284]. Although PS is transiently exposed to the surface upon increased intracellular Ca^{2+} levels [93], our analysis of PS^+ cells by IFC revealed that a high frequency of B cells and activated $CD8^+$ T cells were decorated with PS^+EVs upon LCMV infection, rather than exposing PS on the surface themselves. As no image analysis was performed, it might be possible that a significant fraction of Annexin V^+ activated lymphocytes detected in previous reports were, in fact, associated with PS^+ EVs.

Together, we show that the injection of MFG-E8-eGFP followed by deep learning-based image analysis of PS^+ cells is a reliable method to faithfully examine and discriminate apoptotic cells from EV-decorated cells *in vivo.*

7.2 EV-T cell interactions *in vivo*

EVs have been considered to enable cell-to-cell communication that initiates and regulates immune responses [reviewed in 183]. Particularly, EVs secreted by mature APCs were described to act as antigen-presenting platforms that contribute to the priming and activation of T cells *in vitro* and *in vivo* [158, 165, 166, 189, 193, 194, 285].

DC- and B cell-derived EVs that carry MHC-II, CD86, and CD54 have been shown to activate naïve and primed $CD4^+$ T cells *in vitro* [155, 165, 169, 177, 189]. Furthermore, also naïve $CD8^+$ T cells could be directly stimulated *in vitro* by APC-derived EVs that express the cognate pMHC, CD54 and CD80 [193, 194, 196]. However, the stimulatory activity of free EVs, especially the priming of naïve T cells, greatly increased when EVs interacted with bystander DCs [158, 189, 199, 200, 213]. Moreover, previous *in vivo* studies demonstrated that pMHC complexes could be transferred intercellularly by EVs to mature DCs or B cells, which then efficiently primed cognate $CD8^+$ and $CD4^+$ T cell responses [158, 172, 177, 189, 198, 200]. Therefore, pMHC carrying EVs are currently considered to activate and amplify T cell responses *in vivo* only when captured and presented by recipient APCs [172, 189, 198-200]. In line with this, we found high frequencies of EV^+ DC and B cells in LCMV-infected mice, suggesting that these cells may participate in the stimulation of T cells by acquiring circulating EVs. As an example, FDCs, which do not express MHC-II molecules, were shown to be decorated with MHC-II carrying EVs that

might contribute to the stimulation of T cells in GCs [168]. Besides that, the associated EVs may be derived from the APC itself, which upon secretion, remained attached to their surface and thereby present pMHC complexes to T cells [reviewed in 183]. However, whether T cells, in addition to their interaction with APC-associated EVs, capture free EVs *in vivo* has not been reported yet. In this study, we show for the first time that free APC-derived EVs bind to $CD4^+$ and $CD8^+$ T cells *in vivo* in the spleen and blood of infected mice and vaccinated humans. Although T cells themselves may release EVs upon TCR stimulation *in vitro* [167, 286, 287], we found the majority of $CD8^+$ T cell-associated EVs to be enriched for the aforementioned EV and APC markers (CD63, CD9, MHC-II, CD86, CD54). The fact that murine $CD44^+$ T cells do not express MHC-II [288] or CD86 [256] strongly indicates that the T cell-associated EVs are APC-derived and carry the molecules necessary for the co-stimulation of $CD8^+$ T cells and the activation of $CD4^+$ T cells. However, we were not able to determine the presence of MHC-I on $CD8^+$ T cell-associated MFG-$E8^+$ EVs. MHC-I is constitutively expressed on all nucleated cells [289], including $CD8^+$ T cells, making it challenging to distinguish MHC-I molecules present on APC-derived MFG-$E8^+$ EVs from those on the T cell surface itself. As we used the BDS feature to determine co-localisation of APC molecules and MFG-E8-eGFP on EVs, which quantifies the similarity between localised bright spots in two selected images [290], MHC-I expression on $CD8^+$ T cells distort the co-localisation analysis of the two markers.

However, several reports demonstrate that human and murine DC-derived EVs contain functional MHC-I that could stimulate $CD8^+$ T cell clones [150, 193, 194, 201]. Additionally, we showed that MFG-$E8^+EV^+CD8^+$ T cells display increased nuclear levels of the TCR-induced transcription factor NFATc1 (discussed in detail later), strongly suggesting either the presence of MHC-I or other stimulatory components on associated EVs.

In addition to MHC and co-stimulatory molecules, T cell-associated MFG-$E8^+$ EVs carry the exosome-associated tetraspanins CD9 and CD63 [125, 166]. Furthermore, as demonstrated by TEM analysis, MFG-$E8^+$ EVs display a diameter of about 30- 200 nm and are attached to the cell surface in clusters. Together these results strongly indicate that T cell-bound EVs comprise exosomes of APC origin.

At this stage, we do not know the specific cellular source of the detected MFG-$E8^+$ EVs. As infected cells were shown to release higher amounts of EVs than their uninfected counterparts [160, 285, 291], the EV-secreting cells probably include LCMV-infected cells, such as F4/80 macrophages and DCs [106, 246].

Increased EV levels were detected in the serum of *M. bovis*-infected mice [160]. Consistent with that, the frequency of EV^+ T cells considerably increased upon LCMV infection compared to non-infected mice, suggesting that EVs may serve as a way of communication between APCs and T cells during infection [reviewed in 183].

Similar to murine T cells, immunisation with live attenuated YFV and a subunit-influenza vaccine induced EV-decoration of human peripheral $CD4^+$ and $CD8^+$ T cells, demonstrating a direct interaction of EVs with T cells also occurs in human blood.

$CD4^+$ T cells were reported to be dispensable for eliminating an acute LCMV infection, whereas $CD8^+$ T cell responses are crucial for viral clearance [67]. Although APC-derived EVs were shown to bind to and regulate both $CD4^+$ and $CD8^+$ T cell function [reviewed in 183], we found 10 % of EV^+CD4^+ T cells and around 45 % of EV^+CD8^+ T cells. These data suggest that EVs act on $CD8^+$ T cells rather than on $CD4^+$ T cells and preferentially modulate T cells that play a central role in the anti-viral immune response against LCMV.

However, the stimulatory capacity of EVs is 10-20 times less efficient in activating Ag-specific T cells than that of their parent APC [165, 199]. Naïve T cells require high levels of TCR cross-linking and co-stimulatory signals for their activation [292-294]; therefore, APC-derived EVs have been proposed to not directly induce the activation of naïve T cells *in vivo* [183]. In line with this, we hardly detected EV^+ naïve T cells in LCMV and non-infected mice but instead found 55 % of $CD44^+CD8^+$ and 25 % of $CD44^+CD4^+$ effector T cells that were decorated with EVs.

Our *in vivo* data further support the idea that free EVs are probably not involved in the priming of naïve T cells but instead may contribute to the regulation of Ag-experienced T cells.

Together, in addition to the described binding of T cells to APC-associated EVs [158, 198, 200], we show that a large number of activated $CD8^+$ T cells directly interact with free circulating APC-derived EVs, which may preferentially modulate $CD8^+$ T cells responses.

7.3 The preferential binding of EVs to activated $CD8^+$ T cells

Why are EVs mainly captured by splenic effector $CD8^+$ T cells while being absent on naïve T cell surfaces? The molecules that mediate the interaction of EVs with their target cells remain a central question in the EV field [reviewed in 163]. Some cells may attract or reject the binding of free EVs by the expression of surface molecules that impact EV attachment [reviewed in 163].

Upon T cell activation, TCR stimulation induces a transient conformational change in LFA-1 that increases its avidity for CD54 [295]. Interestingly murine DC-derived EVs have been shown to

bind activated $CD4^+$ T cells probably via CD54-LFA-1 interactions *in vitro* [169]. While the expression of CD80 on EVs is crucial for the activation of T cells, CD80/CD86-CD28 interactions may only enhance but are not critical for actual EV binding to occur [196]. Furthermore, CD44 expression on T cells and DCs is essential for forming an immunological synapse [296], and the CD44 receptor hyaluronan on human mesenchymal stem cell- and tumour-derived EVs was shown to mediate their docking to $CD44^+$ target cells [297, 298]. In line with these *in vitro* studies, we found EVs preferentially associated with activated $CD4^+$ and $CD8^+$ T cells, which express high levels of CD44 and the high-affinity conformation of LFA-1 [295, 299]. By inducing a firm adhesion of activated T cells to integrin-bearing EVs, these molecules may favour activated T cells over naïve T cells, which do not express activated LFA-1 or CD44.

In vitro, cognate TCR:pMHC interactions are required for EV binding to T cells [196], while another study demonstrated that $CD4^+$ T cells capture EVs independently of TCR specificity [169]. We found 25 to 30 % of Ag-specific $tetramer^+$ and 20 % of P14 $CD8^+$ T cells associated with EVs in LCMV-infected mice. Furthermore, LCMV non-specific OT-I cells displayed a slight but not significantly decreased frequency of EV-decoration compared to P14 T cells in the same infected animals. Although we could not show the peptide specificity of EVs, these results suggest that APC-derived EVs are efficiently captured by activated $CD8^+$ T cells irrespective of their TCR specificity. Though we found higher frequencies of EV^+ P14 cells and endogenous $CD44^+CD8^+$ T cells (which probably are LCMV-specific) than EV^+ OT-I cells, cognate TCR:pMHC binding might stabilise EV-T cell interactions. Furthermore, TCR:pMHC interaction might reflect the importance of recent T cell activation by APC, a process where T cells also might obtain EVs directly.

In line with a previous *in vitro* study [169], our *in vivo* results suggest that EV-decoration of T cells is dependent on their activation status, which is associated with the expression of activated integrins and selectins that display a high affinity for adhesion molecules present on the EV surface. The importance of LFA-1 and CD44 for EV-T cell interactions could be addressed by injecting mononuclear antibodies directed against CD44 or LFA-1 in future experiments.

Another possibility for the different EV-binding properties of splenic naïve and effector $CD8^+$ T cells may be their different localisation within lymphoid organs during acute infections [300, 301]. While naïve T cells are mostly confined to the T cell zone of the white pulp, where they interact with APCs, activated effector $CD8^+$ T cells migrate to and accumulate in the red pulp and marginal zone [300-302]. Here, effector $CD8^+$ T cells may capture EVs from the blood and lymph, resulting in a preferential EV-decoration of these cells. The idea that the localisation of

a given T cell could impact its EV-decoration might explain the observed binding of EVs by naïve and non-activated T cells in the blood of LCMV-infected mice and human vaccinees, where free-floating EVs should be equally available for all T cell subsets.

However, as priming of naïve T cells primarily occurs in lymphoid organs, it is unlikely that EV-decoration of T_N cells in the blood influences their activation status. Furthermore, it remains to be determined whether EVs in the blood have the same origin and display similar molecular properties as those detected in the spleen.

The substantial increase of EV-decoration upon LCMV-infection, together with the fact that EVs carrying MHC and co-stimulatory molecules primarily bind to activated T cells in the spleen, suggests a role in the modulation of an ongoing T cell immune response. Notably, as EV binding occurs independently of Ag specificity, EVs are not restricted to specific T cell clones but act on all T cells activated during infection. EV binding to effector $CD8^+$ T cells may promote infection and immune evasion by downregulating T cell-mediated immune responses or impede infection by promoting T cell activation and antiviral immunity [reviewed in 303].

7.4 Increased nuclear NFATc1 levels in EV-decorated $CD8^+$ T cells

EVs have been shown to regulate T cell activity by inducing proliferation and cytotoxic responses or suppressing T cell immune responses *in vivo* [158, 166, 193, 304-307]. However, only a few reports demonstrate a direct effect of free EVs on effector T cell biology, and these experiments were mainly performed *in vitro*. While the binding of DC-derived pMHC-bearing EVs to activated $CD4^+$ T cells has been proposed to be involved in the T-cell mediated downregulation of an ongoing immune response [169], another report suggests a continuous stimulation of primed $CD4^+$ T cells by pMHC-bearing exosomes, resulting in increased proliferation and IFN-γ secretion [197].

It is still unclear whether and to what extent free EVs contribute to the inhibition or activation of T cell immune responses *in vivo*. We demonstrate that MFG-$E8^+EV^+$ effector $CD8^+$ T cells display higher levels of nuclear NFATc1 as compared to their MFG-$E8^-$ counterparts in LCMV-infected mice. NFATc1 is a key transcription factor that regulates the gene expression of T cell effector molecules [28, 29]. The nuclear import of NFAT proteins has been described to occur rapidly after TCR stimulation and their nuclear export within 20 min when TCR signalling stops [23, 29]. Therefore, our results imply that MFG-$E8^+EV^+$ T cells received recent TCR stimulation, either by APC, target cells, or EVs themselves.

Activated MFG-E8$^+$EV$^+$ CD8$^+$ T cells displayed a slightly but not significantly higher expression of Nur77, which is commonly used as a specific marker for Ag receptor signalling [258], thereby further implying a current TCR-mediated activation of MFG-E8$^+$EV$^+$CD8$^+$ T cells. Furthermore, we also detected a higher percentage of nuclear NFATc1 in Ag-specific MFG-E8$^+$EV$^+$ P14 T cells than MFG-E8$^-$ P14 T cells. These results demonstrate that EV-decoration correlates with increased levels of nuclear NFATc1, which contradicts an immune-suppressing function of EVs generated during acute LCMV infection.

Notably, in activated MFG-E8$^+$EV$^+$ OT-I cells carrying non-cognate TCR in our experimental LCMV-setup, NFATc1 nuclear translocation was sharply reduced compared to activated MFG-E8$^+$EV$^+$ P14 T cells. Therefore, MFG-E8$^+$ EV$^+$ P14 T cells either had recent APC or target cell contact or received TCR signals directly from EVs, resulting in enhanced nuclear translocation of NFATc1 in these cells.

Upon cognate T cell interactions, APCs release EVs carrying pMHC, which can subsequently be captured directly by CD4$^+$ T cells [125, 202]. In another study, CD4$^+$ T cells acquired fibroblast-derived pMHC complexes upon cellular dissociation that co-localised with signal molecules involved in TCR signalling [308]. Thus, the authors suggested that the captured pMHCs maintain intracellular T cell signalling pathways [308]. Although another intercellular transfer mechanism was proposed, it is possible that fibroblast-derived pMHC complexes were acquired by T cells through EVs.

In this scenario, EV-decoration during LCMV infection would mark P14 T cells that recently encountered and were activated by pMHCs on APCs, which in turn released EVs into the immunological synapse that then bind to the activated T cell. However, the activation of naïve CD8$^+$ T cells induces their clonal proliferation, resulting in a 50 000-fold increase in the number of Ag-specific T cells on day 8 after LCMV infection [309]. It seems unlikely that all the detected 10^6 EV$^+$ effector CD8$^+$ T cells had APC contact, especially in the short time frame of NFAT nuclear translocation [23, 29]; instead, progeny CD8$^+$ T cells may capture free APC-derived EVs from the surroundings. The binding of pMHC complexes on EVs to TCRs on activated P14 CD8$^+$ T cells may then sustain TCR signalling, as illustrated by the higher levels of nuclear NFATc1 found in MFG-E8$^+$ cells.

The fact that MFG-E8$^+$EV$^+$ OT-I cells, which do not interact with pMHC on DCs, displayed a small but significant increase of nuclear NFATc1 compared to MFG-E8$^-$ OT-I cells, further supports the idea that EVs are captured in the absence of DC-T cell interactions and provide at least co-stimulatory signals that might prolong effector functions of target cells.

In T cells, CD28 mediated signals induce Ca^{2+} signalling [310] and activate the kinase Akt [36, 37]. Akt phosphorylates and thereby inactivates GSK3, which promotes the nuclear export of NFAT [36, 37]. Therefore, CD28 signalling by increasing intracellular Ca^{2+} levels and preventing the export of nuclear NFAT extends the transcription of NFAT-regulated T cell effector genes, including IL-2 and IFN-γ [28, 311-313]. It is possible that the binding of CD86 on EVs to CD28 on activated $CD8^+$ T cells triggers similar signalling pathways.

Moreover, NFATc1 has been shown to regulate cell proliferation and glycolysis positively and to repress cell death [28, 32, 314]. Consistent with that, we found higher levels of proteins involved in gene expression/DNA replication (Pwp1, Wdr43, Pole), protein synthesis, de-novo protein folding (Eiff3f, Eif4a1, Cluh, Clpb) and proliferation (Grn, Cdk4, Hells) [260] in MFG-$E8^+$ effector $CD8^+$ T cells compared to their MFG-$E8^-$ counterparts. Furthermore, we detected a higher amount of Pdcd4 in MFG-$E8^-CD44^+CD8^+$ T cells, a molecule involved in the negative regulation of translation [260]. These data reveal that different signalling pathways are active in MFG-$E8^+EV^+$ and MFG-$E8^-$ effector $CD8^+$ T cells that might be affiliated to a differential T cell metabolism.

Due to their increased proliferation, DNA replication, and protein synthesis, activated T cells require high energy demands and therefore switch their metabolism to glycolysis [reviewed in 315]. The activation of the protein kinase mTOR (mechanistic Target of Rapamycin) is induced upon T cell activation and controls cell growth, proliferation, and glycolytic metabolism [reviewed in 316]. Interestingly, mTOR has been identified to control $CD8^+$ T cell memory differentiation during LCMV infection [317]. Considering an increased amount of proteins involved in proliferation and protein synthesis in MFG-$E8^+EV^+CD8^+$ T cells, it would be interesting to analyse mTOR signalling in EV^+ and MFG-$E8^-$ $CD8^+$ T cells.

Moreover, we found a higher expression of the co-stimulatory molecule CD137 (4-1BB) in EV^+ $CD8^+$ T cells, which is transiently expressed 24 hours after their activation *in vivo* and promotes proliferation, survival and cytotoxic effector function [269, 270]. In macrophages, CD137 ligation induces cell survival and cytokine expression by activating mTOR and Akt [318]. In $CD8^+$ T cells, enhancing CD137 co-stimulation 3 days post LCMV infection significantly increased anti-viral immunity [271]. As we detected the highest frequency of EV-decorated $CD8^+$ T cells on day 5 p.i., APC-derived EVs, by expressing CD137 ligand (CD137L) on their surface, might positively modulate $CD137^+CD8^+$ T cell responses. The expression of CD137L on APC-derived EVs should be addressed in future studies.

It is still unclear whether the release of EV cargo into the cell is necessary for their biological function [reviewed in 163]. The sole binding of EVs to particular surface molecules on the T cell surface has been suggested to be sufficient to influence T cell responses [169, 197]. In line with this, our TEM analysis demonstrates that the majority of EVs are found on the surface of $CD45^+$ cells. We did not observe fusion with the plasma membrane or endocytosis of the associated EVs, suggesting that EV binding is sufficient to induce nuclear translocation of NFATc1 in recipient cells. However, it does not exclude this possibility.

Several studies demonstrate a TCR down-modulation after pMHC ligation [319-321]. Interestingly, APC-derived GFP-tagged pMHC that were transferred during cognate APC-T cell interactions and co-localised with TCRs on activated $CD4^+$ T cells disappeared from the surface over time, and the authors claimed that pMHC complexes were internalised during TCR down-regulation [308]. As EVs were shown to enter cells through receptor-mediated endocytosis [reviewed in 322], T-cell bound EVs may be endocytosed during TCR internalisation.

Furthermore, the conformational change of LFA-1 induced by TCR-engagement is temporary [295]. Whether surface-bound EVs are taken up upon TCR internalisation or dissociate from T cells when LFA-1 returns to its low-avidity state have yet to be determined.

In LCMV-infected mice, the peak of the $CD8^+$ T cell immune response, as well as the elimination of LCMV from tissues, has been described to occur on day 6 to 8 p.i. [78, 248, 249]. In line with this, we found the highest frequency of EV-decorated cells on day 5 p.i., which gradually declined on day 10 to 15 p.i., indicating that EV-decoration of $CD8^+$ T cells is transient. Hence EVs may indicate an ongoing infection and, by delivering stimulatory signals, may keep $CD44^+$ $CD8^+$ T cells in an activated state until the pathogen is eliminated. Furthermore, the rapid decline of EV-decorated $CD8^+$ T cells after day 5 p.i. implies that the absence of EVs may contribute to immune regulation and T cell contraction (discussed later).

Taken together, our results suggest that EVs may not be neutral waste products but instead, by carrying MHC and co-stimulatory molecules, may act as stimulating mini platforms that positively regulate and sustain the activation status of Ag-experienced effector $CD8^+$ T cells *in vivo*. However, at this point, we do not have direct proof that EV-decoration causes higher nuclear NFATc1 levels in the associated T cells, as the possibility exists that EVs are just preferentially captured by T cells with an activated phenotype. Further experiments using knockdowns, knockouts, or specific inhibitors that interfere with EV production or docking to T cells, are necessary to solve these questions. Recently, Rab27a-deficient mice that were compromised in releasing EVs were shown to have a diminished capacity to stimulate T cells

and control *M. tuberculosis* infection [323]. A similar approach could help to clarify the role of EV-decoration during infection further.

7.5 EVs and CD8$^+$ T cell memory development

The molecular pathways that regulate memory differentiation of effector CD8$^+$ T cells are still incompletely understood [reviewed in 15]. Multiple signals have been shown to regulate the expression and activity of transcription factors that play a crucial role in CD8$^+$ T cell fate decisions [reviewed in 15]. During acute infections, high levels of inflammatory cytokines such as IL-12 and TCR signal strength have been shown to induce T-bet expression early following T cell activation [17, 42, 45]. High T-bet expression levels, in turn, cause the differentiation into KLRG1^{hi}CD127^{lo} terminally differentiated SLECs, that are prone to die, while a low expression promotes cells to develop into surviving MPECs that are KLRG1^{lo}CD127^{hi} [42]. Furthermore, memory T cells display increased expression levels of anti-apoptotic Bcl-2, which is crucial to dominate the pro-apoptotic activity of Bim for cell survival [254, 255].

We found a lower expression of T-bet in MFG-E8$^+$ effector CD8$^+$ T cells compared to cells without bound MFG-E8$^+$EVs. Furthermore, KLRG1^{hi}CD127^{lo} cells gradually lose EV-decoration, while the frequency of EV$^+$KLRG1^{lo}CD127^{hi} CD8$^+$ T cells augmented during later time points of LCMV infection. Although the expression of these molecules should not be considered a universal marker for identifying memory precursor cells, they can be helpful to define the memory potential of a given CD8$^+$ T cell [reviewed in 15]. Therefore, our results suggest that EVs preferentially associate with cells that primarily belong to the memory precursor population.

As mentioned before, EV-decoration gradually declines after viral clearance, and we detected maximally 10 % of EV$^+$ effector CD8$^+$ T cells on day 10 after infection. EVs may provide these T cells with signals that support their survival, while MFG-E8$^-$CD8$^+$ T cells might undergo cell death during the contraction phase. Consistent with this hypothesis, we found higher levels of Bcl-2 and an increased Bcl-2/Bim ratio in MFG-E8$^+$ compared to MFG-E8$^-$ CD8$^+$ T cells.

The stimulation of co-stimulatory receptors promotes the survival of effector T cells by increasing the expression of anti-apoptotic Bcl-2 and Bcl-XL [324-327]. The co-stimulatory molecules present on EVs may induce the expression of anti-apoptotic Bcl-2 proteins in bound effector CD8$^+$ T cells, thereby inducing their preferential survival.

Together, EVs may, by delivering stimulatory signals, on the one hand, keep effector CD8$^+$ T cells in an activated state until the pathogen is cleared. On the other hand, EVs may provide

survival signals to effector T cells after pathogen elimination, thereby maintaining memory T cells. The differential functions of EVs during LCMV infection might be context-dependent. EV binding in the presence of pro-inflammatory signals IL-12 and IFN-γ may promote T cell activation [10-12], while EV-decoration together with IL-15 or IL-7 signalling may promote the survival of EV^+ effector $CD8^+$ T cells [44, 328, 329]. However, enhanced survival of EV^+ effector $CD8^+$ T cells has to be determined in the future, e.g., by adoptive transfer of congenically marked EV^+ and MFG-$E8^-$ P14 $CD8^+$ T cells into uninfected C57BL/6 wild type mice.

7.6 EVs as biomarkers for T cell activation?

EVs have been shown to carry different cargoes such as proteins, nucleic acids, and lipids, which strongly reflect their parental cells' molecular signature [reviewed in 114]. Therefore, the molecular composition of EVs may reveal changes in the physiology of the producing cell, including activated or pathological states [reviewed in 156]. Besides, EVs can be easily detected and collected from all kinds of body fluids [reviewed in 115, 147]. For these reasons, EV components are regarded as promising candidates as biomarkers for the diagnosis, prognosis, and monitoring of several diseases, including infections, tumours, metabolic and neurological diseases [reviewed in 147, 156, 330, 331]. In addition to EV content, EV number may also serve as a diagnostic marker for infection, as a few reports demonstrate that the number of secreted EVs significantly increased upon pathogen infection [reviewed in 303, 331].

In vitro, human Rotavirus (RV)-infected cells were shown to secrete more significant amounts of EVs than uninfected control cells [291]. Furthermore, in *M. bovis*-infected mice, the concentration of serum EVs was strongly increased compared to mice that cleared the infection and strongly correlated with bacterial load, supporting the idea that infection promotes EV secretion [160]. Consistent with these reports, our *in vivo* results show that EV-decoration, particularly of $CD44^+CD8^+$ T_E cells, raised strongly in the blood and the spleen of LCMV-infected mice. However, in the absence of infection, we observed only low frequencies of EV^+ splenocytes and no EV-decoration of $CD8^+$ T cells. Similar to the data of *M. bovis*-infected mice, we could show that the decoration $CD8^+$ T cells with EVs was transient and correlated with the published kinetics of LCMV titre [248]. Moreover, we observed the highest number of EV-decorated T cells to occur around the peak (day 7 p.i.) of LCMV-specific $CD8^+$ T cell responses [249], suggesting that EV-decoration of $CD8^+$ T cells may also be related to $CD8^+$ T cell activation in LCMV-infected mice.

In addition to murine model systems, two human studies showed a relationship between pathology and plasma EV numbers [161, 162]. In patients infected with *Plasmodium vivax,* the frequency of platelet-derived EVs strongly increased compared to healthy age-matched malaria-unexposed controls and was significantly associated with fever and length of malaria symptoms [162]. Notably, the levels of plasma EVs significantly decreased after 21 days of anti-malaria treatment [162]. Similarly, in patients infected with *Plasmodium falciparum,* Annexin V^+ EV levels significantly increased and correlated with the severity of the disease but returned to the levels of healthy controls after treatment [161]. In line with these reports, we also observed increased EV-decoration of T cells in human peripheral blood after immunisation with a live-attenuated YFV 17D-based vaccine. The virus titre of 17D has been described to peak around days 5-7 post-vaccination [332]. However, in contrast to EV-decoration in murine spleens, the peak of EV-decoration of both $CD8^+$ and $CD4^+$ T cells did not correlate with the viral load but was associated with the peak of activated HLA-DR^+CD38^+ $CD8^+$ T cells and HLA-DR^+CD38^+ $CD4^+$ T cells on day 14 post-immunisation. Even though animal models cannot directly be used to predict human immune responses [333], it should be noted that human samples were harvested from peripheral blood, which might show different kinetics of EV-decoration than that observed in the spleen. Notably, 28 days after YFV immunisation, the frequency of EV-decorated and activated $CD8^+$ T cells returned to similar levels observed before immunisation, implying that EV positivity coincides with the kinetics of T cell activation during YFV vaccination. For YFV 17D immunisation, the initial viral load has been shown to correlate with the magnitude of $CD8^+$ T cell response [332]. It would be interesting to determine the relationship between EV-decoration and the quality of the anti-viral $CD8^+$ T cell response in YFV 17D-vaccinated donors.

Considering the potential use of EVs as biomarkers, we show that the frequency of EV-decoration sharply increased upon infection and correlated with the activation of $CD8^+$ T cells in mice and humans. We propose that besides their molecular signature, also EV quantity could be used as a biomarker for acute infections or an ongoing immune response.

8 Conclusions

This study aimed to analyse PS^+EV^+ and apoptotic $CD8^+$ T cells during LCMV infection *in vivo*. To detect and discriminate the two PS^+ populations, we injected MFG-E8-eGFP i.v. into mice and analysed apoptotic and EV^+ cells by IFC and a deep learning-based classifier. We further aimed to determine the origin, target cells, and function of unmanipulated, endogenous EVs during immune responses *in vivo*.

By using this approach, we reliably visualised and quantified apoptotic and EV-decorated cells *in vivo*. However, we found only low frequencies of apoptotic cells in LCMV-infected mice, and the majority of MFG-$E8^+$ cells were live cells associated with PS^+ EVs.

Here, we show for the first time that free naturally occurring EVs preferentially bind to activated $CD8^+$ T cells in LCMV-infected mice and vaccinated human donors. $CD8^+$ T cell-associated EVs contain MHC-II, co-stimulatory molecules and the tetraspanins CD9/CD63, classifying them as exosomes of APC-origin. EV-decoration of $CD8^+$ T cells correlated with increased TCR signalling and an activated phenotype.

Furthermore, EV-decoration of $CD8^+$ T cells was transient and was associated with the published kinetics of LCMV titre. These results suggest that EVs bind T cells during acute infection and thereby may sustain effector $CD8^+$ T cell immune responses. Furthermore, at later time points of LCMV infection, EVs were associated with effector $CD8^+$ T cells showing memory precursor characteristics. Therefore, EVs may be involved in the regulation of $CD8^+$ T cell memory differentiation by providing survival signals to EV^+ activated $CD8^+$ T cells after viral clearance. Finally, we propose that the level of EV-decoration could be used as a biological marker for an acute infection or an ongoing $CD8^+$ T cell response.

This study represents a proof of concept for the analysis of EV^+ and apoptotic cells *in vivo* by MFG-E8-eGFP injection and CAE-RF-based image analysis. It also contributes to a better understanding of the complex role and properties of naturally produced EVs during acute infections *in vivo*. On the one hand, our findings may help establish a new MFG-E8-based method for analysing EV-decorated cells in various *in vivo* settings that might eventually advance the EV field. On the other hand, this study may help develop new or improve existing EV-based therapies or get more insights into EVs as potential biomarkers.

9 References

1. Charles A. Janeway, J. and R. Medzhitov, *Innate Immune Recognition.* Annual Review of Immunology, 2002. **20**(1): p. 197-216.
2. Mogensen, T.H., *Pathogen recognition and inflammatory signaling in innate immune defenses.* Clin Microbiol Rev, 2009. **22**(2): p. 240-273, Table of Contents.
3. Bonilla, F.A. and H.C. Oettgen, *Adaptive immunity.* Journal of Allergy and Clinical Immunology, 2010. **125**(2, Supplement 2): p. S33-S40.
4. Pennock, N.D., J.T. White, E.W. Cross, E.E. Cheney, B.A. Tamburini, and R.M. Kedl, *T cell responses: naive to memory and everything in between.* Advances in physiology education, 2013. **37**(4): p. 273-283.
5. von Andrian, U.H. and T.R. Mempel, *Homing and cellular traffic in lymph nodes.* Nature Reviews Immunology, 2003. **3**(11): p. 867-878.
6. Mescher, M.F., J.M. Curtsinger, P. Agarwal, K.A. Casey, M. Gerner, C.D. Hammerbeck, F. Popescu, and Z. Xiao, *Signals required for programming effector and memory development by CD8+ T cells.* Immunological Reviews, 2006. **211**(1): p. 81-92.
7. Kalia, V., S. Sarkar, and R. Ahmed, *CD8 T-cell memory differentiation during acute and chronic viral infections.* Adv Exp Med Biol, 2010. **684**: p. 79-95.
8. Kuwana, M., *Induction of anergic and regulatory T cells by plasmacytoid dendritic cells and other dendritic cell subsets.* Hum Immunol, 2002. **63**(12): p. 1156-1163.
9. Steinman, R.M., D. Hawiger, and M.C. Nussenzweig, *Tolerogenic Dendritic Cells.* Annual Review of Immunology, 2003. **21**(1): p. 685-711.
10. Curtsinger, J.M., C.S. Schmidt, A. Mondino, D.C. Lins, R.M. Kedl, M.K. Jenkins, and M.F. Mescher, *Inflammatory cytokines provide a third signal for activation of naive CD4+ and CD8+ T cells.* J Immunol, 1999. **162**(6): p. 3256-3262.
11. Curtsinger, J.M., D.C. Lins, and M.F. Mescher, *Signal 3 determines tolerance versus full activation of naive CD8 T cells: dissociating proliferation and development of effector function.* J Exp Med, 2003. **197**(9): p. 1141-1151.
12. Curtsinger, J.M., J.O. Valenzuela, P. Agarwal, D. Lins, and M.F. Mescher, *Type I IFNs provide a third signal to CD8 T cells to stimulate clonal expansion and differentiation.* J Immunol, 2005. **174**(8): p. 4465-4469.
13. Mempel, T.R., S.E. Henrickson, and U.H. Von Andrian, *T-cell priming by dendritic cells in lymph nodes occurs in three distinct phases.* Nature, 2004. **427**(6970): p. 154-159.
14. Bousso, P. and E. Robey, *Dynamics of CD8+ T cell priming by dendritic cells in intact lymph nodes.* Nat Immunol, 2003. **4**(6): p. 579-585.
15. Kaech, S.M. and W. Cui, *Transcriptional control of effector and memory CD8+ T cell differentiation.* Nat Rev Immunol, 2012. **12**(11): p. 749-761.
16. Agarwal, S. and A. Rao, *Modulation of chromatin structure regulates cytokine gene expression during T cell differentiation.* Immunity, 1998. **9**(6): p. 765-775.
17. Takemoto, N., A.M. Intlekofer, J.T. Northrup, E.J. Wherry, and S.L. Reiner, *Cutting Edge: IL-12 inversely regulates T-bet and eomesodermin expression during pathogen-induced CD8+ T cell differentiation.* J Immunol, 2006. **177**(11): p. 7515-7519.
18. Cruz-Guilloty, F., M.E. Pipkin, I.M. Djuretic, D. Levanon, J. Lotem, M.G. Lichtenheld, Y. Groner, and A. Rao, *Runx3 and T-box proteins cooperate to establish the transcriptional program of effector CTLs.* J Exp Med, 2009. **206**(1): p. 51-59.
19. Weninger, W., M.A. Crowley, N. Manjunath, and U.H. von Andrian, *Migratory properties of naive, effector, and memory CD8(+) T cells.* J Exp Med, 2001. **194**(7): p. 953-966.
20. Oehen, S. and K. Brduscha-Riem, *Differentiation of naive CTL to effector and memory CTL: correlation of effector function with phenotype and cell division.* J Immunol, 1998. **161**(10): p. 5338-5346.
21. DeGrendele, H.C., P. Estess, and M.H. Siegelman, *Requirement for CD44 in activated T cell extravasation into an inflammatory site.* Science, 1997. **278**(5338): p. 672-675.

22. Mobley, J.L. and M.O. Dailey, *Regulation of adhesion molecule expression by CD8 T cells in vivo. I. Differential regulation of gp90MEL-14 (LECAM-1), Pgp-1, LFA-1, and VLA-4 alpha during the differentiation of cytotoxic T lymphocytes induced by allografts.* J Immunol, 1992. **148**(8): p. 2348-2356.
23. Marangoni, F., T.T. Murooka, T. Manzo, E.Y. Kim, E. Carrizosa, N.M. Elpek, and T.R. Mempel, *The transcription factor NFAT exhibits signal memory during serial T cell interactions with antigen-presenting cells.* Immunity, 2013. **38**(2): p. 237-249.
24. Mancini, M. and A. Toker, *NFAT proteins: emerging roles in cancer progression.* Nature Reviews Cancer, 2009. **9**(11): p. 810-820.
25. Jain, J., E. Burgeon, T.M. Badalian, P.G. Hogan, and A. Rao, *A similar DNA-binding motif in NFAT family proteins and the Rel homology region.* J Biol Chem, 1995. **270**(8): p. 4138-4145.
26. Lopez-Rodriguez, C., J. Aramburu, A.S. Rakeman, and A. Rao, *NFAT5, a constitutively nuclear NFAT protein that does not cooperate with Fos and Jun.* Proc Natl Acad Sci U S A, 1999. **96**(13): p. 7214-7219.
27. Macian, F., *NFAT proteins: key regulators of T-cell development and function.* Nat Rev Immunol, 2005. **5**(6): p. 472-484.
28. Klein-Hessling, S., K. Muhammad, M. Klein, T. Pusch, R. Rudolf, J. Floter, M. Qureischi, A. Beilhack, M. Vaeth, C. Kummerow, C. Backes, R. Schoppmeyer, U. Hahn, M. Hoth, T. Bopp, F. Berberich-Siebelt, A. Patra, A. Avots, N. Muller, A. Schulze, and E. Serfling, *NFATc1 controls the cytotoxicity of CD8(+) T cells.* Nat Commun, 2017. **8**(1): p. 511.
29. Hogan, P.G., L. Chen, J. Nardone, and A. Rao, *Transcriptional regulation by calcium, calcineurin, and NFAT.* Genes Dev, 2003. **17**(18): p. 2205-2232.
30. Feske, S., H. Okamura, P.G. Hogan, and A. Rao, *Ca2+/calcineurin signalling in cells of the immune system.* Biochemical and Biophysical Research Communications, 2003. **311**(4): p. 1117-1132.
31. Nguyen, T.N., L.J. Kim, R.D. Walters, L.F. Drullinger, T.N. Lively, J.F. Kugel, and J.A. Goodrich, *The C-terminal region of human NFATc2 binds cJun to synergistically activate interleukin-2 transcription.* Mol Immunol, 2010. **47**(14): p. 2314-2322.
32. Mognol, G.P., F.R.G. Carneiro, B.K. Robbs, D.V. Faget, and J.P.B. Viola, *Cell cycle and apoptosis regulation by NFAT transcription factors: new roles for an old player.* Cell death & disease, 2016. **7**(4): p. e2199-e2199.
33. Xu, T., A. Keller, and G.J. Martinez, *NFAT1 and NFAT2 Differentially Regulate CTL Differentiation Upon Acute Viral Infection.* Frontiers in Immunology, 2019. **10**(184).
34. Neal, J.W. and N.A. Clipstone, *Glycogen synthase kinase-3 inhibits the DNA binding activity of NFATc.* J Biol Chem, 2001. **276**(5): p. 3666-3673.
35. Beals, C.R., C.M. Sheridan, C.W. Turck, P. Gardner, and G.R. Crabtree, *Nuclear export of NF-ATc enhanced by glycogen synthase kinase-3.* Science, 1997. **275**(5308): p. 1930-1934.
36. Diehn, M., A.A. Alizadeh, O.J. Rando, C.L. Liu, K. Stankunas, D. Botstein, G.R. Crabtree, and P.O. Brown, *Genomic expression programs and the integration of the CD28 costimulatory signal in T cell activation.* Proc Natl Acad Sci U S A, 2002. **99**(18): p. 11796-11801.
37. Appleman, L.J., A.A. van Puijenbroek, K.M. Shu, L.M. Nadler, and V.A. Boussiotis, *CD28 costimulation mediates down-regulation of p27kip1 and cell cycle progression by activation of the PI3K/PKB signaling pathway in primary human T cells.* J Immunol, 2002. **168**(6): p. 2729-2736.
38. Ahmed, R. and D. Gray, *Immunological memory and protective immunity: understanding their relation.* Science, 1996. **272**(5258): p. 54-60.
39. Cui, W. and S.M. Kaech, *Generation of effector CD8+ T cells and their conversion to memory T cells.* Immunological Reviews, 2010. **236**: p. 151-166.
40. Chang, J.T., E.J. Wherry, and A.W. Goldrath, *Molecular regulation of effector and memory T cell differentiation.* Nat Immunol, 2014. **15**(12): p. 1104-1115.
41. Kaech, S.M., J.T. Tan, E.J. Wherry, B.T. Konieczny, C.D. Surh, and R. Ahmed, *Selective expression of the interleukin 7 receptor identifies effector CD8 T cells that give rise to long-lived memory cells.* Nat Immunol, 2003. **4**(12): p. 1191-1198.

42. Joshi, N.S., W. Cui, A. Chandele, H.K. Lee, D.R. Urso, J. Hagman, L. Gapin, and S.M. Kaech, *Inflammation directs memory precursor and short-lived effector CD8(+) T cell fates via the graded expression of T-bet transcription factor.* Immunity, 2007. **27**(2): p. 281-295.
43. Sarkar, S., V. Kalia, W.N. Haining, B.T. Konieczny, S. Subramaniam, and R. Ahmed, *Functional and genomic profiling of effector CD8 T cell subsets with distinct memory fates.* J Exp Med, 2008. **205**(3): p. 625-640.
44. Schluns, K.S., W.C. Kieper, S.C. Jameson, and L. Lefrancois, *Interleukin-7 mediates the homeostasis of naive and memory CD8 T cells in vivo.* Nat Immunol, 2000. **1**(5): p. 426-432.
45. Knudson, K.M., N.P. Goplen, C.A. Cunningham, M.A. Daniels, and E. Teixeiro, *Low-affinity T cells are programmed to maintain normal primary responses but are impaired in their recall to low-affinity ligands.* Cell Rep, 2013. **4**(3): p. 554-565.
46. Intlekofer, A.M., N. Takemoto, C. Kao, A. Banerjee, F. Schambach, J.K. Northrop, H. Shen, E.J. Wherry, and S.L. Reiner, *Requirement for T-bet in the aberrant differentiation of unhelped memory CD8+ T cells.* The Journal of experimental medicine, 2007. **204**(9): p. 2015-2021.
47. Zinkernagel, R.M. and P.C. Doherty, *Restriction of in vitro T cell-mediated cytotoxicity in lymphocytic choriomeningitis within a syngeneic or semiallogeneic system.* Nature, 1974. **248**(5450): p. 701-702.
48. Doherty, P.C. and R.M. Zinkernagel, *H-2 compatibility is required for T-cell-mediated lysis of target cells infected with lymphocytic choriomeningitis virus.* J Exp Med, 1975. **141**(2): p. 502-507.
49. Homann, D., L. Teyton, and M.B. Oldstone, *Differential regulation of antiviral T-cell immunity results in stable CD8+ but declining CD4+ T-cell memory.* Nat Med, 2001. **7**(8): p. 913-919.
50. Wherry, E.J., V. Teichgraber, T.C. Becker, D. Masopust, S.M. Kaech, R. Antia, U.H. von Andrian, and R. Ahmed, *Lineage relationship and protective immunity of memory CD8 T cell subsets.* Nat Immunol, 2003. **4**(3): p. 225-234.
51. Baenziger, J., H. Hengartner, R.M. Zinkernagel, and G.A. Cole, *Induction or prevention of immunopathological disease by cloned cytotoxic T cell lines specific for lymphocytic choriomeningitis virus.* Eur J Immunol, 1986. **16**(4): p. 387-393.
52. Fung-Leung, W.P., T.M. Kundig, R.M. Zinkernagel, and T.W. Mak, *Immune response against lymphocytic choriomeningitis virus infection in mice without CD8 expression.* J Exp Med, 1991. **174**(6): p. 1425-1429.
53. Kagi, D., B. Ledermann, K. Burki, P. Seiler, B. Odermatt, K.J. Olsen, E.R. Podack, R.M. Zinkernagel, and H. Hengartner, *Cytotoxicity mediated by T cells and natural killer cells is greatly impaired in perforin-deficient mice.* Nature, 1994. **369**(6475): p. 31-37.
54. Barber, D.L., E.J. Wherry, D. Masopust, B. Zhu, J.P. Allison, A.H. Sharpe, G.J. Freeman, and R. Ahmed, *Restoring function in exhausted CD8 T cells during chronic viral infection.* Nature, 2006. **439**(7077): p. 682-687.
55. Moskophidis, D., F. Lechner, H. Pircher, and R.M. Zinkernagel, *Virus persistence in acutely infected immunocompetent mice by exhaustion of antiviral cytotoxic effector T cells.* Nature, 1993. **362**(6422): p. 758-761.
56. Wherry, E.J., S.J. Ha, S.M. Kaech, W.N. Haining, S. Sarkar, V. Kalia, S. Subramaniam, J.N. Blattman, D.L. Barber, and R. Ahmed, *Molecular signature of CD8+ T cell exhaustion during chronic viral infection.* Immunity, 2007. **27**(4): p. 670-684.
57. Zajac, A.J., J.N. Blattman, K. Murali-Krishna, D.J. Sourdive, M. Suresh, J.D. Altman, and R. Ahmed, *Viral immune evasion due to persistence of activated T cells without effector function.* J Exp Med, 1998. **188**(12): p. 2205-2213.
58. Armstrong, C. and R.D. Lillie, *Experimental Lymphocytic Choriomeningitis of Monkeys and Mice Produced by a Virus Encountered in Studies of the 1933 St. Louis Encephalitis Epidemic.* Public Health Reports (1896-1970), 1934. **49**(35): p. 1019-1027.
59. MUCKENFUSS, R.S., C. ARMSTRONG, and L.T. WEBSTER, *ETIOLOGY OF THE 1933 EPIDEMIC OF ENCEPHALITIS.* Journal of the American Medical Association, 1934. **103**(10): p. 731-733.
60. Byrne, J.A. and M.B. Oldstone, *Biology of cloned cytotoxic T lymphocytes specific for lymphocytic choriomeningitis virus: clearance of virus in vivo.* J Virol, 1984. **51**(3): p. 682-686.

61. Lehmann-Grube, F., D. Moskophidis, and J. Lohler, *Recovery from acute virus infection. Role of cytotoxic T lymphocytes in the elimination of lymphocytic choriomeningitis virus from spleens of mice.* Ann N Y Acad Sci, 1988. **532**: p. 238-256.
62. Moskophidis, D., S.P. Cobbold, H. Waldmann, and F. Lehmann-Grube, *Mechanism of recovery from acute virus infection: treatment of lymphocytic choriomeningitis virus-infected mice with monoclonal antibodies reveals that Lyt-2+ T lymphocytes mediate clearance of virus and regulate the antiviral antibody response.* J Virol, 1987. **61**(6): p. 1867-1874.
63. Buchmeier, M., M.D. Bowen, and C.J. Peters, *Arenaviridae: The viruses and their replication.* Fields Virology, 2001. **2**: p. 1635-1668.
64. Salvato, M.S. and E.M. Shimomaye, *The completed sequence of lymphocytic choriomeningitis virus reveals a unique RNA structure and a gene for a zinc finger protein.* Virology, 1989. **173**(1): p. 1-10.
65. Southern, P.J., M.K. Singh, Y. Riviere, D.R. Jacoby, M.J. Buchmeier, and M.B. Oldstone, *Molecular characterization of the genomic S RNA segment from lymphocytic choriomeningitis virus.* Virology, 1987. **157**(1): p. 145-155.
66. Wright, K.E., R.C. Spiro, J.W. Burns, and M.J. Buchmeier, *Post-translational processing of the glycoproteins of lymphocytic choriomeningitis virus.* Virology, 1990. **177**(1): p. 175-183.
67. Matloubian, M., R.J. Concepcion, and R. Ahmed, *CD4+ T cells are required to sustain CD8+ cytotoxic T-cell responses during chronic viral infection.* J Virol, 1994. **68**(12): p. 8056-8063.
68. Cao, W., M.D. Henry, P. Borrow, H. Yamada, J.H. Elder, E.V. Ravkov, S.T. Nichol, R.W. Compans, K.P. Campbell, and M.B. Oldstone, *Identification of alpha-dystroglycan as a receptor for lymphocytic choriomeningitis virus and Lassa fever virus.* Science, 1998. **282**(5396): p. 2079-2081.
69. Kunz, S., N. Sevilla, D.B. McGavern, K.P. Campbell, and M.B. Oldstone, *Molecular analysis of the interaction of LCMV with its cellular receptor [alpha]-dystroglycan.* J Cell Biol, 2001. **155**(2): p. 301-310.
70. Sevilla, N., S. Kunz, D. McGavern, and M.B. Oldstone, *Infection of dendritic cells by lymphocytic choriomeningitis virus.* Curr Top Microbiol Immunol, 2003. **276**: p. 125-144.
71. Ciurea, A., L. Hunziker, P. Klenerman, H. Hengartner, and R.M. Zinkernagel, *Impairment of CD4(+) T cell responses during chronic virus infection prevents neutralizing antibody responses against virus escape mutants.* J Exp Med, 2001. **193**(3): p. 297-305.
72. Borrow, P. and M.B. Oldstone, *Characterization of lymphocytic choriomeningitis virus-binding protein(s): a candidate cellular receptor for the virus.* J Virol, 1992. **66**(12): p. 7270-7281.
73. Ahmed, R., L.D. Butler, and L. Bhatti, *T4+ T helper cell function in vivo: differential requirement for induction of antiviral cytotoxic T-cell and antibody responses.* J Virol, 1988. **62**(6): p. 2102-2106.
74. Odermatt, B., M. Eppler, T.P. Leist, H. Hengartner, and R.M. Zinkernagel, *Virus-Triggered Acquired Immunodeficiency by Cytotoxic T-Cell-Dependent Destruction of Antigen-Presenting Cells and Lymph Follicle Structure.* Proceedings of the National Academy of Sciences of the United States of America, 1991. **88**(18): p. 8252-8256.
75. Matter, M.S., T. Hilmenyuk, C. Claus, R. Marone, C. Schürch, M. Tinguely, L. Terracciano, S.A. Luther, and A.F. Ochsenbein, *Destruction of lymphoid organ architecture and hepatitis caused by CD4+ T cells.* PLoS One, 2011. **6**(9): p. e24772-e24772.
76. Kurtulus, S. and D. Hildeman, *Assessment of CD4(+) and CD8 (+) T cell responses using MHC class I and II tetramers.* Methods in molecular biology (Clifton, N.J.), 2013. **979**: p. 71-79.
77. Pircher, H., K. Burki, R. Lang, H. Hengartner, and R.M. Zinkernagel, *Tolerance induction in double specific T-cell receptor transgenic mice varies with antigen.* Nature, 1989. **342**(6249): p. 559-561.
78. Murali-Krishna, K., J.D. Altman, M. Suresh, D.J. Sourdive, A.J. Zajac, J.D. Miller, J. Slansky, and R. Ahmed, *Counting antigen-specific CD8 T cells: a reevaluation of bystander activation during viral infection.* Immunity, 1998. **8**(2): p. 177-187.
79. Lau, L.L., B.D. Jamieson, T. Somasundaram, and R. Ahmed, *Cytotoxic T-cell memory without antigen.* Nature, 1994. **369**(6482): p. 648-652.

80. Kotturi, M.F., B. Peters, F. Buendia-Laysa, Jr., J. Sidney, C. Oseroff, J. Botten, H. Grey, M.J. Buchmeier, and A. Sette, *The CD8+ T-cell response to lymphocytic choriomeningitis virus involves the L antigen: uncovering new tricks for an old virus.* J Virol, 2007. **81**(10): p. 4928-4940.
81. van der Most, R.G., K. Murali-Krishna, J.L. Whitton, C. Oseroff, J. Alexander, S. Southwood, J. Sidney, R.W. Chesnut, A. Sette, and R. Ahmed, *Identification of Db- and Kb-restricted subdominant cytotoxic T-cell responses in lymphocytic choriomeningitis virus-infected mice.* Virology, 1998. **240**(1): p. 158-167.
82. Kaech, S.M., S. Hemby, E. Kersh, and R. Ahmed, *Molecular and Functional Profiling of Memory CD8 T Cell Differentiation.* Cell, 2002. **111**(6): p. 837-851.
83. Zhou, X., S. Ramachandran, M. Mann, and D.L. Popkin, *Role of lymphocytic choriomeningitis virus (LCMV) in understanding viral immunology: past, present and future.* Viruses, 2012. **4**(11): p. 2650-2669.
84. Ahmed, R., A. Salmi, L.D. Butler, J.M. Chiller, and M.B. Oldstone, *Selection of genetic variants of lymphocytic choriomeningitis virus in spleens of persistently infected mice. Role in suppression of cytotoxic T lymphocyte response and viral persistence.* J Exp Med, 1984. **160**(2): p. 521-540.
85. Häcker, G., *Apoptosis in infection.* Microbes and Infection, 2018. **20**(9): p. 552-559.
86. D'Cruz, L.M., M.P. Rubinstein, and A.W. Goldrath, *Surviving the crash: transitioning from effector to memory CD8+ T cell.* Semin Immunol, 2009. **21**(2): p. 92-98.
87. Galluzzi, L., I. Vitale, S.A. Aaronson, J.M. Abrams, D. Adam, P. Agostinis, E.S. Alnemri, L. Altucci, I. Amelio, D.W. Andrews, M. Annicchiarico-Petruzzelli, A.V. Antonov, E. Arama, E.H. Baehrecke, N.A. Barlev, N.G. Bazan, F. Bernassola, M.J.M. Bertrand, K. Bianchi, M.V. Blagosklonny, K. Blomgren, C. Borner, P. Boya, C. Brenner, M. Campanella, E. Candi, D. Carmona-Gutierrez, F. Cecconi, F.K.M. Chan, N.S. Chandel, E.H. Cheng, J.E. Chipuk, J.A. Cidlowski, A. Ciechanover, G.M. Cohen, M. Conrad, J.R. Cubillos-Ruiz, P.E. Czabotar, V. D'Angiolella, T.M. Dawson, V.L. Dawson, V. De Laurenzi, R. De Maria, K.-M. Debatin, R.J. DeBerardinis, M. Deshmukh, N. Di Daniele, F. Di Virgilio, V.M. Dixit, S.J. Dixon, C.S. Duckett, B.D. Dynlacht, W.S. El-Deiry, J.W. Elrod, G.M. Fimia, S. Fulda, A.J. García-Sáez, A.D. Garg, C. Garrido, E. Gavathiotis, P. Golstein, E. Gottlieb, D.R. Green, L.A. Greene, H. Gronemeyer, A. Gross, G. Hajnoczky, J.M. Hardwick, I.S. Harris, M.O. Hengartner, C. Hetz, H. Ichijo, M. Jäättelä, B. Joseph, P.J. Jost, P.P. Juin, W.J. Kaiser, M. Karin, T. Kaufmann, O. Kepp, A. Kimchi, R.N. Kitsis, D.J. Klionsky, R.A. Knight, S. Kumar, S.W. Lee, J.J. Lemasters, B. Levine, A. Linkermann, S.A. Lipton, R.A. Lockshin, C. López-Otín, S.W. Lowe, T. Luedde, E. Lugli, M. MacFarlane, F. Madeo, M. Malewicz, W. Malorni, G. Manic, J.-C. Marine, S.J. Martin, J.-C. Martinou, J.P. Medema, P. Mehlen, P. Meier, S. Melino, E.A. Miao, J.D. Molkentin, U.M. Moll, C. Muñoz-Pinedo, S. Nagata, G. Nuñez, A. Oberst, M. Oren, M. Overholtzer, M. Pagano, T. Panaretakis, M. Pasparakis, J.M. Penninger, D.M. Pereira, S. Pervaiz, M.E. Peter, M. Piacentini, P. Pinton, J.H.M. Prehn, H. Puthalakath, G.A. Rabinovich, M. Rehm, R. Rizzuto, C.M.P. Rodrigues, D.C. Rubinsztein, T. Rudel, K.M. Ryan, E. Sayan, L. Scorrano, F. Shao, Y. Shi, J. Silke, H.-U. Simon, A. Sistigu, B.R. Stockwell, A. Strasser, G. Szabadkai, S.W.G. Tait, D. Tang, N. Tavernarakis, A. Thorburn, Y. Tsujimoto, B. Turk, T. Vanden Berghe, P. Vandenabeele, M.G. Vander Heiden, A. Villunger, H.W. Virgin, K.H. Vousden, D. Vucic, E.F. Wagner, H. Walczak, D. Wallach, Y. Wang, J.A. Wells, W. Wood, J. Yuan, Z. Zakeri, B. Zhivotovsky, L. Zitvogel, G. Melino and G. Kroemer, *Molecular mechanisms of cell death: recommendations of the Nomenclature Committee on Cell Death 2018.* Cell Death & Differentiation, 2018. **25**(3): p. 486-541.
88. Nagata, S., *Apoptosis and Clearance of Apoptotic Cells.* Annu Rev Immunol, 2018. **36**: p. 489-517.
89. Leventis, P.A. and S. Grinstein, *The distribution and function of phosphatidylserine in cellular membranes.* Annu Rev Biophys, 2010. **39**: p. 407-427.

90. Segawa, K., S. Kurata, Y. Yanagihashi, T.R. Brummelkamp, F. Matsuda, and S. Nagata, *Caspase-mediated cleavage of phospholipid flippase for apoptotic phosphatidylserine exposure.* Science, 2014. **344**(6188): p. 1164-1168.
91. Suzuki, J., D.P. Denning, E. Imanishi, H.R. Horvitz, and S. Nagata, *Xk-related protein 8 and CED-8 promote phosphatidylserine exposure in apoptotic cells.* Science, 2013. **341**(6144): p. 403-406.
92. Segawa, K., S. Kurata, and S. Nagata, *Human Type IV P-type ATPases That Work as Plasma Membrane Phospholipid Flippases and Their Regulation by Caspase and Calcium.* J Biol Chem, 2016. **291**(2): p. 762-772.
93. Suzuki, J., M. Umeda, P.J. Sims, and S. Nagata, *Calcium-dependent phospholipid scrambling by TMEM16F.* Nature, 2010. **468**(7325): p. 834-838.
94. Fadok, V.A., D.R. Voelker, P.A. Campbell, J.J. Cohen, D.L. Bratton, and P.M. Henson, *Exposure of phosphatidylserine on the surface of apoptotic lymphocytes triggers specific recognition and removal by macrophages.* J Immunol, 1992. **148**(7): p. 2207-2216.
95. Nagata, S., J. Suzuki, K. Segawa, and T. Fujii, *Exposure of phosphatidylserine on the cell surface.* Cell Death Differ, 2016. **23**(6): p. 952-961.
96. Kroemer, G., L. Galluzzi, P. Vandenabeele, J. Abrams, E.S. Alnemri, E.H. Baehrecke, M.V. Blagosklonny, W.S. El-Deiry, P. Golstein, D.R. Green, M. Hengartner, R.A. Knight, S. Kumar, S.A. Lipton, W. Malorni, G. Nuñez, M.E. Peter, J. Tschopp, J. Yuan, M. Piacentini, B. Zhivotovsky, G. Melino, and D. Nomenclature Committee on Cell, *Classification of cell death: recommendations of the Nomenclature Committee on Cell Death 2009.* Cell death and differentiation, 2009. **16**(1): p. 3-11.
97. Shlomovitz, I., M. Speir, and M. Gerlic, *Flipping the dogma – phosphatidylserine in non-apoptotic cell death.* Cell Communication and Signaling, 2019. **17**(1): p. 139.
98. D'Arcy, M.S., *Cell death: a review of the major forms of apoptosis, necrosis and autophagy.* Cell Biology International, 2019. **43**(6): p. 582-592.
99. Bertheloot, D., E. Latz, and B.S. Franklin, *Necroptosis, pyroptosis and apoptosis: an intricate game of cell death.* Cellular & Molecular Immunology, 2021. **18**(5): p. 1106-1121.
100. Gong, Y.N., C. Guy, H. Olauson, J.U. Becker, M. Yang, P. Fitzgerald, A. Linkermann, and D.R. Green, *ESCRT-III Acts Downstream of MLKL to Regulate Necroptotic Cell Death and Its Consequences.* Cell, 2017. **169**(2): p. 286-300.e216.
101. Chen, J., S. Kuroki, M. Someda, and S. Yonehara, *Interferon-γ induces the cell surface exposure of phosphatidylserine by activating the protein MLKL in the absence of caspase-8 activity.* Journal of Biological Chemistry, 2019. **294**(32): p. 11994-12006.
102. Shlomovitz, I., S. Zargarian, Z. Erlich, L. Edry-Botzer, and M. Gerlic, *Distinguishing Necroptosis from Apoptosis.* Methods Mol Biol, 2018. **1857**: p. 35-51.
103. de Vasconcelos, N.M., N. Van Opdenbosch, H. Van Gorp, E. Parthoens, and M. Lamkanfi, *Single-cell analysis of pyroptosis dynamics reveals conserved GSDMD-mediated subcellular events that precede plasma membrane rupture.* Cell Death & Differentiation, 2019. **26**(1): p. 146-161.
104. Pinton, P., C. Giorgi, R. Siviero, E. Zecchini, and R. Rizzuto, *Calcium and apoptosis: ER-mitochondria Ca2+ transfer in the control of apoptosis.* Oncogene, 2008. **27**(50): p. 6407-6418.
105. Bots, M. and J.P. Medema, *Granzymes at a glance.* Journal of Cell Science, 2006. **119**(24): p. 5011-5014.
106. Borrow, P., C.F. Evans, and M.B. Oldstone, *Virus-induced immunosuppression: immune system-mediated destruction of virus-infected dendritic cells results in generalized immune suppression.* J Virol, 1995. **69**(2): p. 1059-1070.
107. McNally, J.M., C.C. Zarozinski, M.Y. Lin, M.A. Brehm, H.D. Chen, and R.M. Welsh, *Attrition of bystander CD8 T cells during virus-induced T-cell and interferon responses.* J Virol, 2001. **75**(13): p. 5965-5976.

108. Bahl, K., S.-K. Kim, C. Calcagno, D. Ghersi, R. Puzone, F. Celada, L.K. Selin, and R.M. Welsh, *IFN-Induced Attrition of CD8 T Cells in the Presence or Absence of Cognate Antigen during the Early Stages of Viral Infections.* The Journal of Immunology, 2006. **176**(7): p. 4284-4295.
109. Peacock, C.D., S.-K. Kim, and R.M. Welsh, *Attrition of Virus-Specific Memory CD8⁺ T Cells During Reconstitution of Lymphopenic Environments.* The Journal of Immunology, 2003. **171**(2): p. 655-663.
110. Elliott, M.R. and K.S. Ravichandran, *The Dynamics of Apoptotic Cell Clearance.* Dev Cell, 2016. **38**(2): p. 147-160.
111. Hugel, B., M.C. Martinez, C. Kunzelmann, and J.M. Freyssinet, *Membrane microparticles: two sides of the coin.* Physiology (Bethesda), 2005. **20**: p. 22-27.
112. Thery, C., M. Ostrowski, and E. Segura, *Membrane vesicles as conveyors of immune responses.* Nat Rev Immunol, 2009. **9**(8): p. 581-593.
113. Deatherage, B.L. and B.T. Cookson, *Membrane vesicle release in bacteria, eukaryotes, and archaea: a conserved yet underappreciated aspect of microbial life.* Infect Immun, 2012. **80**(6): p. 1948-1957.
114. van Niel, G., G. D'Angelo, and G. Raposo, *Shedding light on the cell biology of extracellular vesicles.* Nature Reviews Molecular Cell Biology, 2018. **19**(4): p. 213-228.
115. Doyle, L.M. and M.Z. Wang, *Overview of Extracellular Vesicles, Their Origin, Composition, Purpose, and Methods for Exosome Isolation and Analysis.* Cells, 2019. **8**(7): p. 727.
116. van Niel, G., S. Charrin, S. Simoes, M. Romao, L. Rochin, P. Saftig, M.S. Marks, E. Rubinstein, and G. Raposo, *The tetraspanin CD63 regulates ESCRT-independent and -dependent endosomal sorting during melanogenesis.* Dev Cell, 2011. **21**(4): p. 708-721.
117. Hurley, J.H., *ESCRTs are everywhere.* Embo j, 2015. **34**(19): p. 2398-2407.
118. Katzmann, D.J., M. Babst, and S.D. Emr, *Ubiquitin-dependent sorting into the multivesicular body pathway requires the function of a conserved endosomal protein sorting complex, ESCRT-I.* Cell, 2001. **106**(2): p. 145-155.
119. Babst, M., D.J. Katzmann, W.B. Snyder, B. Wendland, and S.D. Emr, *Endosome-Associated Complex, ESCRT-II, Recruits Transport Machinery for Protein Sorting at the Multivesicular Body.* Developmental Cell, 2002. **3**(2): p. 283-289.
120. Babst, M., B. Wendland, E.J. Estepa, and S.D. Emr, *The Vps4p AAA ATPase regulates membrane association of a Vps protein complex required for normal endosome function.* Embo j, 1998. **17**(11): p. 2982-2993.
121. Babst, M., D.J. Katzmann, E.J. Estepa-Sabal, T. Meerloo, and S.D. Emr, *Escrt-III: an endosome-associated heterooligomeric protein complex required for mvb sorting.* Dev Cell, 2002. **3**(2): p. 271-282.
122. Raiborg, C., K.G. Bache, A. Mehlum, E. Stang, and H. Stenmark, *Hrs recruits clathrin to early endosomes.* Embo j, 2001. **20**(17): p. 5008-5021.
123. Aline, F., D. Bout, S. Amigorena, P. Roingeard, and I. Dimier-Poisson, *Toxoplasma gondii antigen-pulsed-dendritic cell-derived exosomes induce a protective immune response against T. gondii infection.* Infection and immunity, 2004. **72**(7): p. 4127-4137.
124. Baietti, M.F., Z. Zhang, E. Mortier, A. Melchior, G. Degeest, A. Geeraerts, Y. Ivarsson, F. Depoortere, C. Coomans, E. Vermeiren, P. Zimmermann, and G. David, *Syndecan-syntenin-ALIX regulates the biogenesis of exosomes.* Nat Cell Biol, 2012. **14**(7): p. 677-685.
125. Buschow, S.I., E.N. Nolte-'t Hoen, G. van Niel, M.S. Pols, T. ten Broeke, M. Lauwen, F. Ossendorp, C.J. Melief, G. Raposo, R. Wubbolts, M.H. Wauben, and W. Stoorvogel, *MHC II in dendritic cells is targeted to lysosomes or T cell-induced exosomes via distinct multivesicular body pathways.* Traffic, 2009. **10**(10): p. 1528-1542.
126. Andreu, Z. and M. Yáñez-Mó, *Tetraspanins in extracellular vesicle formation and function.* Frontiers in Immunology, 2014. **5**: p. 442-442.
127. Trajkovic, K., C. Hsu, S. Chiantia, L. Rajendran, D. Wenzel, F. Wieland, P. Schwille, B. Brugger, and M. Simons, *Ceramide triggers budding of exosome vesicles into multivesicular endosomes.* Science, 2008. **319**(5867): p. 1244-1247.

128. Menck, K., C. Sönmezer, T.S. Worst, M. Schulz, G.H. Dihazi, F. Streit, G. Erdmann, S. Kling, M. Boutros, C. Binder, and J.C. Gross, *Neutral sphingomyelinases control extracellular vesicles budding from the plasma membrane.* Journal of Extracellular Vesicles, 2017. **6**(1): p. 1378056-1378056.
129. Villarroya-Beltri, C., C. Gutierrez-Vazquez, F. Sanchez-Cabo, D. Perez-Hernandez, J. Vazquez, N. Martin-Cofreces, D.J. Martinez-Herrera, A. Pascual-Montano, M. Mittelbrunn, and F. Sanchez-Madrid, *Sumoylated hnRNPA2B1 controls the sorting of miRNAs into exosomes through binding to specific motifs.* Nat Commun, 2013. **4**: p. 2980.
130. Irion, U. and D. St Johnston, *bicoid RNA localization requires specific binding of an endosomal sorting complex.* Nature, 2007. **445**(7127): p. 554-558.
131. Mateescu, B., E.J.K. Kowal, B.W.M. van Balkom, S. Bartel, S.N. Bhattacharyya, E.I. Buzás, A.H. Buck, P. de Candia, F.W.N. Chow, S. Das, T.A.P. Driedonks, L. Fernández-Messina, F. Haderk, A.F. Hill, J.C. Jones, K.R. Van Keuren-Jensen, C.P. Lai, C. Lässer, I.d. Liegro, T.R. Lunavat, M.J. Lorenowicz, S.L.N. Maas, I. Mäger, M. Mittelbrunn, S. Momma, K. Mukherjee, M. Nawaz, D.M. Pegtel, M.W. Pfaffl, R.M. Schiffelers, H. Tahara, C. Théry, J.P. Tosar, M.H.M. Wauben, K.W. Witwer, and E.N.M. Nolte-'t Hoen, *Obstacles and opportunities in the functional analysis of extracellular vesicle RNA - an ISEV position paper.* Journal of Extracellular Vesicles, 2017. **6**(1): p. 1286095-1286095.
132. Ostrowski, M., N.B. Carmo, S. Krumeich, I. Fanget, G. Raposo, A. Savina, C.F. Moita, K. Schauer, A.N. Hume, R.P. Freitas, B. Goud, P. Benaroch, N. Hacohen, M. Fukuda, C. Desnos, M.C. Seabra, F. Darchen, S. Amigorena, L.F. Moita, and C. Thery, *Rab27a and Rab27b control different steps of the exosome secretion pathway.* Nat Cell Biol, 2010. **12**(1): p. 19-30; sup pp 11-13.
133. Sinha, S., D. Hoshino, N.H. Hong, K.C. Kirkbride, N.E. Grega-Larson, M. Seiki, M.J. Tyska, and A.M. Weaver, *Cortactin promotes exosome secretion by controlling branched actin dynamics.* J Cell Biol, 2016. **214**(2): p. 197-213.
134. Savina, A., M. Vidal, and M.I. Colombo, *The exosome pathway in K562 cells is regulated by Rab11.* J Cell Sci, 2002. **115**(Pt 12): p. 2505-2515.
135. Zheng, Y., E.C. Campbell, J. Lucocq, A. Riches, and S.J. Powis, *Monitoring the Rab27 associated exosome pathway using nanoparticle tracking analysis.* Exp Cell Res, 2013. **319**(12): p. 1706-1713.
136. Fader, C.M., D.G. Sanchez, M.B. Mestre, and M.I. Colombo, *TI-VAMP/VAMP7 and VAMP3/cellubrevin: two v-SNARE proteins involved in specific steps of the autophagy/multivesicular body pathways.* Biochim Biophys Acta, 2009. **1793**(12): p. 1901-1916.
137. Del Conde, I., C.N. Shrimpton, P. Thiagarajan, and J.A. Lopez, *Tissue-factor-bearing microvesicles arise from lipid rafts and fuse with activated platelets to initiate coagulation.* Blood, 2005. **106**(5): p. 1604-1611.
138. Bianco, F., C. Perrotta, L. Novellino, M. Francolini, L. Riganti, E. Menna, L. Saglietti, E.H. Schuchman, R. Furlan, E. Clementi, M. Matteoli, and C. Verderio, *Acid sphingomyelinase activity triggers microparticle release from glial cells.* Embo j, 2009. **28**(8): p. 1043-1054.
139. Li, B., M.A. Antonyak, J. Zhang, and R.A. Cerione, *RhoA triggers a specific signaling pathway that generates transforming microvesicles in cancer cells.* Oncogene, 2012. **31**(45): p. 4740-4749.
140. Yang, J.M. and S.J. Gould, *The cis-acting signals that target proteins to exosomes and microvesicles.* Biochem Soc Trans, 2013. **41**(1): p. 277-282.
141. Fang, Y., N. Wu, X. Gan, W. Yan, J.C. Morrell, and S.J. Gould, *Higher-order oligomerization targets plasma membrane proteins and HIV gag to exosomes.* PLoS Biol, 2007. **5**(6): p. e158.
142. Shen, B., Y. Fang, N. Wu, and S.J. Gould, *Biogenesis of the posterior pole is mediated by the exosome/microvesicle protein-sorting pathway.* The Journal of biological chemistry, 2011. **286**(51): p. 44162-44176.

143. Muralidharan-Chari, V., J. Clancy, C. Plou, M. Romao, P. Chavrier, G. Raposo, and C. D'Souza-Schorey, *ARF6-regulated shedding of tumor cell-derived plasma membrane microvesicles.* Curr Biol, 2009. **19**(22): p. 1875-1885.
144. Sedgwick, A.E., J.W. Clancy, M. Olivia Balmert, and C. D'Souza-Schorey, *Extracellular microvesicles and invadopodia mediate non-overlapping modes of tumor cell invasion.* Scientific reports, 2015. **5**(1): p. 14748.
145. Schlienger, S., S. Campbell, and A. Claing, *ARF1 regulates the Rho/MLC pathway to control EGF-dependent breast cancer cell invasion.* Molecular Biology of the Cell, 2013. **25**(1): p. 17-29.
146. Nabhan, J.F., R. Hu, R.S. Oh, S.N. Cohen, and Q. Lu, *Formation and release of arrestin domain-containing protein 1-mediated microvesicles (ARMMs) at plasma membrane by recruitment of TSG101 protein.* Proc Natl Acad Sci U S A, 2012. **109**(11): p. 4146-4151.
147. Urabe, F., N. Kosaka, K. Ito, T. Kimura, S. Egawa, and T. Ochiya, *Extracellular vesicles as biomarkers and therapeutic targets for cancer.* American Journal of Physiology-Cell Physiology, 2020. **318**(1): p. C29-C39.
148. Willms, E., H.J. Johansson, I. Mäger, Y. Lee, K.E.M. Blomberg, M. Sadik, A. Alaarg, C.I.E. Smith, J. Lehtiö, S. El Andaloussi, M.J.A. Wood, and P. Vader, *Cells release subpopulations of exosomes with distinct molecular and biological properties.* Scientific reports, 2016. **6**(1): p. 22519.
149. Bobrie, A., M. Colombo, S. Krumeich, G. Raposo, and C. Thery, *Diverse subpopulations of vesicles secreted by different intracellular mechanisms are present in exosome preparations obtained by differential ultracentrifugation.* J Extracell Vesicles, 2012. **1**.
150. Kowal, J., G. Arras, M. Colombo, M. Jouve, J.P. Morath, B. Primdal-Bengtson, F. Dingli, D. Loew, M. Tkach, and C. Thery, *Proteomic comparison defines novel markers to characterize heterogeneous populations of extracellular vesicle subtypes.* Proc Natl Acad Sci U S A, 2016. **113**(8): p. E968-977.
151. Lane, R.E., D. Korbie, M.M. Hill, and M. Trau, *Extracellular vesicles as circulating cancer biomarkers: opportunities and challenges.* Clinical and translational medicine, 2018. **7**(1): p. 14-14.
152. Gould, S.J. and G. Raposo, *As we wait: coping with an imperfect nomenclature for extracellular vesicles.* J Extracell Vesicles, 2013. **2**.
153. Théry, C., K.W. Witwer, E. Aikawa, M.J. Alcaraz, J.D. Anderson, R. Andriantsitohaina, A. Antoniou, T. Arab, F. Archer, G.K. Atkin-Smith, D.C. Ayre, J.-M. Bach, D. Bachurski, H. Baharvand, L. Balaj, S. Baldacchino, N.N. Bauer, A.A. Baxter, M. Bebawy, C. Beckham, A. Bedina Zavec, A. Benmoussa, A.C. Berardi, P. Bergese, E. Bielska, C. Blenkiron, S. Bobis-Wozowicz, E. Boilard, W. Boireau, A. Bongiovanni, F.E. Borràs, S. Bosch, C.M. Boulanger, X. Breakefield, A.M. Breglio, M.Á. Brennan, D.R. Brigstock, A. Brisson, M.L.D. Broekman, J.F. Bromberg, P. Bryl-Górecka, S. Buch, A.H. Buck, D. Burger, S. Busatto, D. Buschmann, B. Bussolati, E.I. Buzás, J.B. Byrd, G. Camussi, D.R.F. Carter, S. Caruso, L.W. Chamley, Y.-T. Chang, C. Chen, S. Chen, L. Cheng, A.R. Chin, A. Clayton, S.P. Clerici, A. Cocks, E. Cocucci, R.J. Coffey, A. Cordeiro-da-Silva, Y. Couch, F.A.W. Coumans, B. Coyle, R. Crescitelli, M.F. Criado, C. D'Souza-Schorey, S. Das, A. Datta Chaudhuri, P. de Candia, E.F. De Santana, O. De Wever, H.A. del Portillo, T. Demaret, S. Deville, A. Devitt, B. Dhondt, D. Di Vizio, L.C. Dieterich, V. Dolo, A.P. Dominguez Rubio, M. Dominici, M.R. Dourado, T.A.P. Driedonks, F.V. Duarte, H.M. Duncan, R.M. Eichenberger, K. Ekström, S. El Andaloussi, C. Elie-Caille, U. Erdbrügger, J.M. Falcón-Pérez, F. Fatima, J.E. Fish, M. Flores-Bellver, A. Försönits, A. Frelet-Barrand, F. Fricke, G. Fuhrmann, S. Gabrielsson, A. Gámez-Valero, C. Gardiner, K. Gärtner, R. Gaudin, Y.S. Gho, B. Giebel, C. Gilbert, M. Gimona, I. Giusti, D.C.I. Goberdhan, A. Görgens, S.M. Gorski, D.W. Greening, J.C. Gross, A. Gualerzi, G.N. Gupta, D. Gustafson, A. Handberg, R.A. Haraszti, P. Harrison, H. Hegyesi, A. Hendrix, A.F. Hill, F.H. Hochberg, K.F. Hoffmann, B. Holder, H. Holthofer, B. Hosseinkhani, G. Hu, Y. Huang, V. Huber, S. Hunt, A.G.-E. Ibrahim, T. Ikezu, J.M. Inal, M. Isin, A. Ivanova, H.K. Jackson, S. Jacobsen, S.M. Jay, M. Jayachandran, G. Jenster, L. Jiang, S.M. Johnson, J.C. Jones, A. Jong, T. Jovanovic-Talisman, S. Jung, R. Kalluri, S.-i. Kano, S.

Kaur, Y. Kawamura, E.T. Keller, D. Khamari, E. Khomyakova, A. Khvorova, P. Kierulf, K.P. Kim, T. Kislinger, M. Klingeborn, D.J. Klinke, M. Kornek, M.M. Kosanović, Á.F. Kovács, E.-M. Krämer-Albers, S. Krasemann, M. Krause, I.V. Kurochkin, G.D. Kusuma, S. Kuypers, S. Laitinen, S.M. Langevin, L.R. Languino, J. Lannigan, C. Lässer, L.C. Laurent, G. Lavieu, E. Lázaro-Ibáñez, S. Le Lay, M.-S. Lee, Y.X.F. Lee, D.S. Lemos, M. Lenassi, A. Leszczynska, I.T.S. Li, K. Liao, S.F. Libregts, E. Ligeti, R. Lim, S.K. Lim, A. Linē, K. Linnemannstöns, A. Llorente, C.A. Lombard, M.J. Lorenowicz, Á.M. Lörincz, J. Lötvall, J. Lovett, M.C. Lowry, X. Loyer, Q. Lu, B. Lukomska, T.R. Lunavat, S.L.N. Maas, H. Malhi, A. Marcilla, J. Mariani, J. Mariscal, E.S. Martens-Uzunova, L. Martin-Jaular, M.C. Martinez, V.R. Martins, M. Mathieu, S. Mathivanan, M. Maugeri, L.K. McGinnis, M.J. McVey, D.G. Meckes, K.L. Meehan, I. Mertens, V.R. Minciacchi, A. Möller, M. Møller Jørgensen, A. Morales-Kastresana, J. Morhayim, F. Mullier, M. Muraca, L. Musante, V. Mussack, D.C. Muth, K.H. Myburgh, T. Najrana, M. Nawaz, I. Nazarenko, P. Nejsum, C. Neri, T. Neri, R. Nieuwland, L. Nimrichter, J.P. Nolan, E.N.M. Nolte-'t Hoen, N. Noren Hooten, L. O'Driscoll, T. O'Grady, A. O'Loghlen, T. Ochiya, M. Olivier, A. Ortiz, L.A. Ortiz, X. Osteikoetxea, O. Østergaard, M. Ostrowski, J. Park, D.M. Pegtel, H. Peinado, F. Perut, M.W. Pfaffl, D.G. Phinney, B.C.H. Pieters, R.C. Pink, D.S. Pisetsky, E. Pogge von Strandmann, I. Polakovicova, I.K.H. Poon, B.H. Powell, I. Prada, L. Pulliam, P. Quesenberry, A. Radeghieri, R.L. Raffai, S. Raimondo, J. Rak, M.I. Ramirez, G. Raposo, M.S. Rayyan, N. Regev-Rudzki, F.L. Ricklefs, P.D. Robbins, D.D. Roberts, S.C. Rodrigues, E. Rohde, S. Rome, K.M.A. Rouschop, A. Rughetti, A.E. Russell, P. Saá, S. Sahoo, E. Salas-Huenuleo, C. Sánchez, J.A. Saugstad, M.J. Saul, R.M. Schiffelers, R. Schneider, T.H. Schøyen, A. Scott, E. Shahaj, S. Sharma, O. Shatnyeva, F. Shekari, G.V. Shelke, A.K. Shetty, K. Shiba, P.R.M. Siljander, A.M. Silva, A. Skowronek, O.L. Snyder, R.P. Soares, B.W. Sódar, C. Soekmadji, J. Sotillo, P.D. Stahl, W. Stoorvogel, S.L. Stott, E.F. Strasser, S. Swift, H. Tahara, M. Tewari, K. Timms, S. Tiwari, R. Tixeira, M. Tkach, W.S. Toh, R. Tomasini, A.C. Torrecilhas, J.P. Tosar, V. Toxavidis, L. Urbanelli, P. Vader, B.W.M. van Balkom, S.G. van der Grein, J. Van Deun, M.J.C. van Herwijnen, K. Van Keuren-Jensen, G. van Niel, M.E. van Royen, A.J. van Wijnen, M.H. Vasconcelos, I.J. Vechetti, T.D. Veit, L.J. Vella, É. Velot, F.J. Verweij, B. Vestad, J.L. Viñas, T. Visnovitz, K.V. Vukman, J. Wahlgren, D.C. Watson, M.H.M. Wauben, A. Weaver, J.P. Webber, V. Weber, A.M. Wehman, D.J. Weiss, J.A. Welsh, S. Wendt, A.M. Wheelock, Z. Wiener, L. Witte, J. Wolfram, A. Xagorari, P. Xander, J. Xu, X. Yan, M. Yáñez-Mó, H. Yin, Y. Yuana, V. Zappulli, J. Zarubova, V. Žėkas, J.-y. Zhang, Z. Zhao, L. Zheng, A.R. Zheutlin, A.M. Zickler, P. Zimmermann, A.M. Zivkovic, D. Zocco and E.K. Zuba-Surma, *Minimal information for studies of extracellular vesicles 2018 (MISEV2018): a position statement of the International Society for Extracellular Vesicles and update of the MISEV2014 guidelines.* Journal of Extracellular Vesicles, 2018. **7**(1): p. 8,9

154. Carayon, K., K. Chaoui, E. Ronzier, I. Lazar, J. Bertrand-Michel, V. Roques, S. Balor, F. Terce, A. Lopez, L. Salome, and E. Joly, *Proteolipidic composition of exosomes changes during reticulocyte maturation.* J Biol Chem, 2011. **286**(39): p. 34426-34439.
155. Segura, E., S. Amigorena, and C. Thery, *Mature dendritic cells secrete exosomes with strong ability to induce antigen-specific effector immune responses.* Blood Cells Mol Dis, 2005. **35**(2): p. 89-93.
156. Console, L., M. Scalise, and C. Indiveri, *Exosomes in inflammation and role as biomarkers.* Clin Chim Acta, 2019. **488**: p. 165-171.
157. Kim, J.-H., E. Kim, and M.Y. Lee, *Exosomes as diagnostic biomarkers in cancer.* Molecular & Cellular Toxicology, 2018. **14**(2): p. 113-122.
158. Giri, P.K. and J.S. Schorey, *Exosomes derived from M. Bovis BCG infected macrophages activate antigen-specific CD4+ and CD8+ T cells in vitro and in vivo.* PLoS One, 2008. **3**(6): p. e2461.
159. Kruh-Garcia, N.A., L.M. Wolfe, L.H. Chaisson, W.O. Worodria, P. Nahid, J.S. Schorey, J.L. Davis, and K.M. Dobos, *Detection of Mycobacterium tuberculosis peptides in the exosomes of patients with active and latent M. tuberculosis infection using MRM-MS.* PLoS One, 2014. **9**(7): p. e103811.

160. Singh, P.P., V.L. Smith, P.C. Karakousis, and J.S. Schorey, *Exosomes isolated from mycobacteria-infected mice or cultured macrophages can recruit and activate immune cells in vitro and in vivo.* J Immunol, 2012. **189**(2): p. 777-785.
161. Pankoui Mfonkeu, J.B., I. Gouado, H. Fotso Kuate, O. Zambou, P.H. Amvam Zollo, G.E. Grau, and V. Combes, *Elevated cell-specific microparticles are a biological marker for cerebral dysfunctions in human severe malaria.* PLoS One, 2010. **5**(10): p. e13415.
162. Campos, F.M.F., B.S. Franklin, A. Teixeira-Carvalho, A.L.S. Filho, S.C.O. de Paula, C.J. Fontes, C.F. Brito, and L.H. Carvalho, *Augmented plasma microparticles during acute Plasmodium vivax infection.* Malaria Journal, 2010. **9**(1): p. 327.
163. Margolis, L. and Y. Sadovsky, *The biology of extracellular vesicles: The known unknowns.* PLoS Biol, 2019. **17**(7): p. e3000363.
164. Valadi, H., K. Ekstrom, A. Bossios, M. Sjostrand, J.J. Lee, and J.O. Lotvall, *Exosome-mediated transfer of mRNAs and microRNAs is a novel mechanism of genetic exchange between cells.* Nat Cell Biol, 2007. **9**(6): p. 654-659.
165. Raposo, G., H.W. Nijman, W. Stoorvogel, R. Liejendekker, C.V. Harding, C.J. Melief, and H.J. Geuze, *B lymphocytes secrete antigen-presenting vesicles.* J Exp Med, 1996. **183**(3): p. 1161-1172.
166. Zitvogel, L., A. Regnault, A. Lozier, J. Wolfers, C. Flament, D. Tenza, P. Ricciardi-Castagnoli, G. Raposo, and S. Amigorena, *Eradication of established murine tumors using a novel cell-free vaccine: dendritic cell-derived exosomes.* Nat Med, 1998. **4**(5): p. 594-600.
167. Mittelbrunn, M., C. Gutierrez-Vazquez, C. Villarroya-Beltri, S. Gonzalez, F. Sanchez-Cabo, M.A. Gonzalez, A. Bernad, and F. Sanchez-Madrid, *Unidirectional transfer of microRNA-loaded exosomes from T cells to antigen-presenting cells.* Nat Commun, 2011. **2**: p. 282.
168. Denzer, K., M. van Eijk, M.J. Kleijmeer, E. Jakobson, C. de Groot, and H.J. Geuze, *Follicular dendritic cells carry MHC class II-expressing microvesicles at their surface.* J Immunol, 2000. **165**(3): p. 1259-1265.
169. Nolte-'t Hoen, E.N., S.I. Buschow, S.M. Anderton, W. Stoorvogel, and M.H. Wauben, *Activated T cells recruit exosomes secreted by dendritic cells via LFA-1.* Blood, 2009. **113**(9): p. 1977-1981.
170. Mallegol, J., G. Van Niel, C. Lebreton, Y. Lepelletier, C. Candalh, C. Dugave, J.K. Heath, G. Raposo, N. Cerf-Bensussan, and M. Heyman, *T84-intestinal epithelial exosomes bear MHC class II/peptide complexes potentiating antigen presentation by dendritic cells.* Gastroenterology, 2007. **132**(5): p. 1866-1876.
171. Hoshino, A., B. Costa-Silva, T.L. Shen, G. Rodrigues, A. Hashimoto, M. Tesic Mark, H. Molina, S. Kohsaka, A. Di Giannatale, S. Ceder, S. Singh, C. Williams, N. Soplop, K. Uryu, L. Pharmer, T. King, L. Bojmar, A.E. Davies, Y. Ararso, T. Zhang, H. Zhang, J. Hernandez, J.M. Weiss, V.D. Dumont-Cole, K. Kramer, L.H. Wexler, A. Narendran, G.K. Schwartz, J.H. Healey, P. Sandstrom, K.J. Labori, E.H. Kure, P.M. Grandgenett, M.A. Hollingsworth, M. de Sousa, S. Kaur, M. Jain, K. Mallya, S.K. Batra, W.R. Jarnagin, M.S. Brady, O. Fodstad, V. Muller, K. Pantel, A.J. Minn, M.J. Bissell, B.A. Garcia, Y. Kang, V.K. Rajasekhar, C.M. Ghajar, I. Matei, H. Peinado, J. Bromberg, and D. Lyden, *Tumour exosome integrins determine organotropic metastasis.* Nature, 2015. **527**(7578): p. 329-335.
172. Segura, E., C. Guerin, N. Hogg, S. Amigorena, and C. Thery, *CD8+ dendritic cells use LFA-1 to capture MHC-peptide complexes from exosomes in vivo.* J Immunol, 2007. **179**(3): p. 1489-1496.
173. Rana, S., S. Yue, D. Stadel, and M. Zoller, *Toward tailored exosomes: the exosomal tetraspanin web contributes to target cell selection.* Int J Biochem Cell Biol, 2012. **44**(9): p. 1574-1584.
174. Morelli, A.E., A.T. Larregina, W.J. Shufesky, M.L. Sullivan, D.B. Stolz, G.D. Papworth, A.F. Zahorchak, A.J. Logar, Z. Wang, S.C. Watkins, L.D. Falo, Jr., and A.W. Thomson, *Endocytosis, intracellular sorting, and processing of exosomes by dendritic cells.* Blood, 2004. **104**(10): p. 3257-3266.

175. Purushothaman, A., S.K. Bandari, J. Liu, J.A. Mobley, E.E. Brown, and R.D. Sanderson, *Fibronectin on the Surface of Myeloma Cell-derived Exosomes Mediates Exosome-Cell Interactions.* J Biol Chem, 2016. **291**(4): p. 1652-1663.
176. Barres, C., L. Blanc, P. Bette-Bobillo, S. Andre, R. Mamoun, H.J. Gabius, and M. Vidal, *Galectin-5 is bound onto the surface of rat reticulocyte exosomes and modulates vesicle uptake by macrophages.* Blood, 2010. **115**(3): p. 696-705.
177. Segura, E., C. Nicco, B. Lombard, P. Veron, G. Raposo, F. Batteux, S. Amigorena, and C. Thery, *ICAM-1 on exosomes from mature dendritic cells is critical for efficient naive T-cell priming.* Blood, 2005. **106**(1): p. 216-223.
178. Bruno, S., C. Grange, M.C. Deregibus, R.A. Calogero, S. Saviozzi, F. Collino, L. Morando, A. Busca, M. Falda, B. Bussolati, C. Tetta, and G. Camussi, *Mesenchymal stem cell-derived microvesicles protect against acute tubular injury.* Journal of the American Society of Nephrology : JASN, 2009. **20**(5): p. 1053-1067.
179. Atai, N.A., L. Balaj, H. van Veen, X.O. Breakefield, P.A. Jarzyna, C.J. Van Noorden, J. Skog, and C.A. Maguire, *Heparin blocks transfer of extracellular vesicles between donor and recipient cells.* J Neurooncol, 2013. **115**(3): p. 343-351.
180. Christianson, H.C., K.J. Svensson, T.H. van Kuppevelt, J.P. Li, and M. Belting, *Cancer cell exosomes depend on cell-surface heparan sulfate proteoglycans for their internalization and functional activity.* Proc Natl Acad Sci U S A, 2013. **110**(43): p. 17380-17385.
181. French, K.C., M.A. Antonyak, and R.A. Cerione, *Extracellular vesicle docking at the cellular port: Extracellular vesicle binding and uptake.* Seminars in cell & developmental biology, 2017. **67**: p. 48-55.
182. Skog, J., T. Würdinger, S. van Rijn, D.H. Meijer, L. Gainche, M. Sena-Esteves, W.T. Curry, Jr., B.S. Carter, A.M. Krichevsky, and X.O. Breakefield, *Glioblastoma microvesicles transport RNA and proteins that promote tumour growth and provide diagnostic biomarkers.* Nature cell biology, 2008. **10**(12): p. 1470-1476.
183. Lindenbergh, M.F.S. and W. Stoorvogel, *Antigen Presentation by Extracellular Vesicles from Professional Antigen-Presenting Cells.* Annu Rev Immunol, 2018. **36**: p. 435-459.
184. Lundy, S.K. and M.W. Klinker, *Characterization and activity of Fas ligand producing CD5(+) B cells.* Methods Mol Biol, 2014. **1190**: p. 81-102.
185. Klinker, M.W., V. Lizzio, T.J. Reed, D.A. Fox, and S.K. Lundy, *Human B Cell-Derived Lymphoblastoid Cell Lines Constitutively Produce Fas Ligand and Secrete MHCII(+)FasL(+) Killer Exosomes.* Front Immunol, 2014. **5**: p. 144.
186. Latifkar, A., Y.H. Hur, J.C. Sanchez, R.A. Cerione, and M.A. Antonyak, *New insights into extracellular vesicle biogenesis and function.* J Cell Sci, 2019. **132**(13).
187. Raab-Traub, N. and D.P. Dittmer, *Viral effects on the content and function of extracellular vesicles.* Nat Rev Microbiol, 2017. **15**(9): p. 559-572.
188. Rodrigues, M., J. Fan, C. Lyon, M. Wan, and Y. Hu, *Role of Extracellular Vesicles in Viral and Bacterial Infections: Pathogenesis, Diagnostics, and Therapeutics.* Theranostics, 2018. **8**(10): p. 2709-2721.
189. Thery, C., L. Duban, E. Segura, P. Veron, O. Lantz, and S. Amigorena, *Indirect activation of naive CD4+ T cells by dendritic cell-derived exosomes.* Nat Immunol, 2002. **3**(12): p. 1156-1162.
190. Cheng, Y. and J.S. Schorey, *Exosomes carrying mycobacterial antigens can protect mice against Mycobacterium tuberculosis infection.* Eur J Immunol, 2013. **43**(12): p. 3279-3290.
191. Walker, J.D., C.L. Maier, and J.S. Pober, *Cytomegalovirus-infected human endothelial cells can stimulate allogeneic CD4+ memory T cells by releasing antigenic exosomes.* Journal of immunology (Baltimore, Md. : 1950), 2009. **182**(3): p. 1548-1559.
192. Nolte-'t Hoen, E.N., E.J. van der Vlist, M. de Boer-Brouwer, G.J. Arkesteijn, W. Stoorvogel, and M.H. Wauben, *Dynamics of dendritic cell-derived vesicles: high-resolution flow cytometric analysis of extracellular vesicle quantity and quality.* J Leukoc Biol, 2013. **93**(3): p. 395-402.

193. Hao, S., O. Bai, F. Li, J. Yuan, S. Laferte, and J. Xiang, *Mature dendritic cells pulsed with exosomes stimulate efficient cytotoxic T-lymphocyte responses and antitumour immunity.* Immunology, 2007. **120**(1): p. 90-102.
194. Utsugi-Kobukai, S., H. Fujimaki, C. Hotta, M. Nakazawa, and M. Minami, *MHC class I-mediated exogenous antigen presentation by exosomes secreted from immature and mature bone marrow derived dendritic cells.* Immunol Lett, 2003. **89**(2-3): p. 125-131.
195. Schnitzer, J.K., S. Berzel, M. Fajardo-Moser, K.A. Remer, and H. Moll, *Fragments of antigen-loaded dendritic cells (DC) and DC-derived exosomes induce protective immunity against Leishmania major.* Vaccine, 2010. **28**(36): p. 5785-5793.
196. Hwang, I., X. Shen, and J. Sprent, *Direct stimulation of naive T cells by membrane vesicles from antigen-presenting cells: distinct roles for CD54 and B7 molecules.* Proc Natl Acad Sci U S A, 2003. **100**(11): p. 6670-6675.
197. Muntasell, A., A.C. Berger, and P.A. Roche, *T cell-induced secretion of MHC class II-peptide complexes on B cell exosomes.* Embo j, 2007. **26**(19): p. 4263-4272.
198. Montecalvo, A., W.J. Shufesky, D.B. Stolz, M.G. Sullivan, Z. Wang, S.J. Divito, G.D. Papworth, S.C. Watkins, P.D. Robbins, A.T. Larregina, and A.E. Morelli, *Exosomes as a short-range mechanism to spread alloantigen between dendritic cells during T cell allorecognition.* J Immunol, 2008. **180**(5): p. 3081-3090.
199. Vincent-Schneider, H., P. Stumptner-Cuvelette, D. Lankar, S. Pain, G. Raposo, P. Benaroch, and C. Bonnerot, *Exosomes bearing HLA-DR1 molecules need dendritic cells to efficiently stimulate specific T cells.* Int Immunol, 2002. **14**(7): p. 713-722.
200. Andre, F., N. Chaput, N.E. Schartz, C. Flament, N. Aubert, J. Bernard, F. Lemonnier, G. Raposo, B. Escudier, D.H. Hsu, T. Tursz, S. Amigorena, E. Angevin, and L. Zitvogel, *Exosomes as potent cell-free peptide-based vaccine. I. Dendritic cell-derived exosomes transfer functional MHC class I/peptide complexes to dendritic cells.* J Immunol, 2004. **172**(4): p. 2126-2136.
201. Admyre, C., S.M. Johansson, S. Paulie, and S. Gabrielsson, *Direct exosome stimulation of peripheral human T cells detected by ELISPOT.* Eur J Immunol, 2006. **36**(7): p. 1772-1781.
202. Patel, D.M., R.W. Dudek, and M.D. Mannie, *Intercellular exchange of class II MHC complexes: ultrastructural localization and functional presentation of adsorbed I-A/peptide complexes.* Cell Immunol, 2001. **214**(1): p. 21-34.
203. Arnold, P.Y. and M.D. Mannie, *Vesicles bearing MHC class II molecules mediate transfer of antigen from antigen-presenting cells to CD4+ T cells.* Eur J Immunol, 1999. **29**(4): p. 1363-1373.
204. Monleon, I., M.J. Martinez-Lorenzo, L. Monteagudo, P. Lasierra, M. Taules, M. Iturralde, A. Pineiro, L. Larrad, M.A. Alava, J. Naval, and A. Anel, *Differential secretion of Fas ligand- or APO2 ligand/TNF-related apoptosis-inducing ligand-carrying microvesicles during activation-induced death of human T cells.* J Immunol, 2001. **167**(12): p. 6736-6744.
205. Alonso, R., M.C. Rodriguez, J. Pindado, E. Merino, I. Merida, and M. Izquierdo, *Diacylglycerol kinase alpha regulates the secretion of lethal exosomes bearing Fas ligand during activation-induced cell death of T lymphocytes.* J Biol Chem, 2005. **280**(31): p. 28439-28450.
206. Andreola , G., L. Rivoltini , C. Castelli , V. Huber , P. Perego , P. Deho , P. Squarcina , P. Accornero , F. Lozupone , L. Lugini , A. Stringaro , A. Molinari , G. Arancia , M. Gentile , G. Parmiani , and S. Fais *Induction of Lymphocyte Apoptosis by Tumor Cell Secretion of FasL-bearing Microvesicles.* Journal of Experimental Medicine, 2002. **195**(10): p. 1303-1316.
207. Kim, J.W., E. Wieckowski, D.D. Taylor, T.E. Reichert, S. Watkins, and T.L. Whiteside, *Fas ligand-positive membranous vesicles isolated from sera of patients with oral cancer induce apoptosis of activated T lymphocytes.* Clin Cancer Res, 2005. **11**(3): p. 1010-1020.
208. Escudier, B., T. Dorval, N. Chaput, F. Andre, M.P. Caby, S. Novault, C. Flament, C. Leboulaire, C. Borg, S. Amigorena, C. Boccaccio, C. Bonnerot, O. Dhellin, M. Movassagh, S. Piperno, C. Robert, V. Serra, N. Valente, J.B. Le Pecq, A. Spatz, O. Lantz, T. Tursz, E. Angevin, and L. Zitvogel, *Vaccination of metastatic melanoma patients with autologous dendritic cell (DC) derived-exosomes: results of thefirst phase I clinical trial.* J Transl Med, 2005. **3**(1): p. 10.

209. Morse, M.A., J. Garst, T. Osada, S. Khan, A. Hobeika, T.M. Clay, N. Valente, R. Shreeniwas, M.A. Sutton, A. Delcayre, D.H. Hsu, J.B. Le Pecq, and H.K. Lyerly, *A phase I study of dexosome immunotherapy in patients with advanced non-small cell lung cancer.* J Transl Med, 2005. **3**(1): p. 9.
210. Besse, B., M. Charrier, V. Lapierre, E. Dansin, O. Lantz, D. Planchard, T. Le Chevalier, A. Livartoski, F. Barlesi, A. Laplanche, S. Ploix, N. Vimond, I. Peguillet, C. Thery, L. Lacroix, I. Zoernig, K. Dhodapkar, M. Dhodapkar, S. Viaud, J.C. Soria, K.S. Reiners, E. Pogge von Strandmann, F. Vely, S. Rusakiewicz, A. Eggermont, J.M. Pitt, L. Zitvogel, and N. Chaput, *Dendritic cell-derived exosomes as maintenance immunotherapy after first line chemotherapy in NSCLC.* Oncoimmunology, 2016. **5**(4): p. e1071008.
211. Viaud, S., S. Ploix, V. Lapierre, C. Thery, P.H. Commere, D. Tramalloni, K. Gorrichon, P. Virault-Rocroy, T. Tursz, O. Lantz, L. Zitvogel, and N. Chaput, *Updated technology to produce highly immunogenic dendritic cell-derived exosomes of clinical grade: a critical role of interferon-gamma.* J Immunother, 2011. **34**(1): p. 65-75.
212. Pitt, J.M., F. Andre, S. Amigorena, J.C. Soria, A. Eggermont, G. Kroemer, and L. Zitvogel, *Dendritic cell-derived exosomes for cancer therapy.* J Clin Invest, 2016. **126**(4): p. 1224-1232.
213. Robbins, P.D. and A.E. Morelli, *Regulation of immune responses by extracellular vesicles.* Nat Rev Immunol, 2014. **14**(3): p. 195-208.
214. Imai, T., Y. Takahashi, M. Nishikawa, K. Kato, M. Morishita, T. Yamashita, A. Matsumoto, C. Charoenviriyakul, and Y. Takakura, *Macrophage-dependent clearance of systemically administered B16BL6-derived exosomes from the blood circulation in mice.* J Extracell Vesicles, 2015. **4**: p. 26238.
215. Takahashi, Y., M. Nishikawa, H. Shinotsuka, Y. Matsui, S. Ohara, T. Imai, and Y. Takakura, *Visualization and in vivo tracking of the exosomes of murine melanoma B16-BL6 cells in mice after intravenous injection.* J Biotechnol, 2013. **165**(2): p. 77-84.
216. Lai, C.P., E.Y. Kim, C.E. Badr, R. Weissleder, T.R. Mempel, B.A. Tannous, and X.O. Breakefield, *Visualization and tracking of tumour extracellular vesicle delivery and RNA translation using multiplexed reporters.* Nat Commun, 2015. **6**: p. 7029.
217. Lai, C.P., O. Mardini, M. Ericsson, S. Prabhakar, C. Maguire, J.W. Chen, B.A. Tannous, and X.O. Breakefield, *Dynamic biodistribution of extracellular vesicles in vivo using a multimodal imaging reporter.* ACS Nano, 2014. **8**(1): p. 483-494.
218. Hyenne, V., S. Ghoroghi, M. Collot, J. Bons, G. Follain, S. Harlepp, B. Mary, J. Bauer, L. Mercier, I. Busnelli, O. Lefebvre, N. Fekonja, M.J. Garcia-Leon, P. Machado, F. Delalande, A.A. López, S.G. Silva, F.J. Verweij, G. van Niel, F. Djouad, H. Peinado, C. Carapito, A.S. Klymchenko, and J.G. Goetz, *Studying the Fate of Tumor Extracellular Vesicles at High Spatiotemporal Resolution Using the Zebrafish Embryo.* Developmental Cell, 2019. **48**(4): p. 554-572.e557.
219. Chuo, S.T., J.C. Chien, and C.P. Lai, *Imaging extracellular vesicles: current and emerging methods.* J Biomed Sci, 2018. **25**(1): p. 91.
220. Heijnen, H.F., A.E. Schiel, R. Fijnheer, H.J. Geuze, and J.J. Sixma, *Activated platelets release two types of membrane vesicles: microvesicles by surface shedding and exosomes derived from exocytosis of multivesicular bodies and alpha-granules.* Blood, 1999. **94**(11): p. 3791-3799.
221. Meers, P. and T. Mealy, *Calcium-dependent annexin V binding to phospholipids: stoichiometry, specificity, and the role of negative charge.* Biochemistry, 1993. **32**(43): p. 11711-11721.
222. Larson, M.C., M.R. Luthi, N. Hogg, and C.A. Hillery, *Calcium-phosphate microprecipitates mimic microparticles when examined with flow cytometry.* Cytometry A, 2013. **83**(2): p. 242-250.
223. Kaminska, A., F.J. Enguita, and E.L. Stepien, *Lactadherin: An unappreciated haemostasis regulator and potential therapeutic agent.* Vascul Pharmacol, 2018. **101**: p. 21-28.

224. Hanayama, R., M. Tanaka, K. Miyasaka, K. Aozasa, M. Koike, Y. Uchiyama, and S. Nagata, *Autoimmune disease and impaired uptake of apoptotic cells in MFG-E8-deficient mice.* Science, 2004. **304**(5674): p. 1147-1150.
225. Stubbs, J.D., C. Lekutis, K.L. Singer, A. Bui, D. Yuzuki, U. Srinivasan, and G. Parry, *cDNA cloning of a mouse mammary epithelial cell surface protein reveals the existence of epidermal growth factor-like domains linked to factor VIII-like sequences.* Proc Natl Acad Sci U S A, 1990. **87**(21): p. 8417-8421.
226. Oshima, K., N. Aoki, M. Negi, M. Kishi, K. Kitajima, and T. Matsuda, *Lactation-dependent expression of an mRNA splice variant with an exon for a multiply O-glycosylated domain of mouse milk fat globule glycoprotein MFG-E8.* Biochem Biophys Res Commun, 1999. **254**(3): p. 522-528.
227. Hanayama, R. and S. Nagata, *Impaired involution of mammary glands in the absence of milk fat globule EGF factor 8.* Proc Natl Acad Sci U S A, 2005. **102**(46): p. 16886-16891.
228. Miyasaka, K., R. Hanayama, M. Tanaka, and S. Nagata, *Expression of milk fat globule epidermal growth factor 8 in immature dendritic cells for engulfment of apoptotic cells.* Eur J Immunol, 2004. **34**(5): p. 1414-1422.
229. Hanayama, R., M. Tanaka, K. Miwa, A. Shinohara, A. Iwamatsu, and S. Nagata, *Identification of a factor that links apoptotic cells to phagocytes.* Nature, 2002. **417**(6885): p. 182-187.
230. Kranich, J., N.J. Krautler, E. Heinen, M. Polymenidou, C. Bridel, A. Schildknecht, C. Huber, M.H. Kosco-Vilbois, R. Zinkernagel, G. Miele, and A. Aguzzi, *Follicular dendritic cells control engulfment of apoptotic bodies by secreting Mfge8.* J Exp Med, 2008. **205**(6): p. 1293-1302.
231. Yamaguchi, H., J. Takagi, T. Miyamae, S. Yokota, T. Fujimoto, S. Nakamura, S. Ohshima, T. Naka, and S. Nagata, *Milk fat globule EGF factor 8 in the serum of human patients of systemic lupus erythematosus.* J Leukoc Biol, 2008. **83**(5): p. 1300-1307.
232. Shi, J., Y. Shi, L.N. Waehrens, J.T. Rasmussen, C.W. Heegaard, and G.E. Gilbert, *Lactadherin detects early phosphatidylserine exposure on immortalized leukemia cells undergoing programmed cell death.* Cytometry A, 2006. **69**(12): p. 1193-1201.
233. Dasgupta, S.K., P. Guchhait, and P. Thiagarajan, *Lactadherin binding and phosphatidylserine expression on cell surface-comparison with annexin A5.* Transl Res, 2006. **148**(1): p. 19-25.
234. Hu, T., J. Shi, X. Jiao, J. Zhou, and X. Yin, *Measurement of annexin V uptake and lactadherin labeling for the quantification of apoptosis in adherent Tca8113 and ACC-2 cells.* Braz J Med Biol Res, 2008. **41**(9): p. 750-757.
235. Falborg, L., L.N. Waehrens, J. Alsner, H. Bluhme, J. Frokiaer, C.W. Heegaard, M.R. Horsman, J.T. Rasmussen, and M. Rehling, *Biodistribution of 99mTc-HYNIC-lactadherin in mice--a potential tracer for visualizing apoptosis in vivo.* Scand J Clin Lab Invest, 2010. **70**(3): p. 209-216.
236. Shi, J., C.W. Heegaard, J.T. Rasmussen, and G.E. Gilbert, *Lactadherin binds selectively to membranes containing phosphatidyl-L-serine and increased curvature.* Biochim Biophys Acta, 2004. **1667**(1): p. 82-90.
237. Otzen, D.E., K. Blans, H. Wang, G.E. Gilbert, and J.T. Rasmussen, *Lactadherin binds to phosphatidylserine-containing vesicles in a two-step mechanism sensitive to vesicle size and composition.* Biochim Biophys Acta, 2012. **1818**(4): p. 1019-1027.
238. Nielsen, M.H., H. Beck-Nielsen, M.N. Andersen, and A. Handberg, *A flow cytometric method for characterization of circulating cell-derived microparticles in plasma.* Journal of Extracellular Vesicles, 2014. **3**: p. 10.3402/jev.v3403.20795.
239. Kranich, J., N.-K. Chlis, L. Rausch, A. Latha, M. Schifferer, T. Kurz, A. Foltyn-Arfa Kia, M. Simons, F.J. Theis, and T. Brocker, *In vivo identification of apoptotic and extracellular vesicle-bound live cells using image-based deep learning.* Journal of extracellular vesicles, 2020. **9**(1): p. 1792683-1792683.
240. Hogquist, K.A., S.C. Jameson, W.R. Heath, J.L. Howard, M.J. Bevan, and F.R. Carbone, *T cell receptor antagonist peptides induce positive selection.* Cell, 1994. **76**(1): p. 17-27.

241. Moran, A.E., K.L. Holzapfel, Y. Xing, N.R. Cunningham, J.S. Maltzman, J. Punt, and K.A. Hogquist, *T cell receptor signal strength in Treg and iNKT cell development demonstrated by a novel fluorescent reporter mouse.* J Exp Med, 2011. **208**(6): p. 1279-1289.
242. Baer, A. and K. Kehn-Hall, *Viral concentration determination through plaque assays: using traditional and novel overlay systems.* Journal of visualized experiments : JoVE, 2014(93): p. e52065-e52065.
243. Matter, M., B. Odermatt, H. Yagita, J.-M. Nuoffer, and A.F. Ochsenbein, *Elimination of chronic viral infection by blocking CD27 signaling.* The Journal of experimental medicine, 2006. **203**(9): p. 2145-2155.
244. Willms, E., C. Cabañas, I. Mäger, M.J.A. Wood, and P. Vader, *Extracellular Vesicle Heterogeneity: Subpopulations, Isolation Techniques, and Diverse Functions in Cancer Progression.* Frontiers in Immunology, 2018. **9**(738).
245. Hao, Y., Z. Li, Y. Wang, X. Liu, and L. Ye, *Analyzing Mouse B Cell Responses Specific to LCMV Infection.* Methods Mol Biol, 2018. **1707**: p. 15-38.
246. Sevilla, N., S. Kunz, A. Holz, H. Lewicki, D. Homann, H. Yamada, K.P. Campbell, J.C. de La Torre, and M.B. Oldstone, *Immunosuppression and resultant viral persistence by specific viral targeting of dendritic cells.* The Journal of experimental medicine, 2000. **192**(9): p. 1249-1260.
247. Jameson, S.C. and D. Masopust, *Understanding Subset Diversity in T Cell Memory.* Immunity, 2018. **48**(2): p. 214-226.
248. Wherry, E.J., J.N. Blattman, K. Murali-Krishna, R. van der Most, and R. Ahmed, *Viral persistence alters CD8 T-cell immunodominance and tissue distribution and results in distinct stages of functional impairment.* J Virol, 2003. **77**(8): p. 4911-4927.
249. Althaus, C.L., V.V. Ganusov, and R.J. De Boer, *Dynamics of CD8+ T cell responses during acute and chronic lymphocytic choriomeningitis virus infection.* J Immunol, 2007. **179**(5): p. 2944-2951.
250. Zarozinski, C.C. and R.M. Welsh, *Minimal bystander activation of CD8 T cells during the virus-induced polyclonal T cell response.* J Exp Med, 1997. **185**(9): p. 1629-1639.
251. Subedi, P., M. Schneider, J. Philipp, O. Azimzadeh, F. Metzger, S. Moertl, M.J. Atkinson, and S. Tapio, *Comparison of methods to isolate proteins from extracellular vesicles for mass spectrometry-based proteomic analyses.* Analytical Biochemistry, 2019. **584**: p. 113390.
252. Osteikoetxea, X., B. Sodar, A. Nemeth, K. Szabo-Taylor, K. Paloczi, K.V. Vukman, V. Tamasi, A. Balogh, A. Kittel, E. Pallinger, and E.I. Buzas, *Differential detergent sensitivity of extracellular vesicle subpopulations.* Org Biomol Chem, 2015. **13**(38): p. 9775-9782.
253. Wojciechowski , S., P. Tripathi , T. Bourdeau , L. Acero , H.L. Grimes , J.D. Katz , F.D. Finkelman , and D.A. Hildeman *Bim/Bcl-2 balance is critical for maintaining naive and memory T cell homeostasis.* Journal of Experimental Medicine, 2007. **204**(7): p. 1665-1675.
254. Grayson, J.M., A.J. Zajac, J.D. Altman, and R. Ahmed, *Cutting edge: increased expression of Bcl-2 in antigen-specific memory CD8+ T cells.* J Immunol, 2000. **164**(8): p. 3950-3954.
255. Kurtulus, S., P. Tripathi, M.E. Moreno-Fernandez, A. Sholl, J.D. Katz, H.L. Grimes, and D.A. Hildeman, *Bcl-2 allows effector and memory CD8+ T cells to tolerate higher expression of Bim.* J Immunol, 2011. **186**(10): p. 5729-5737.
256. Eberlein, J., B. Davenport, T.T. Nguyen, F. Victorino, T. Sparwasser, and D. Homann, *Multiple layers of CD80/86-dependent costimulatory activity regulate primary, memory, and secondary lymphocytic choriomeningitis virus-specific T cell immunity.* Journal of Virology, 2012. **86**(4): p. 1955-1970.
257. Frebel, H., V. Nindl, R.A. Schuepbach, T. Braunschweiler, K. Richter, J. Vogel, C.A. Wagner, D. Loffing-Cueni, M. Kurrer, B. Ludewig, and A. Oxenius, *Programmed death 1 protects from fatal circulatory failure during systemic virus infection of mice.* J Exp Med, 2012. **209**(13): p. 2485-2499.
258. Ashouri, J.F. and A. Weiss, *Endogenous Nur77 Is a Specific Indicator of Antigen Receptor Signaling in Human T and B Cells.* J Immunol, 2017. **198**(2): p. 657-668.

259. Au-Yeung, B.B., J. Zikherman, J.L. Mueller, J.F. Ashouri, M. Matloubian, D.A. Cheng, Y. Chen, K.M. Shokat, and A. Weiss, *A sharp T-cell antigen receptor signaling threshold for T-cell proliferation.* Proceedings of the National Academy of Sciences, 2014. **111**: p. E3679-E3688.
260. Consortium, T.U., *UniProt: a worldwide hub of protein knowledge.* Nucleic Acids Research, 2018. **47**(D1): p. D506-D515.
261. Spessott, W.A., M.L. Sanmillan, V.V. Kulkarni, M.E. McCormick, and C.G. Giraudo, *Syntaxin 4 mediates endosome recycling for lytic granule exocytosis in cytotoxic T-lymphocytes.* Traffic, 2017. **18**(7): p. 442-452.
262. Suzuki, C., R.G. Garces, K.A. Edmonds, S. Hiller, S.G. Hyberts, A. Marintchev, and G. Wagner, *PDCD4 inhibits translation initiation by binding to eIF4A using both its MA3 domains.* Proceedings of the National Academy of Sciences, 2008. **105**(9): p. 3274-3279.
263. Liwak, U., N. Thakor, L.E. Jordan, R. Roy, S.M. Lewis, O.E. Pardo, M. Seckl, and M. Holcik, *Tumor Suppressor PDCD4 Represses Internal Ribosome Entry Site-Mediated Translation of Antiapoptotic Proteins and Is Regulated by S6 Kinase 2.* Molecular and Cellular Biology, 2012. **32**(10): p. 1818-1829.
264. Lingel, H., J. Wissing, A. Arra, D. Schanze, S. Lienenklaus, F. Klawonn, M. Pierau, M. Zenker, L. Jänsch, and M.C. Brunner-Weinzierl, *CTLA-4-mediated posttranslational modifications direct cytotoxic T-lymphocyte differentiation.* Cell death and differentiation, 2017. **24**(10): p. 1739-1749.
265. Yasuda, K., Y. Ueda, M. Ozawa, T. Matsuda, and T. Kinashi, *Enhanced cytotoxic T-cell function and inhibition of tumor progression by Mst1 deficiency.* FEBS Letters, 2016. **590**(1): p. 68-75.
266. Secrist, J.P., L. Karnitz, and R.T. Abraham, *T-cell antigen receptor ligation induces tyrosine phosphorylation of phospholipase C-gamma 1.* J Biol Chem, 1991. **266**(19): p. 12135-12139.
267. Cox, J., M.Y. Hein, C.A. Luber, I. Paron, N. Nagaraj, and M. Mann, *Accurate proteome-wide label-free quantification by delayed normalization and maximal peptide ratio extraction, termed MaxLFQ.* Molecular & cellular proteomics : MCP, 2014. **13**(9): p. 2513-2526.
268. Vinay, D.S. and B.S. Kwon, *Role of 4-1BB in immune responses.* Semin Immunol, 1998. **10**(6): p. 481-489.
269. Cannons, J.L., P. Lau, B. Ghumman, M.A. DeBenedette, H. Yagita, K. Okumura, and T.H. Watts, *4-1BB ligand induces cell division, sustains survival, and enhances effector function of CD4 and CD8 T cells with similar efficacy.* J Immunol, 2001. **167**(3): p. 1313-1324.
270. Dawicki, W. and T.H. Watts, *Expression and function of 4-1BB during CD4 versus CD8 T cell responses in vivo.* Eur J Immunol, 2004. **34**(3): p. 743-751.
271. Zhang, B., C.H. Maris, J. Foell, J. Whitmire, L. Niu, J. Song, B.S. Kwon, A.T. Vella, R. Ahmed, J. Jacob, and R.S. Mittler, *Immune suppression or enhancement by CD137 T cell costimulation during acute viral infection is time dependent.* J Clin Invest, 2007. **117**(10): p. 3029-3041.
272. Akondy, R.S., N.D. Monson, J.D. Miller, S. Edupuganti, D. Teuwen, H. Wu, F. Quyyumi, S. Garg, J.D. Altman, C. Del Rio, H.L. Keyserling, A. Ploss, C.M. Rice, W.A. Orenstein, M.J. Mulligan, and R. Ahmed, *The Yellow Fever Virus Vaccine Induces a Broad and Polyfunctional Human Memory CD8⁺ T Cell Response.* The Journal of Immunology, 2009. **183**(12): p. 7919-7930.
273. Miller, J.D., R.G. van der Most, R.S. Akondy, J.T. Glidewell, S. Albott, D. Masopust, K. Murali-Krishna, P.L. Mahar, S. Edupuganti, S. Lalor, S. Germon, C. Del Rio, M.J. Mulligan, S.I. Staprans, J.D. Altman, M.B. Feinberg, and R. Ahmed, *Human effector and memory CD8+ T cell responses to smallpox and yellow fever vaccines.* Immunity, 2008. **28**(5): p. 710-722.
274. Kongsgaard, M., M.R. Bassi, M. Rasmussen, K. Skjødt, S. Thybo, M. Gabriel, M.B. Hansen, J.P. Christensen, A.R. Thomsen, S. Buus, and A. Stryhn, *Adaptive immune responses to booster vaccination against yellow fever virus are much reduced compared to those after primary vaccination.* Scientific reports, 2017. **7**(1): p. 662-662.
275. Song, C.-B., L.-L. Zhang, X. Wu, Y.-J. Fu, Y.-J. Jiang, H. Shang, and Z.-N. Zhang, *CD4+CD38+ central memory T cells contribute to HIV persistence in HIV-infected individuals on long-term ART.* Journal of Translational Medicine, 2020. **18**(1): p. 95.

276. Sallusto, F., D. Lenig, R. Forster, M. Lipp, and A. Lanzavecchia, *Two subsets of memory T lymphocytes with distinct homing potentials and effector functions.* Nature, 1999. **401**(6754): p. 708-712.
277. Wang, X.Z., S.E. Stepp, M.A. Brehm, H.D. Chen, L.K. Selin, and R.M. Welsh, *Virus-specific CD8 T cells in peripheral tissues are more resistant to apoptosis than those in lymphoid organs.* Immunity, 2003. **18**(5): p. 631-642.
278. Kapoor, V.N., H.M. Shin, O.H. Cho, L.J. Berg, J. Kang, and R.M. Welsh, *Regulation of tissue-dependent differences in CD8+ T cell apoptosis during viral infection.* Journal of Virology, 2014. **88**(17): p. 9490-9503.
279. Henson, P.M. and D.A. Hume, *Apoptotic cell removal in development and tissue homeostasis.* Trends in Immunology, 2006. **27**(5): p. 244-250.
280. Bahl, K., A. Hüebner, R.J. Davis, and R.M. Welsh, *Analysis of apoptosis of memory T cells and dendritic cells during the early stages of viral infection or exposure to toll-like receptor agonists.* Journal of Virology, 2010. **84**(10): p. 4866-4877.
281. Elliott, J.I., A. Surprenant, F.M. Marelli-Berg, J.C. Cooper, R.L. Cassady-Cain, C. Wooding, K. Linton, D.R. Alexander, and C.F. Higgins, *Membrane phosphatidylserine distribution as a non-apoptotic signalling mechanism in lymphocytes.* Nat Cell Biol, 2005. **7**(8): p. 808-816.
282. Fischer, K., S. Voelkl, J. Berger, R. Andreesen, T. Pomorski, and A. Mackensen, *Antigen recognition induces phosphatidylserine exposure on the cell surface of human CD8+ T cells.* Blood, 2006. **108**(13): p. 4094-4101.
283. Dillon, S.R., M. Mancini, A. Rosen, and M.S. Schlissel, *Annexin V binds to viable B cells and colocalizes with a marker of lipid rafts upon B cell receptor activation.* J Immunol, 2000. **164**(3): p. 1322-1332.
284. Dillon, S.R., A. Constantinescu, and M.S. Schlissel, *Annexin V binds to positively selected B cells.* J Immunol, 2001. **166**(1): p. 58-71.
285. Ramachandra, L., Y. Qu, Y. Wang, C.J. Lewis, B.A. Cobb, K. Takatsu, W.H. Boom, G.R. Dubyak, and C.V. Harding, *Mycobacterium tuberculosis synergizes with ATP to induce release of microvesicles and exosomes containing major histocompatibility complex class II molecules capable of antigen presentation.* Infect Immun, 2010. **78**(12): p. 5116-5125.
286. Blanchard, N., D. Lankar, F. Faure, A. Regnault, C. Dumont, G. Raposo, and C. Hivroz, *TCR activation of human T cells induces the production of exosomes bearing the TCR/CD3/zeta complex.* J Immunol, 2002. **168**(7): p. 3235-3241.
287. Choudhuri, K., J. Llodra, E.W. Roth, J. Tsai, S. Gordo, K.W. Wucherpfennig, L.C. Kam, D.L. Stokes, and M.L. Dustin, *Polarized release of T-cell-receptor-enriched microvesicles at the immunological synapse.* Nature, 2014. **507**(7490): p. 118-123.
288. Benoist, C. and D. Mathis, *Regulation of major histocompatibility complex class-II genes: X, Y and other letters of the alphabet.* Annu Rev Immunol, 1990. **8**: p. 681-715.
289. Hewitt, E.W., *The MHC class I antigen presentation pathway: strategies for viral immune evasion.* Immunology, 2003. **110**(2): p. 163-169.
290. IDEAS, *Image Data Exploration and Analysis Software User's Manual Version 6.2*. 2015.
291. Barreto, A., L.S. Rodriguez, O.L. Rojas, M. Wolf, H.B. Greenberg, M.A. Franco, and J. Angel, *Membrane vesicles released by intestinal epithelial cells infected with rotavirus inhibit T-cell function.* Viral Immunol, 2010. **23**(6): p. 595-608.
292. Croft, M., L.M. Bradley, and S.L. Swain, *Naive versus memory CD4 T cell response to antigen. Memory cells are less dependent on accessory cell costimulation and can respond to many antigen-presenting cell types including resting B cells.* J Immunol, 1994. **152**(6): p. 2675-2685.
293. Croft, M., *Activation of naive, memory and effector T cells.* Curr Opin Immunol, 1994. **6**(3): p. 431-437.
294. Fahmy, T.M., J.G. Bieler, M. Edidin, and J.P. Schneck, *Increased TCR Avidity after T Cell Activation: A Mechanism for Sensing Low-Density Antigen.* Immunity, 2001. **14**(2): p. 135-143.
295. Dustin, M.L. and T.A. Springer, *T-cell receptor cross-linking transiently stimulates adhesiveness through LFA-1.* Nature, 1989. **341**(6243): p. 619-624.

296. Hegde, V.L., N.P. Singh, P.S. Nagarkatti, and M. Nagarkatti, *CD44 mobilization in allogeneic dendritic cell-T cell immunological synapse plays a key role in T cell activation.* J Leukoc Biol, 2008. **84**(1): p. 134-142.
297. Rilla, K., H. Siiskonen, M. Tammi, and R. Tammi, *Hyaluronan-coated extracellular vesicles--a novel link between hyaluronan and cancer.* Adv Cancer Res, 2014. **123**: p. 121-148.
298. Arasu, U.T., R. Karna, K. Harkonen, S. Oikari, A. Koistinen, H. Kroger, C. Qu, M.J. Lammi, and K. Rilla, *Human mesenchymal stem cells secrete hyaluronan-coated extracellular vesicles.* Matrix Biol, 2017. **64**: p. 54-68.
299. DeGrendele, H.C., M. Kosfiszer, P. Estess, and M.H. Siegelman, *CD44 activation and associated primary adhesion is inducible via T cell receptor stimulation.* J Immunol, 1997. **159**(6): p. 2549-2553.
300. Potsch, C., D. Vohringer, and H. Pircher, *Distinct migration patterns of naive and effector CD8 T cells in the spleen: correlation with CCR7 receptor expression and chemokine reactivity.* Eur J Immunol, 1999. **29**(11): p. 3562-3570.
301. Jung, Y.W., R.L. Rutishauser, N.S. Joshi, A.M. Haberman, and S.M. Kaech, *Differential localization of effector and memory CD8 T cell subsets in lymphoid organs during acute viral infection.* Journal of immunology (Baltimore, Md. : 1950), 2010. **185**(9): p. 5315-5325.
302. Khanna, K.M., J.T. McNamara, and L. Lefrancois, *In situ imaging of the endogenous CD8 T cell response to infection.* Science, 2007. **318**(5847): p. 116-120.
303. Zhang, W., X. Jiang, J. Bao, Y. Wang, H. Liu, and L. Tang, *Exosomes in Pathogen Infections: A Bridge to Deliver Molecules and Link Functions.* Frontiers in Immunology, 2018. **9**: p. 90-90.
304. Kim, S.H., N.R. Bianco, W.J. Shufesky, A.E. Morelli, and P.D. Robbins, *MHC class II+ exosomes in plasma suppress inflammation in an antigen-specific and Fas ligand/Fas-dependent manner.* J Immunol, 2007. **179**(4): p. 2235-2241.
305. Chen, G., A.C. Huang, W. Zhang, G. Zhang, M. Wu, W. Xu, Z. Yu, J. Yang, B. Wang, H. Sun, H. Xia, Q. Man, W. Zhong, L.F. Antelo, B. Wu, X. Xiong, X. Liu, L. Guan, T. Li, S. Liu, R. Yang, Y. Lu, L. Dong, S. McGettigan, R. Somasundaram, R. Radhakrishnan, G. Mills, Y. Lu, J. Kim, Y.H. Chen, H. Dong, Y. Zhao, G.C. Karakousis, T.C. Mitchell, L.M. Schuchter, M. Herlyn, E.J. Wherry, X. Xu, and W. Guo, *Exosomal PD-L1 contributes to immunosuppression and is associated with anti-PD-1 response.* Nature, 2018. **560**(7718): p. 382-386.
306. Prado, N., E.G. Marazuela, E. Segura, H. Fernández-García, M. Villalba, C. Théry, R. Rodríguez, and E. Batanero, *Exosomes from Bronchoalveolar Fluid of Tolerized Mice Prevent Allergic Reaction.* The Journal of Immunology, 2008. **181**: p. 1519-1525.
307. Xie, Y., H. Zhang, W. Li, Y. Deng, M.A. Munegowda, R. Chibbar, M. Qureshi, and J. Xiang, *Dendritic cells recruit T cell exosomes via exosomal LFA-1 leading to inhibition of CD8+ CTL responses through downregulation of peptide/MHC class I and Fas ligand-mediated cytotoxicity.* J Immunol, 2010. **185**(9): p. 5268-5278.
308. Wetzel, S.A., T.W. McKeithan, and D.C. Parker, *Peptide-specific intercellular transfer of MHC class II to CD4+ T cells directly from the immunological synapse upon cellular dissociation.* J Immunol, 2005. **174**(1): p. 80-89.
309. Blattman, J.N., R. Antia, D.J.D. Sourdive, X. Wang, S.M. Kaech, K. Murali-Krishna, J.D. Altman, and R. Ahmed, *Estimating the precursor frequency of naive antigen-specific CD8 T cells.* The Journal of experimental medicine, 2002. **195**(5): p. 657-664.
310. Acuto, O. and F. Michel, *CD28-mediated co-stimulation: a quantitative support for TCR signalling.* Nat Rev Immunol, 2003. **3**(12): p. 939-951.
311. Fraser, J.D., B.A. Irving, G.R. Crabtree, and A. Weiss, *Regulation of interleukin-2 gene enhancer activity by the T cell accessory molecule CD28.* Science, 1991. **251**(4991): p. 313-316.
312. Granelli-Piperno, A. and P. Nolan, *Nuclear transcription factors that bind to elements of the IL-2 promoter. Induction requirements in primary human T cells.* J Immunol, 1991. **147**(8): p. 2734-2739.
313. Teixeira, L.K., B.P.F. Fonseca, A. Vieira-de-Abreu, B.A. Barboza, B.K. Robbs, P.T. Bozza, and J.P.B. Viola, *IFN-γ Production by CD8⁺ T Cells Depends on NFAT1 Transcription*

Factor and Regulates Th Differentiation. The Journal of Immunology, 2005. **175**(9): p. 5931-5939.
314. Chuvpilo, S., E. Jankevics, D. Tyrsin, A. Akimzhanov, D. Moroz, M.K. Jha, J. Schulze-Luehrmann, B. Santner-Nanan, E. Feoktistova, T. Konig, A. Avots, E. Schmitt, F. Berberich-Siebelt, A. Schimpl, and E. Serfling, *Autoregulation of NFATc1/A expression facilitates effector T cells to escape from rapid apoptosis.* Immunity, 2002. **16**(6): p. 881-895.
315. Finlay, D. and D.A. Cantrell, *Metabolism, migration and memory in cytotoxic T cells.* Nature reviews. Immunology, 2011. **11**(2): p. 109-117.
316. Salmond, R.J., *mTOR Regulation of Glycolytic Metabolism in T Cells.* Frontiers in Cell and Developmental Biology, 2018. **6**(122).
317. Araki, K., A.P. Turner, V.O. Shaffer, S. Gangappa, S.A. Keller, M.F. Bachmann, C.P. Larsen, and R. Ahmed, *mTOR regulates memory CD8 T-cell differentiation.* Nature, 2009. **460**(7251): p. 108-112.
318. Kim, D.K., S.C. Lee, and H.W. Lee, *CD137 ligand-mediated reverse signals increase cell viability and cytokine expression in murine myeloid cells: involvement of mTOR/p70S6 kinase and Akt.* Eur J Immunol, 2009. **39**(9): p. 2617-2628.
319. Minami, Y., L.E. Samelson, and R.D. Klausner, *Internalization and cycling of the T cell antigen receptor. Role of protein kinase C.* J Biol Chem, 1987. **262**(27): p. 13342-13347.
320. Andre, P., J. Boretto, A.O. Hueber, A. Regnier-Vigouroux, J.P. Gorvel, P. Ferrier, and P. Chavrier, *A dominant-negative mutant of the Rab5 GTPase enhances T cell signaling by interfering with TCR down-modulation in transgenic mice.* J Immunol, 1997. **159**(11): p. 5253-5263.
321. Liu, H., M. Rhodes, D.L. Wiest, and D.A. Vignali, *On the dynamics of TCR:CD3 complex cell surface expression and downmodulation.* Immunity, 2000. **13**(5): p. 665-675.
322. Gonda, A., J. Kabagwira, G.N. Senthil, and N.R. Wall, *Internalization of Exosomes through Receptor-Mediated Endocytosis.* Mol Cancer Res, 2019. **17**(2): p. 337-347.
323. Smith, V.L., Y. Cheng, B.R. Bryant, and J.S. Schorey, *Exosomes function in antigen presentation during an in vivo Mycobacterium tuberculosis infection.* Scientific reports, 2017. **7**: p. 43578-43578.
324. Boise, L.H., A.J. Minn, P.J. Noel, C.H. June, M.A. Accavitti, T. Lindsten, and C.B. Thompson, *CD28 costimulation can promote T cell survival by enhancing the expression of Bcl-XL.* Immunity, 1995. **3**(1): p. 87-98.
325. Rogers, P.R., J. Song, I. Gramaglia, N. Killeen, and M. Croft, *OX40 promotes Bcl-xL and Bcl-2 expression and is essential for long-term survival of CD4 T cells.* Immunity, 2001. **15**(3): p. 445-455.
326. Dahl, A.M., C. Klein, P.G. Andres, C.A. London, M.P. Lodge, R.C. Mulligan, and A.K. Abbas, *Expression of bcl-X(L) restores cell survival, but not proliferation off effector differentiation, in CD28-deficient T lymphocytes.* The Journal of experimental medicine, 2000. **191**(12): p. 2031-2038.
327. Kroon, H.M., Q. Li, S. Teitz-Tennenbaum, J.R. Whitfield, A.-M. Noone, and A.E. Chang, *4-1BB Costimulation of Effector T Cells for Adoptive Immunotherapy of Cancer: Involvement of Bcl Gene Family Members.* Journal of Immunotherapy, 2007. **30**(4): p. 406-416.
328. Tan, J.T., B. Ernst, W.C. Kieper, E. LeRoy, J. Sprent, and C.D. Surh, *Interleukin (IL)-15 and IL-7 jointly regulate homeostatic proliferation of memory phenotype CD8+ cells but are not required for memory phenotype CD4+ cells.* J Exp Med, 2002. **195**(12): p. 1523-1532.
329. Berard, M., K. Brandt, S. Bulfone-Paus, and D.F. Tough, *IL-15 promotes the survival of naive and memory phenotype CD8+ T cells.* J Immunol, 2003. **170**(10): p. 5018-5026.
330. Wong, C.-H. and Y.-C. Chen, *Clinical significance of exosomes as potential biomarkers in cancer.* World journal of clinical cases, 2019. **7**(2): p. 171-190.
331. Wang, J., Y. Yao, X. Chen, J. Wu, T. Gu, and X. Tang, *Host derived exosomes-pathogens interactions: Potential functions of exosomes in pathogen infection.* Biomedicine & Pharmacotherapy, 2018. **108**: p. 1451-1459.

332. Akondy, R.S., P.L. Johnson, H.I. Nakaya, S. Edupuganti, M.J. Mulligan, B. Lawson, J.D. Miller, B. Pulendran, R. Antia, and R. Ahmed, *Initial viral load determines the magnitude of the human CD8 T cell response to yellow fever vaccination.* Proc Natl Acad Sci U S A, 2015. **112**(10): p. 3050-3055.
333. Shanks, N., R. Greek, and J. Greek, *Are animal models predictive for humans?* Philosophy, ethics, and humanities in medicine : PEHM, 2009. **4**: p. 2-2.

10 Acknowledgements

Zuallererst möchte ich mich bei Prof. Dr. Thomas Brocker für die Möglichkeit meine Dissertation in seiner Arbeitsgruppe anzufertigen bedanken. Ich danke ihm für den Austausch und die Diskussionen, die dieses Projekt vorangebracht haben und sein Vertrauen in meine wissenschaftliche Arbeit.

Ich möchte mich ganz herzlich bei Jan bedanken, der den schmalen Grad zwischen witzigem Kumpeltyp und professionellem Betreuer zu 100 % beherrscht. Danke für die Einarbeitung, Betreuung, deine unterstützenden Ratschläge aber auch für die Freiheiten die du mir gelassen hast. Danke, dass du bei jedem Experiment mitgefiebert hast und die Scherze deiner Doktoranden nicht so ernst genommen hast ;) und vielen Dank für das Lesen meiner Dr. Arbeit.

Ich danke meinen Kollegen, besonders Ina, Tilman, Anne, Ashreta, Agi, Christine die mich während meiner Dr. Arbeit begleitet haben. Danke dafür, dass wir immer zusammen gehalten haben und füreinander da waren. Danke für die witzigen unsinnigen Blödeleien und die deepen Gespräche, die die langen Tage um einiges schöner gemacht haben. Special thanks to Agi, who helped me producing MFG-E8-eGFP and for the many hours she survived in the cold room. Ich danke der AG Baumjohann für die heitere Stimmung bei den nächtlichen AMNIS Sitzungen.
Ich möchte außerdem Christine Ried für ihre Unterstützung und die tolle Organisation des Labors danken. Auch möchte ich mich bei Lisa Richter, für ihre tolle Organisation der FACS Core Facility und ihre Tipps und Kniffe bedanken.

Ich danke unseren Kooperationspartnern Prof. Dr. Anne Krug, Prof. Dr. Rothenfusser, Dr. Katharina Eisenächer, PhD Felix Meissner, Jingyuan Cheng und Dr. Tobias Straub, Dr. Martina Schifferer und Prof. Dr. Mikael Simons für die Zusammenarbeit und die tollen Ergebnisse die im Rahmen der Kooperation entstanden sind. I would like to thank especially Jingyuan Cheng for her personal crash course on R. Ich bedanke mich außerdem bei allen Mitarbeitern der Tierhaltung und meinen Kollegen am Insituts der Immunologie. Danke für die tolle, witzige Zeit. Ebenso danke ich dem SFB1054 für die finanzielle Unterstützung.

Ich möchte meiner Familie danken, die großes Interesse an meiner Arbeit gezeigt und mich immer unterstützt haben. Ganz besonders danke ich Max, der mir immer den Rücken gestärkt hat, für mich da war, für unsere nächtlichen AMNIS sessions und für seine unendliche Geduld.